2012

Smart Nanocoated Structure for Energy Harvesting at Low Frequency Vibration

Sudhanshu Sharma

SMART NANOCOATED STRUCTURE FOR ENERGY HARVESTING AT LOW FREQUENCY VIBRATION

A Thesis

Presented for the

Master of Science

Degree

In

Engineering Science

The University of Mississippi

Sudhanshu Sharma

May 2012

ABSTRACT

Increasing demands of energy which is cleaner and has an unlimited supply has led development in the field of energy harvesting. Piezoelectric materials can be used as a means of transforming ambient vibrations into electrical energy that can be stored and used to power other devices. With the recent surge of micro scale devices, piezoelectric power generation can provide a convenient alternative to traditional power sources.

In this research, a piezoelectric power generator composite prototype was developed to maximize the power output of the system. A lead zirconate titanate (PZT) composite structure was formed and mounted on a cantilever bar and was studied to convert vibration energy of the low range vibrations at 30 Hz – 1000 Hz. To improve the performance of the PZT, different coatings were made using different percentage of Ferrofluid (FNP) and Zinc Oxide nanoparticles (ZnO) and binder resin. The optimal coating mixture constituent percentage was based on the performance of the composite structure formed by applying the coating on the PZT. The fabricated PZT power generator composite with an effective volume of 0.062 cm^3 produced a maximum of 44.5 μW, or 0.717mW/cm^3 at its resonant frequency of 90 Hz. The optimal coating mixture had the composition of 59.9%FNP + 40% ZnO + 1% Resin Binder. The coating utilizes the opto-magneto-electrical properties of ZnO and Magnetic properties of FNP.

To further enhance the output, the magneto-electric (ME) effect was increased by subjecting the composite to magnetic field where coating acts as a magnetostrictive material. For the effective volume of 0.0062 cm^3, the composite produced a maximum of 68.5 μW, or

1.11mW/cm^3 at its resonant frequency of 90 Hz at 160 gauss. The optimal coating mixture had the composition of 59.9% FNP + 40% ZnO + 1% Resin Binder.

This research also focused on improving the efficiency of solar cells by utilizing the magnetic effect along with gas plasma etching to improve the internal reflection. Preliminary results showed an improvement in solar cell efficiency from 14.6% to 17.1%.

ACKNOWLEDGMENTS

I would like to express my sincere gratitude towards my advisor Dr. J.P.Sharma, for giving me a chance to work with him. He has been a continuous source of knowledge and information during the past two years, making my learning a pleasant and memorable experience. I would also like to express my sincere gratitude to my co-advisor Dr. Tyrus A. McCarty, without his knowledge and assistance this study would not have been successful. I also would like to express my deepest appreciation to Dr. Arunachalam M. Rajendran, Professor and Chair, Mechanical Engineering Department, for his kind financial support. Finally, I would like thank all my family members and friends for their encouragement and support to complete my studies.

TABLE OF CONTENTS

LIST OF TABLES

LIST OF FIGURES

CHAPTER 1

INTRODUCTION

1.1 Motivation – an overview of the problem

There is an abundance of solar and wind energy in the surrounding environment. A large portion of this energy is transformed into heat and vibration and is lost into the atmosphere without being used. It is only 1% of renewable energy resources in the form of solar and wind energy is being currently tapped [1] for power requirements in household applications. These resources are not being used extensively, because of 12 – 16 % efficiency of crystalline solar cells (most widely used [2-3]) and mechanical problems associated with wind mills [4]. Other renewable resources are smart materials in the form of piezoelectric materials which have been considered since the late 1990's for generating small power under mechanical strains [5].

For operation of electronics and wireless applications small power requirements are met currently by utilizing batteries as power sources. However, battery power discharges fast with use and thus lowers the performance of electronic devices and are not considered reliable [5]. Hence, alternates to batteries are now being looked at. The growth of scientific research and tools in the fields of nanotechnology and smart materials are providing indication that these technologies are likely to enhance not only the efficiency of solar power but also to develop new techniques to recover the thermal and vibration energy which is abundant in the atmosphere from infrastructures to machines. Even the human motion and body pulsation can be used to recover power for implants, drug delivery systems, health diagnostics and monitoring electronics.

In the technological world all types of industrial machines, automobiles and other modes of transportation, infrastructures like bridges, defense application devices generate heat and vibrations which dissipate into the atmosphere as waste. Most of the infrastructures in the world like bridges and mass transport systems are aging and thus require medium power supply to activate sensors and associated electronic devices to diagnose and monitor their performance. The large border in the nation also can utilize the smart devices which will get sensitized with vibration to detect illegal immigrants crossing the border.

With the availability of smart materials like piezoelectric materials and the multiple properties exhibited by zinc oxide nanoparticles, ferrofluid and carbon nanoparticles, it is now possible to the form composites utilizing the proposed opto-magneto-electric coupling to enhance the power output of the piezoceramics for energy harvesting at low frequency vibrations. Also, this study delved with solar cells efficiency improvement methods. Preliminary data of commercially procured solar cell also showed an encouraging improvement in the efficiency. Hence the new technological advancements in the field of vibration energy harvesting and other renewable sources of energy which are studied in this research have potentially provided a viable replacement of the conventional power sources like batteries.

1.2 Background Research

Energy harvesting devices capture the ambient energy surrounding a system and convert it into usable electrical energy. The earliest energy harvesting can be traced back to windmills in the ninth century. People have been utilizing light, heat, vibration, and other ambient energy for many decades. A variety of ambient renewable resources such as solar, thermal, and vibration have been studied as an additional resource for power supply for the last decades. Among them, the vibration/kinetic driven power generator has been widely researched because of its ubiquity

and potential for miniaturization. This point is further cleared by Figure 1.1 which shows the patent activities in energy harvesting using PZT in the recent past has increased significantly.

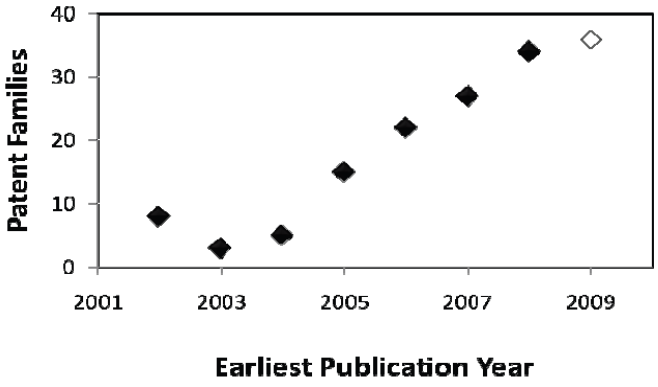

Figure 1.1 Number of patent families that contain piezo for energy harvesting [6].

1.2.1 Energy Harvesting from Smart Piezoelectric Materials

Smart piezoelectric materials, lead zirconate titanate ($Pb[Zr_xTi_{1-x}]O_3$ $0 \leq x \leq 1$), barium titanate ($BaTiO_3$), polyvinylidene fluoride (PVDF), bismuth ferrite (BiFeO3) etc. have the potential of energy harvesting. Extensive research in the field of low vibration energy harvesting has demonstrated encouraging results. Shearwood et al. [7] in 1997 developed an electromagnetic micro-generator with power density of about $2.4\mu W/cm^3$.

Amirtharajah et al. [8-9] in 1998 designed a moving coil electromagnetic transducer used as a power generator, and the calculated power was on the order of 400μW. Also, in 2000 used a MEMS capacitive transducer to convert vibration energy to power micro devices. Li et al. [10] in 2000 performed modeling and simulation of a micromachined vibration-based electromagnetic power generator. Meninger et al. [11] in 2001 proposed a variable capacitor to convert ambient mechanical vibration into electrical energy with the simulated power density being about $3.8\mu W/cm^3$.

El-hami et al. [12] in 2001 fabricated an electromagnetic transducer to convert vibration energy to electricity and generated 4167 $\mu W/cm^3$ at a vibration frequency of 320 Hz. Ching et al. [13] in 2002 presented a laser micro-machined springs to convert mechanical vibration energy into electric power and the output power density was about 830$\mu W/cm^3$ from an input frequency of 60-100 Hz. Roundy et al [14] in 2004 developed a system which was tested on a shaker at a resonant frequency of 120 Hz producing a peak total of 375 μW and were able to successfully power a custom-built radio.

Lu Chao et al [15] in 2007 proposed a vibration driven energy platform based on piezoelectric material. The proposed platform harvests ambient vibration energy as its power source and was capable of self-starting and was self-powered without the need of a battery. A comparison of power density of solar and vibration resources is shown in Table 1.1.

Table 1.1 Power density comparison of ambient energy sources [16].

Energy Source	Power density ($\mu W/cm^3$ or cm^2)
Solar	Outdoor: 15000 Indoor: 10
Vibration	Electrostatic: 50~100 Electromagnetic: 119 Piezoelectric: 250

Most of these woks were carried out between the frequency ranges of 50-400 Hz. As shown in Table 1.2, vibration sources are generally ubiquitous and can be readily found in accessible locations such as air ducts and building structures. From Table 1.2 it can be seen that most vibration sources show a peak frequency below 400 Hz.

Table 1.2 Peak frequency of various vibration sources [16].

Vibration source	Frequency of peak
Kitchen blender casing	121
Clothes dryer	121
Door frame just after door closes	125
Small microwave oven	121
HVAC vents in office building	60
External windows next to a busy street	100
Washing machine	109
Notebook computer while CD is being read	75
Second story of wood frame office building	100
Refrigerator	240
Car engine compartment	200
Handheld tools	8~500
Vehicles	5~2000
Calm winds [17]	300-1100

In the above Table 1.2, it is shown that the available frequency range of daily appliances is from 5 Hz to 2000 Hz. The smart piezoelectric materials have shown the potential to harvest the vibrations from the above range to generate power. Piezoelectric energy harvesting devices have been more intensively studied and present many advantages over other mechanisms such as simple configuration, precise control, higher power output, and potential of miniaturization.

With recent developments in personal electronics and micro-electronics, much research has been dedicated to the development of self-powered devices that can overcome the current reliance and limitations of finite-supply batteries. Figure 1.2 shows the power output densities and the lifetime of various batteries along with the two potential ambient renewable energy sources, solar and vibration, which can generate high power density and an infinite lifetime.

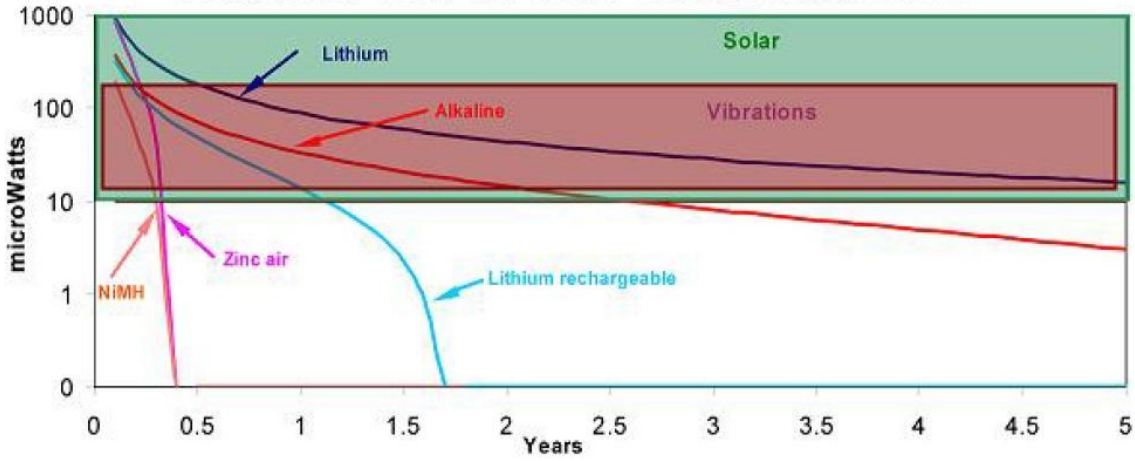

Figure 1.2 Comparison of the output power density and the lifetime among battery, solar and vibration energy sources [6].

1.2.2 Potential of Nano particles in Energy Harvesting

Nanoparticles are the tiny like microscopic particles with the size less than 100 nm. The most researched nanoparticles are carbon nanotubes, quantum dots, ferrous nanoparticles [FNP], zinc oxide nanoparticles [ZnO] and gold [Ag] and copper nanoparticles [Cu]. Wang et al [18] is one of the pioneers in the field of energy generators that use the potential of ZnO. He converted nanoscale mechanical energy into electrical energy by means of piezoelectric zinc oxide nanowire (NW) arrays. They showed that coupling of piezoelectric and semiconducting properties in ZnO creates a strain field and charge separation across the NW as a result of its bending. Lukas et al [19] in his review paper discussed about piezoelectricity, wide-bandgap semiconductivity, room-temperature ferromagnetism, and huge magneto-optic and chemical-sensing effects of ZnO.

Veeregowda [20] from the University of Mississippi, in his experiments showed how ferrous nanoparticle coated from ferrofluid on silver coated PZT material of area 6 in^2 can enhance the energy generation. His experiment reveals an enhancement from 51.123 mV to

115.434 mV comparing a plain PZT with the coated PZT vibrating at a frequency of 90Hz. Bhagmar [21] in his research at University of Mississippi showed an increase in the output from 237 mV to 299.7 mV when coated with FNP-ZnO coat. From the data above it is clear that the nanoparticle coating has good potential for power generation

1.2.3 Potential of Magnetoelectric Effect

Jing et al [22] showed that the Magnetoelectric (ME) response of PZT can be improved by using thin film ferrite coating. To achieve better ME properties, magnetostrictive materials like Terfenol- D (Terbium, Dysprosium, Iron) ($Tb_xDy_{1-x}Fe_2$ ($x \sim 0.3$)) or ferrofluid and Zinc Oxide mixture can be used. A suiTable combination of two phases can yield the desirable property such as a combination of piezomagnetic and piezoelectric phases or a combination of magnetostrictive and piezoelectric phases.

Shenqiang et al [23] developed a magnetoelectric device composed of nano-particulate magnetostrictive ironoxide-cobalt ferrite film on PZT and got a voltage coefficient as high as 10.1V/cm Oe. Junghu et al [24] used Terfnol-D to form a magnetostrictive laminate with different piezoelectric materials like PZT, Lead Magnesium Niobate / Lead Titanate (PMN-PT) ceramics and the highest output for the laminate was 10.30 V/cm Oe which is approximately 80 times higher than either that of naturally occurring MEs or artificially-grown ME composites.

Pan et al [25] discovered very high ME effect in Ni-PZT cylindrical structure when exposed to 8kOe magnetic field at 59.9 kHz frequency at 30V/cm Oe. Kulkarni et al [6] studied the development of energy harvesting modules based on piezoceramics. Table 1.3[6] shows the comparison between the different studies conducted on the ME and the potential of PZT for energy harvesting.

Table 1.3 Summary of energy-harvesting devices [6].

Reference	Device Type	Power [μW]	Frequency [Hz]	Overall Size [mm]	Power Density [$\mu W/cm^3$]
Roundy[14]	Resonant-Cantilever	375	120	30x3.6x7.7	450.9
Sodano[26]	Resonant – Cantilever	2000	50	80x40x1.0	625
Zheng[27]	Resonant- Cantilever	32.5	150	42x22x0.85	41.4
Glynne Jones[28]	Resonant- Cantilever	3	80	23x20x0.1	65.2
Marinkovich[29]	Resonant- Tethered	1	160-400	4x4x0.5	125
Renaud[30]	Impulse Driven	40	1	12x10x5	666.7

Recent advancements in the field of nanotechnology have shown that ZnO possess semiconducting, piezoelectric, and magnetic properties. FNP showed magnetostrictive properties and magnetic properties. Combination of ZnO and FNP are of great interest for power harvesting due to the various advantages as shown in the previous sections.

Application of these particles to form composite structures with the PZT will improve the energy harvesting capabilities of PZT's. The improvement in efficiency of PZT can make it a very viable replacement for the current batteries which may be hazardous and have to be frequently replaced.

1.3 Justification of Work

From the above literature search it is evident that it is possible to use nanoparticles and magnetic effect in combination to enhance the power output of smart piezoelectric materials. This current research is thus focused on development of a smart composite with coating of nanoparticles, FNP and ZnO, under the influence of magnetic field.

This research involves developing a coating which is easier to make and apply on the

PZT. The coating developed in this research is formed using readily available materials like FNP, ZnO nanoparticles, and commercially available magnetic strips and binder resins. The cost involved in developing this coating is also low.

The other advantage of using this coating is that it utilizes the Opto-MagnetoElectric effect which is a due to a combination of the optical effect of ZnO nanoparticles and the advanced magenetoelectric effect of both FNP and ZnO. This improves the power density of the coating and provides an easier and cost effective alternative for improving the energy harvesting capabilities of PZT.

In addition to this the other focus is on making nanodents on commercially available solar cells using gas plasma etching. The nanodent generated improves the internal reflection of light falling on the solar cell. Also, the combination of solar cells and piezoelectric materials can be used to create a composite which has the potential to use both, vibration and solar energy simultaneously.

CHAPTER 2

THEORY

2.1 Piezoelectricity

Piezoelectricity is a form of electricity created when piezo crystals are bent and deformed. The property of piezoelectricity is dictated by both the atoms in the crystal and the particular way in which that crystal was formed. Some of the first substances that were used to demonstrate piezoelectricity are topaz, quartz, and cane sugar. Today, it is known that many crystals are piezoelectric, and certain ceramics and polymers have also exhibited the effect as well.

A piezoelectric crystal consists of multiple interlocking domains which have positive and negative charges. These domains are symmetrical within the crystal, causing the crystal as a whole to be electrically neutral. When stress is put on the crystal, the symmetry is slightly broken, generating voltage as shown in Figure 2.1[31]. Even a tiny bit of piezoelectric crystal can generate very high voltage. Piezoelectric materials are being used in sensors, actuators, motors, clocks, lighters, and transducers. Piezoelectric crystals are used in many high-performance devices to apply tiny mechanical displacements on the scale of nanometers.

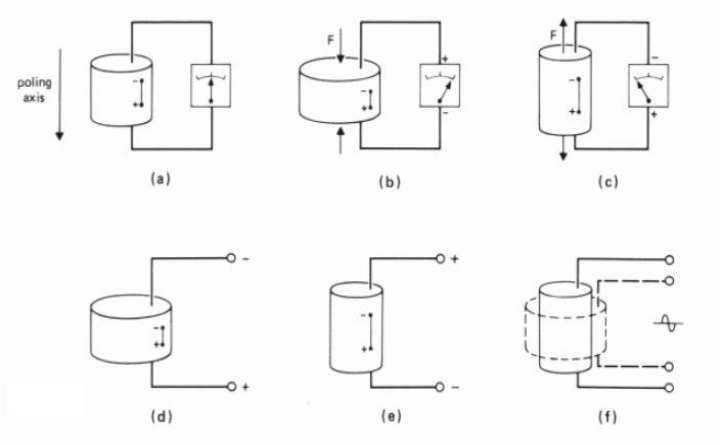

Figure 2.1 Piezoelectric effect in a cylindrical body of piezoelectric ceramic [31].

Even though a piezoelectric crystal never deforms by more than a few nanometers when a current is run through it, the force behind this deformation is extremely high, on the order of meganewtons. Piezoelectric materials are smart materials used in micro electromechanical systems (MEMS). They possess a unique property called as piezoelectricity, which mechanically stressed generates a potential difference given in voltage. Piezoelectric materials are naturally available and are also in the form of multiphase ceramics and films. Some of the man-made piezoelectric ceramics are barium titanate, lead titanate, lead zirconium titanate (PZT), and lithium niobate.

2.2 Lead Zirconium Titanate (PZT)

Lead zirconate titanate ($Pb[Zr_xTi_{1-x}]O_3$, where $0<x<1$) or PZT is a crystal, with lead atoms at corner and oxygen atoms at the face center of unit cell. Atomic size of the lead and oxygen is 1.4Å. Titanium or zirconium atoms are located at the center of unit cell. Lead, oxygen, and titanium/zirconium atoms together form a face centered cubic array, as shown in Figure 2.2 [32].

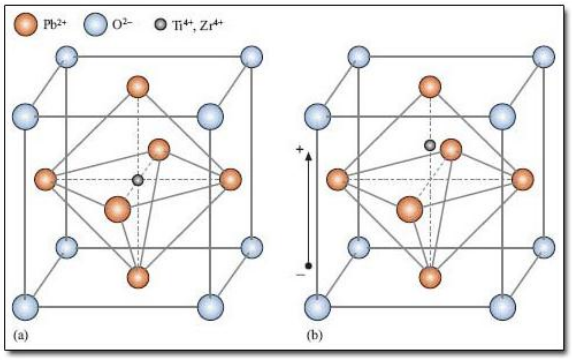

Figure 2.2 (a) Structure of PZT (b) under influence of an electric field [32].

Though all piezoelectric materials work on the same principle, PZT has highly advanced features and properties. PZT has a wide operating frequency range from 10^{-3} Hz to 10^{9} Hz. Also, it has low acoustic impedance, high elastic compliance, high stability, mechanical strength and resistivity against moisture, chemicals etc. making it very suiTable for energy harvesting and thus was chosen over the other piezo materials for this work.

Table 2.1 Properties of different piezoelectric materials [20].

Property	**Units**	**PVDF Film**	**PZT**	**$BaTiO_3$**
Density	10^3 kg/m^3	1.78	7.5	5.7
Relative Permittivity	$\varepsilon/\varepsilon_0$	12	1200	1700
d_{31} Constant	(10^{-12}) C/N	23	110	78
g_{31} Constant	(10^{-3}) Vm/N	216	10	5
k_{31} Constant	% at 1 KHz	12	30	21
Acoustic Impedance	(10^6) kg/m^2-sec	2.7	30	30

The Properties of PZT are defined in terms of constants as permittivity (ε), piezoelectric charge constant (d), piezoelectric voltage constant (g), coupling factor (k) and properties such as

density and acoustic impedance. Table 2.1 [20] demonstrates the superior properties of PZT as compared to other piezoelectric materials.

Piezoelectric Constants

Since piezoelectric ceramics are anisotropic, their physical constants (elasticity, permittivity, etc.) are tensor quantities and relate to both the direction of the applied stress, electric field, etc. and to the directions perpendicular to these. For this reason the constants are generally given two subscript indices which refer to the direction of the two related quantities (e.g. stress and strain for elasticity, displacement and electric field for permittivity). A superscript index is used to indicate a quantity that's kept constant. The direction of positive polarization is usually chosen to coincide with the Z-axis of a rectangular system of crystallographic axes X, Y, Z as shown in Figure 2.3 [31]. If the directions of X, Y and Z are represented by 1, 2 and 3 respectively, and the shear about these axes by 4, 5 and 6 respectively, the various constants may be written with subscripts referring to these.

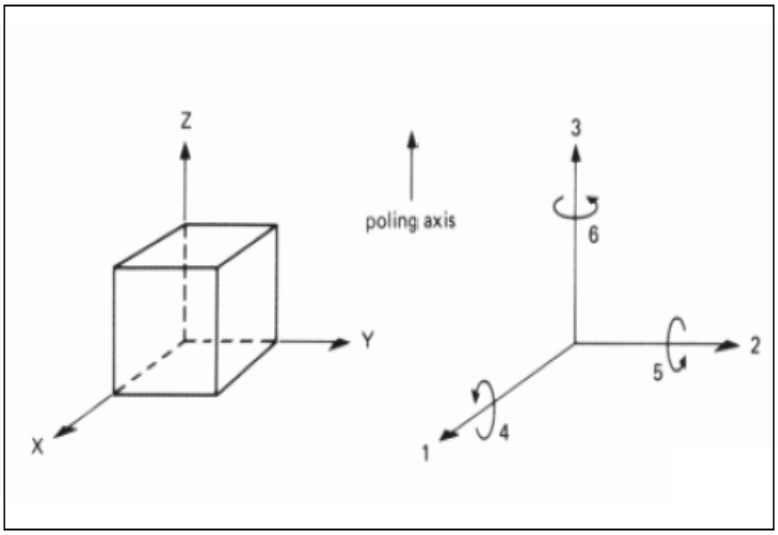

Figure 2.3 Designation of the axes and directions of deformation [31].

Permittivity (ε):

The permittivity (or dielectric constant) is defined as the dielectric displacement per unit electric field. The first subscript gives the direction of the dielectric displacement, the second gives the direction of the electric field. For example:

ε_{11}^{T} is the permittivity for the dielectric displacement and electric field in direction 1 under conditions of constant stress, and

ε_{33}^{S} is the permittivity for the dielectric displacement and electric field in direction 3 under conditions of constant strain.

Piezoelectric charge constants (d):

The piezoelectric charge constant is defined as the electric polarization generated in a material per unit mechanical stress applied to it. Alternatively, it is the mechanical strain experienced by the material per unit electric field applied to it. The first subscript refers to the direction of polarization generated in the material (at E = 0) or to the applied field strength, the second refers respectively to the direction of the applied stress or to the direction of the induced strain. For example:

d_{33} is the induced polarization per unit applied stress in direction 3. Alternatively it is the induced strain per unit electric field in direction 3.

d_{31} is the induced polarization in direction 3 per unit stress applied in direction 1. Alternatively it is the mechanical strain induced in the material in direction 1 per unit electric field applied in direction 3.

Piezoelectric voltage constant (g):

The piezoelectric voltage constant is defined as the electric field generated in a material per unit mechanical stress applied to it. Alternatively, it is the mechanical strain experienced by the material per unit electric displacement applied to it. The first subscript refers to the direction of the electric field generated in the material or to the applied electric displacement, the second refers respectively to the direction of the applied stress or to the direction of the induced strain. For example:

$g_{31}$is the induced electric field in direction per unit stress applied in direction 1. Alternatively it is the mechanical strain induced in the material in direction 1 per unit electric displacement applied in direction 3.

g_{15} is the induced electric field in direction 1 per unit shear stress applied about direction 2. Alternatively it is the shear strain induced in the material about axis 2 per unit electric displacement applied in direction 1.

Coupling factor (k):

Another important constant for piezoelectric materials is the coupling factor k_{eff} which is a measure of the effectiveness with which electrical energy in converted into mechanical energy and vice versa. At frequencies well below the resonant frequency of the piezoelectric body, k_{eff} is given by the expression

$$k_{eff}^2 = \frac{energyconverted}{inputenergy}$$

This expression holds for both electromechanical and mechano-electrical conversions. As with other piezoelectric constants, coupling factors carry subscripts. For instance, k_{33} is the coupling factor for longitudinal vibrations of a very long, very slender rod (in theory infinitely long, in practice, with a length/diameter ratio > 10) under the influence of a longitudinal electric field. K_{31} is the coupling factor for longitudinal vibrations of long rod under the influence of a transverse electric field, and k_{l5} describes shear mode vibrations of a piezoelectric body.

Compliance (S):

The compliance 'S' of a material is defined as the strain produced per unit stress. It's the reciprocal of the modulus of elasticity. The first subscript refers to the direction of strain, the second to direction of stress. For example:

S_{11}^{E} is the compliance for a stress and accompanying stain in direction 1 under conditions of constant electric field, and

S_{36}^{D} is the compliance for a shear stress about axis 3 and accompanying stain in direction 3 under conditions of constant electric displacement.

2.3 Effect of Magnetic Field on PZT

Wolf et al. [33] reported the appearance of a hierarchy of aggregate structures of particle chains on the application of a magnetic field. Sai et al. [34] conducted experiments in which it was shown that the application of magnetic field on the substrate of the piezofilm enhanced the capability of the piezofilm to measure electric fields. The main reason for this improvement in the PZT efficiency is the magneto electric (ME) effect.

Magneto Electric Effect:

ME effect can be defined as coupling of magnetic, mechanical and dielectric behaviors [35]. That is, when a magnetic field is applied to these composites, the ferromagnetic phase changes the shape magnetostrictivity, and the strain is passed to the piezoelectric phase, resulting in an electric polarization. The effect can be observed in single phase and composite materials. Some examples of single phase magnetoelectrics are Cr_2O_3, and multiferroic materials which show a coupling between the magnetic and electric order parameters. Composite magnetoelectrics are combinations of magnetostrictive and electrostrictive materials, such as ferromagnetic and piezoelectric materials. Some of the promising applications of the ME effect are sensitive detection of magnetic fields, advanced logic devices, and tunable microwave filters.

Dielectric polarization of a material under a magnetic field or an induced magnetization under an electric field requires the simultaneous presence of long-range ordering of magnetic moments and electric dipoles. Single phase materials suffer from the drawback that the ME effect is considerably weak even at low temperatures, limiting their applicability in practical devices. Better alternatives are ME composites that have large magnitudes of the ME voltage coefficient. The composites exploit the product property of the materials.

The ME effect can be realized using composites consisting of individual piezomagnetic and piezoelectric phases or individual magnetostrictive and piezoelectric phases [36]. In multiferroic materials magnetism and ferroelectricity do coexist and their mutual coupling is described by magnetoelectric effect [25]. In composite materials, the ME effect is realized by using the concept of product properties. A suiTable combination of two phases can yield the desirable property such as a combination of piezomagnetic and piezoelectric phases or a

combination of magnetostrictive and piezoelectric phases. Most ferromagnetic materials show the magnetostrictive effect, however, piezomagnetic effect in these materials has not been observed. This means that the strain caused by a magnetic field in these materials is not linearly proportional to the field strength but is related to the square of the magnetic field strength. This makes the product property, the magnetoelectric effect in the piezoelectric-magnetostrictive composites, a non-linear effect unlike the single phase materials where the magnetoelectric effect is a linear effect over a wide range of the values of the magnetic or electric field. Also, the magnetoelectric effect in these composites shows a hysteretic behavior.

The ME effect obtained in composites is more than a hundred times that of single-phase ME materials such as Co_2O_3 [24].The basic ideas underlying composite electroceramics can be classified into three categories: (1) sum properties, (2) product properties, and (3) combination properties [24]. A sum property of a composite is a weighted sum of the contributions from the individual component phases, proportional to the volume of weight fractions of these phases in the composite. Physical quantities like density and resistivity are sum properties. The product property is reflected in the composite structure but is absent in the individual phases. To achieve better magnetoelectric properties, magnetostrictive materials like Terfenol- D or ferrofluid [23] and Zinc Oxide mixture can be used which shows product property as giant ME effect is not seen in either the magentostrictive material nor PZT on its own.

2.4 Potential of Nanoparticles

Nanoparticles are the microscopic particles with the size less than 100 nm. Most common are carbon nanotubes, quantum dots, ferrous nanoparticle [FNP], zinc oxide nanoparticle [ZnO], gold [Ag] and copper nanoparticles [Cu]. Nanoparticles have a wide range of applications, such

as in nanoelectronics, magnetic storage devices, optical grating, and energy harvesting to name a few. Sprayable lead sulphide (PbS) nanocrystals dispersed in a chloroform solution of a conductive conjugative polymer, acts as a light harvesting films, shows a photovoltaic effect in the infrared region [37]. Wang et al [38] converted nanoscale mechanical energy to electrical energy using zinc oxide nanowire arrays where the energy transfer efficiency was in the range of 17-30%. Nanoparticle coating for power harvesting or energy harvesting is a field with very good potential. Nanoparticles like zinc oxide and ferrous are in particular focus of research because they possess semiconducting, piezoelectric and magnetic property, which is of great interest for power harvesting.

2.5 Zinc Oxide Nanoparticle (ZnO)

Zinc oxide nanoparticle under the scanning electron microscope as shown in the Figure 2.4 [20] is unique material that exhibits semiconducting and piezoelectric dual properties. These nanoparticles have novel applications in optoelectronics, sensors, transducers and biomedical sciences.

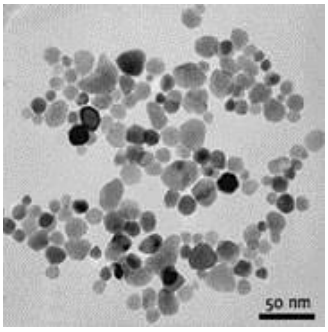

Figure 2.4 ZnO nanoparticles [50nm][20].

Wang et al [39] in his review paper showed various potential application of ZnO as a key technological material. The lack of a center of symmetry in wurtzite, combined with large

electromechanical coupling, results in strong piezoelectric and pyroelectric properties and the consequent use of ZnO in mechanical actuators and piezoelectric sensors. In addition, ZnO is a wide band-gap (3.37 eV) compound semiconductor that is suiTable for short wavelength optoelectronic applications. The high exciton binding energy (60 meV) in ZnO crystal can ensure efficient excitonic emission at room temperature and room temperature ultraviolet (UV) luminescence has been reported in disordered nanoparticles and thin films. ZnO is transparent to visible light and can be made highly conductive by doping.

The advantages of ZnO nanoparticles based on the data collected from several sources are summarized below [20][21][34][38][39]:

- It has the highest piezoelectric effect of ε_{33} = 1.2 C/m^2, among all the semiconductors.
- The thermal conductivity of ZnO is 0.54 $Wcm^{-1}K^{-1}$ which is high as compared to gallium arsenide (GaAs) which has a thermal conductivity of 0.5 $Wcm^{-1}K^{-1}$.
- It has the largest exciton binding energy of 60 meV of all the semiconductors of II-VI group and III-V group.
- ZnO has a very large shear modulus ~45.5 Gpa which indicates the stability of the crystal, as compared with 18.35Gpa for ZnSe, 32.60Gpa for GaAs and 51.37Gpa for Si.)

2.6 Ferrous Nanoparticle

Ferrofluids are colloidal liquids made of nanoscale ferromagnetic, or ferrimagnetic, particles suspended in a carrier fluid (usually an organic solvent or water). Figure 2.5 shows the ferrofluid structure. Each tiny particle is thoroughly coated with a surfactant to inhibit clumping. Oleic acid, citric acid, tetra methyl ammonium hydroxides are the common surfactants used.

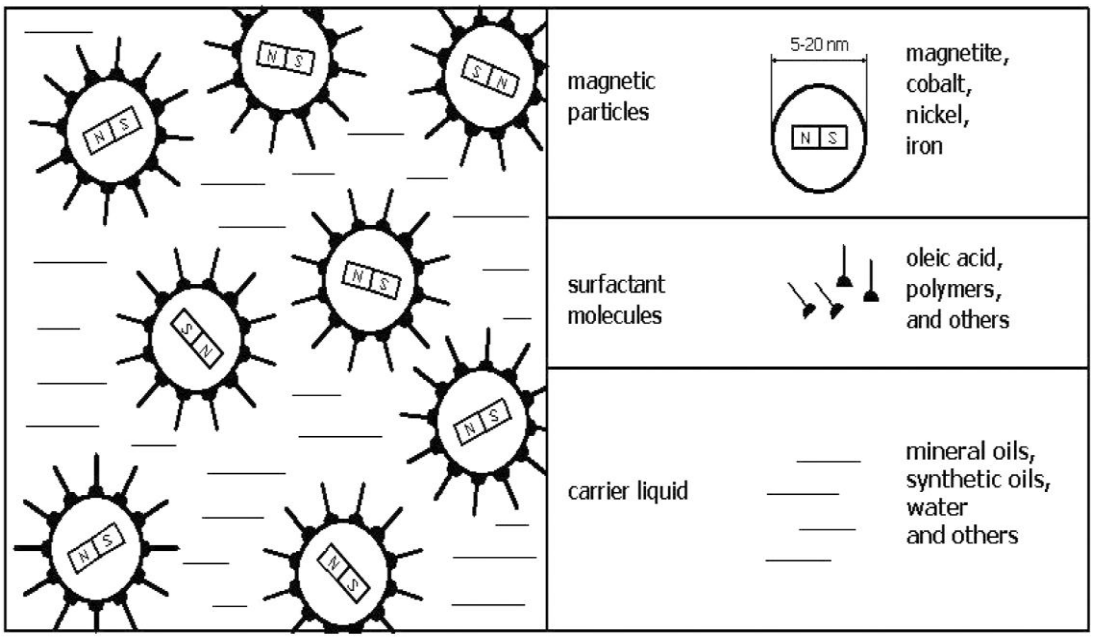

Figure 2.5: Ferrofluid structure [41].

Large ferromagnetic particles can be ripped out of the homogeneous colloidal mixture, forming a separate clump of magnetic dust when exposed to strong magnetic fields. The magnetic attraction of nanoparticles is weak enough that the surfactant's Van der Waals force is sufficient to prevent magnetic clumping or agglomeration. Ferrofluids usually do not retain magnetization in the absence of an externally applied field and thus are often classified as "superparamagnets" rather than ferromagnets [40]. They are used as lubricants, charge injection devices, high memory data storage arrays (5nm FNP could store one bit of information) and actuators. They have an average size of 10nm. Table 2.2 shows the properties of ZnO nanoparticles and ferrous oxide nanoparticles.

Table 2.2: Properties of Nanoparticles

Properties	ZnO Particles	ZnO Solution	Ferrous Oxide Particles	Ferrofluid
Size of Nanoparticles (nm)	01 - 10		20 - 50	
Appearance	White	Colorless	Grey	Black
UV Absorption (λmax) in nm		288		
pH		7-8		
Density(g/cc)	5.643	1.5	5.7	1.21
Melting Point (°C)	1975		1370	
Boiling Point (°C)	2360	100	3414	205-255
Young Modulus (Gpa)	12		214-350	
Poissons ratio	0.31		0.2	
Specific Heat @ 25°C ($Jmol^{-1}K^{-1)}$	0.12			
Thermal Conductivity(Cal/m/K)	0.6			
Magnetic Ordering	Diamagnetic		Paramagnetic	
Band Gap (eV)	3.3			
Excitation Binding Energy (meV)	60			
Piezo Electric effect (F/m^2)	1.2			
Electron Mobility cm2/(V·s) @ 80 K	27			
Initial Susceptibility			1.7	
Flash Point (°C)	1436			71.1
Pour Point (°C)				-94
Volatility 1hr @50℃				9%
Viscosity (cp@27°C)				6
Surface Tension (dy/cm)				29
Acoustic Impedance (g/cm^2-sec)	$36.4x10^5$			

Veergowda [20] in his research showed that the ferrofluid coating over PZT can be used for condition monitoring and diagnostic purposes. Bhagmar [21] in his work also showed the potential of ferrofluid in increasing the power output of PVDF by up to 55% from 457.9 µW to 740.7 µW. FNP coating under the influence of magnetic field on PZT improved the magnetoelectric property of the PZT. Magnetoelectric property of PZT increases the polarization, due to the additional magnetic energy on PZT surface [23]. Ferrofluid can act as a magetostrictive material and hence can be used to enhance the ME effect of the composite. Recent developments have shown that giant magnetoelectric effects [25] has been observed in PZT when a composite has been made using magnetostricitve materials and PZT under the influence of magnetic field and the potential of ferrofluid in that field is immense.

2.7 ZnO Nanoparticles with the Ferrofluid

The magnetic property of the FNP in the ferrofluid encouraged Sai [35] to prepare ferrofluid coating on the PZT which acted as a magnetostrictive layer on the PZT surface. Comparison of the voltage responses of PZT, ferrofluid coated PZT and PZT treated under the magnetic field is represented in Figure 2.6.

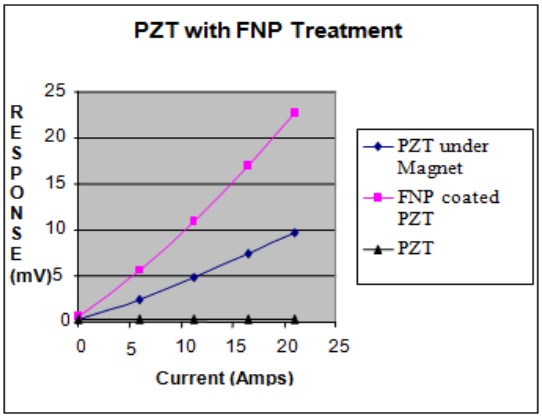

Figure 2.6: Voltage response variation [35]

Other studies have shown that ZnO has very good optical and semiconducting properties. Taking into account the opto-electric properties of ZnO and magnetostrictive properties of ferrofluid the improvement in the output of PZT will be because of the opto-magneto-electrical properties of the mixture formed by these two materials. Therefore, combination of ferrofluid and ZnO can be of immense potential in improving the energy harvesting capabilities of PZT.

2.8 Theoretical Background

When a dynamic system is subjected to a steady-state harmonic excitation, it is forced to vibrate at the same frequency as that of the excitation. The harmonic excitation can be given in many ways like with constant frequency and variable frequency or a swept-sine frequency. If the frequency of excitation coincides with one of the natural frequencies of the system, a condition of resonance is encountered. At the point of resonance the displacement of the system is a maximum. Thus calculation of natural frequencies is of major importance in the study of vibrations.

Vibration in a Continuous Beam: The beam is a continuous system, i.e. the mass along with the stiffness is distributed throughout the beam which is excited using an exciter.

The equation of motion [42] for a cantilever beam shown in Figure 2.7 is given as

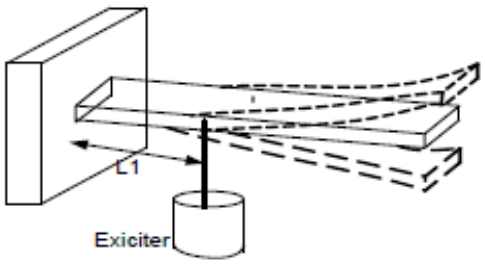

Figure 2.7 Cantilever Beam under Forced Vibration [42].

$$\frac{\partial^2}{\partial x^2}\left\{EI(x)\frac{\partial^2 y(x,t)}{\partial x^2}\right\} = m(x)\frac{\partial^2 y(x,t)}{\partial t^2} + f(t)\delta(x - L_1) \qquad (2.1)$$

E = Modulus of Rigidity,

I = Area moment of inertia

y(x, t) = displacement in y direction at distance x from fixed end,

m = mass per unit length,

m= ρA(x), ρ is the material density, A(x) is the area of cross-section of the beam,

f (t) = Forced applied to the system at x = L_1 . In the case of this study L_1 = 0.

Free Vibration Solution: The following boundary conditions for a cantilever beam

$$\text{at } x = 0,\ Y(x) = 0,\ \frac{dY(x)}{dx} = 0 \qquad (2.2)$$

and

$$\text{at } x = l,\ \frac{d^2Y(x)}{dx^2} = 0,\ \frac{d^3Y(x)}{dx^3} = 0 \qquad (2.3)$$

For a uniform beam under free vibration from equation (2.1), we get

$$\frac{d^4Y(x)}{dx^4} - \beta^4 Y(x) = 0 \qquad (2.4)$$

with $$\beta^4 = \frac{\omega^2 m}{EI} \qquad (2.5)$$

from above equation of motion, the first mode can be written as

$$\omega_{nf} = 1.875^2 \sqrt{\frac{EI}{\rho A L^4}} \quad \text{rad/sec} \qquad (2.6)$$

the second natural frequency as

$$\omega_{nf2} = 4.694^2 \sqrt{\frac{EI}{\rho A L^4}} \quad \text{rad/sec} \qquad (2.7)$$

and the third natural frequency as

$$\omega_{nf3} = 7.855^2 \sqrt{\frac{EI}{\rho A L^4}} \quad \text{rad/sec} \qquad (2.8)$$

$$f_{nf} = \frac{\omega_{nf}}{2\pi} Hz \qquad (2.9)$$

For different boundary conditions these expressions would be different. In this study the mass of the accelerometer was taken into account thus changing the equation of the natural frequency.

2.9 Photovoltaics

Photovoltaic (PV) is the direct conversion of light into electricity at the atomic level. Some materials exhibit a property known as the photoelectric effect that causes them to absorb photons of light and release electrons. When these free electrons are captured, an electric current is produced which can be used as electricity. Solar cells are made of the same kinds of semiconductor materials, such as silicon, used in the microelectronics industry.

For solar cells, a thin semiconductor wafer is specially treated [43] to form an electric field, positive on one side and negative on the other. When light energy strikes the solar cell,

electrons are knocked loose from the atoms in the semiconductor material. If electrical conductors are attached to the positive and negative sides, forming an electrical circuit, the electrons can be captured in the form of an electric current i.e. electricity as shown in Figure 2.8 [43]. This electricity can then be used to power a load, such as a light or a tool.

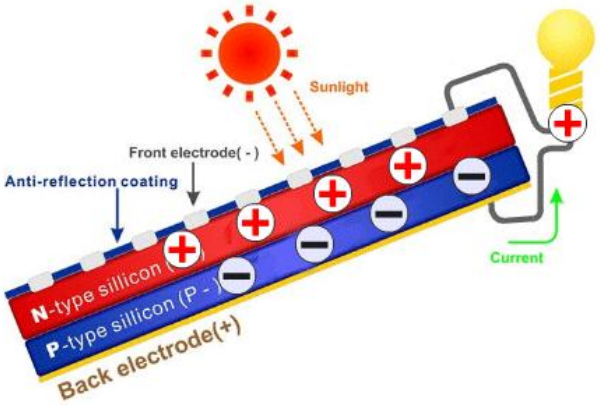

Figure 2.8: Principle of photovoltaics [43].

A solar cell's energy conversion efficiency (η) is the percentage of incident light energy that actually ends up as electric power. This is calculated at the maximum power point, P_m, divided by the product of input light irradiance (E, in W/m^2) and the surface area of the solar cell (A_c in m^2).

$$\eta = \frac{P_m}{E \times A_C} \qquad (2.10)$$

Maximum power is not maximum voltage or maximum current by itself, but it is when voltage and current combine to produce maximum power. More power can be achieved with solar panels in parallel as compared with solar panels in series. A number of solar cells electrically connected to each other and mounted in a support structure or frame is called a

photovoltaic module. These modules are designed to supply electricity at a certain voltage, such as a common 12 volts system.

The current produced is directly dependent on how much light strikes the module. Today's most common PV devices use a single junction, or interface, to create an electric field within a semiconductor such as a PV cell. In a single-junction PV cell, only photons whose energy is equal to or greater than the band gap of the cell material can free an electron for an electric circuit. In other words, the photovoltaic response of single-junction cells is limited to the portion of the sun's spectrum whose energy is above the band gap of the absorbing material, and lower-energy photons are not used. Figure 2.9 reproduced from NREL [44] shows the progressive development in the efficiency of different solar cell technologies from 1975 to 2010 along with the efficiency improvement techniques used.

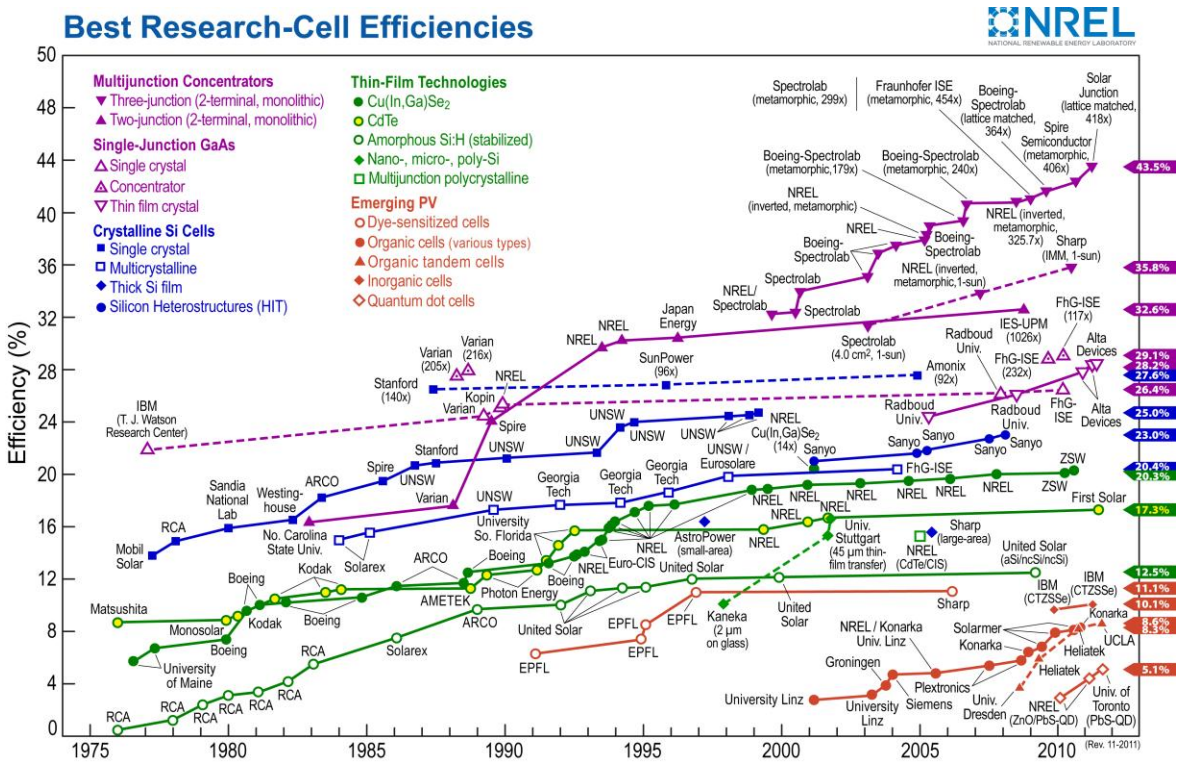

Figure 2.9 Efficiency chart of different solar cell technologies [44].

2.10 Gas Plasma Etching

In the gas plasma etching process the surface becomes highly ionized. Also, etching causes formation of nanodents due to surface erosion. These nanodents are responsible for trapping the incident light by internal reflection and refraction from the nanodents or nanorods formed by the process. This phenomenon can be used to improve the efficiency of the solar cell. Figure 2.10 shows the principle behind the improvement of the solar cell performance.

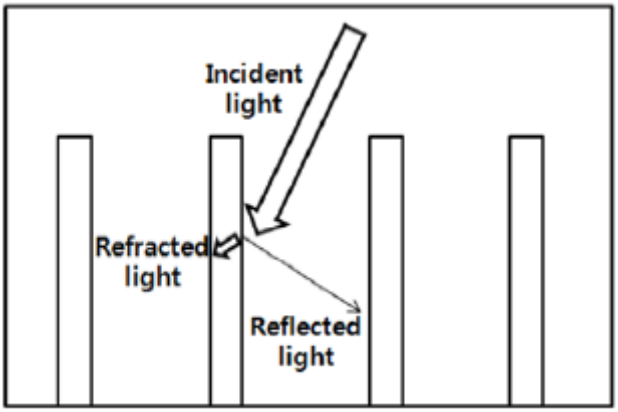

Figure 2.10 Trajectory of incident light on the gas plasma etched surface [45].

Ryu et al [45] in their experiments have demonstrated that the reflectance of the solar cells can be reduced by gas plasma etching The reflectance before the etching process was in the range of 30 – 50 % which was reduced to ~3% after the process.

CHAPTER 3

EXPERIMENTAL SETUP

This chapter contains the details of the procedures followed for making the composites, excitation of the cantilever, preparations of nanoparticles mixtures for coating and details about the tools and instruments used in performing the experiments. Two sets of experiments were carried out with focus on (a) energy harvesting from vibration of the nanocoated composites and (b) improving the efficiency of crystalline solar cell using gas plasma etching.

For the first set of experiments relating to the energy harvesting using nanocoated PZT composites, two types of composite structures were developed. The first was nanocoated PZT composite mounted on the stainless steel cantilever beam and the second one was nanocoated PZT composite mounted on the magnetic strip attached over the stainless steel cantilever beam. The PZT composites were exposed to different magnetic fields in a special apparatus developed in the department laboratory for the study of the effect of magnetic field on the nanocoated composites. The optimum exposure level of magnetic field was recorded by analyzing the performance of different composites. All further composites were exposed to the same magnetic field of 500 gauss for a period of 24 hours. The nanocoated PZT composite structure with magnetic strip was never exposed to external magnetic field.

For the second part of this work, the crystalline solar cell obtained from a commercial supplier was etched with gas plasma and then exposed to sun to study the effect of gas plasma

etching on the efficiency of solar cell. Then the etched solar cell's output was measured under the influence of magnetic field to study their combined effect on the efficiency of the crystalline solar cell.

3.1 Preparation of nanoparticle mixture solution for coating

A total of 10 nanoparticle coating mixtures were using ferrofluid and ZnO solutions. These coating mixtures varied in the percentage of their constituents having epoxy resin binder to hold the coating on the PZT substrate of the composite. Table 3.1 shows the different types of coating mixtures and their constituent percentages.

Table 3.1 Different compositions of composite coatings.

S. No.	Percentage of Ferrofluid %	Percentage of ZnO %	Percentage of Epoxy Resin Binder %
1	99.9	0	0.1
2	98.9	1	0.1
3	89.9	10	0.1
4	79.9	20	0.1
5	69.9	30	0.1
6	59.9	40	0.1
7	49.9	50	0.1
8	39.9	60	0.1
9	19.9	80	0.1
10	0	99.9	0.1

Ferrofluid consists of 5% magnetic particles, 10 % surfactant and 85% carrier fluid. The average size of ferromagnetic nanoparticles is 10 nm. Zinc oxide nanoparticles had an average particle size ranging from 24 nm to 71 nm. The epoxy helps in better adherence of the coating on

the piezoelectric substrate. The main constituents of the coating mixture were obtained from the market as listed in Table 3.2.

Table 3.2 Mixture constituents and the suppliers.

S.No	Material	Supplier Address
1	Ferrofluid – EMG 300	Ferrotec (USA) Corporation 33 Constitution Drive, Bedford, N.H. 03110
2	ZnO Nanoparticles – Z-MITE - AP	American Elements 1093 Broxton Ave. Suite 2000, L.A, CA 90024
3	Epoxy Resin - ITW Consumer 62345 - 437541	Ron's Home And Hardware 215 North College Avenue Indianapolis, IN 46204

The coatings were identified based on the percentage of ZnO nanoparticles in them. All the above materials were mixed together by weight to make a mixture. Percentage calculation for the mixture was done for a mixture weighing 10 grams. For 1% ZnO mixture, 0.1 gram of ZnO nanoparticles was mixed with 0.1 gram of binder resin and 9.8 grams ferrofluid. After the constituents were weighed on the lab balance Mettler –PE 3000, they were mixed together in a plastic petri dish using a thin plastic pipette to form a mixture of the uniform consistency.

Similarly, for the 10% ZnO coating, 1gram of ZnO nanoparticle powder was mixed with 8.9 grams of ferrofluid and 0.1gram of resin. The viscosity of the mixture varied with the percentage of ZnO powder in it but it was not measured.

3.2 Coating of PZT Substrate

After the mixture was prepared, a layer of uniform thickness was coated with a brush on the PZT substrate supplied by Murata [part number - 7BB-27-4L0]. The piezo substrate shown in the Figure 3.1 [46] and has the following dimensions as shown Table 3.3.

Table 3.3 Dimension of the piezo substrate.

Plate size dia **ø D (mm)**	Piezo element dia. **ø a (mm)**	Silver coated electrode diameter **ø b (mm)**	Total Thickness **T (mm)**	Brass Plate Thickness **t (mm)**	Plate Material
27.0	19.7	18.2	0.54	0.30	Brass

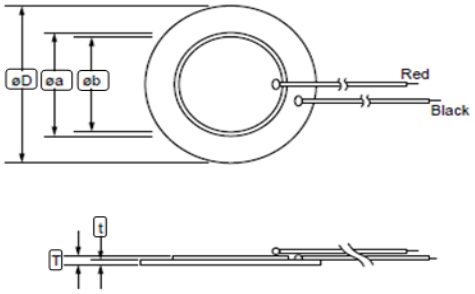

Figure 3.1 PZT substrate [46].

The coating mixture was applied such that the leads on the PZT substrate do not come in contact with the coating otherwise the output signal from the PZT would be disturbed or even lost due to discontinuity in the circuit. The coating thickness was measured between 0.04 mm-0.05 mm using a vernier caliper (Mitutoyo 01407A). To measure the thickness of the coating the coated PZT substrate's thickness was measured and then the thickness of uncoated PZT was subtracted to find the thickness of the coating. A total of 4 substrates were prepared for each mixture and the thickness of the coating was taken as the average of all the coating thicknesses.

3.3 Curing of coating by UV

The nanocoated PZT substrate was then exposed to Ultraviolet light (UV) for curing. The UV curing process is based on a photochemical reaction. An UV lamp (Entela UVL-56) having a wavelength 365 nm was used for curing. The curing time was 36 hours for all the test specimens.

3.4 Magnetic Field exposure on coatings

After the samples were cured they were set in the magnetic field for the orientation of the magnetic nanoparticles. Three levels of magnetic fields were selected for coating exposures. The levels of exposure were 500 Gauss, 750 Gauss and 1000 Gauss in addition to non-exposed coating. The magnetic field was measured using a gauss meter (DC Gauss meter Model 1). The schematic diagram along with the actual picture of the chamber used for magnetic exposure is shown in Figure 3.2(a) and (b) respectively. The two magnets were facing each other and the magnetic field intensity was varied by changing the distance of the magnets. The top magnet has S pole whereas the bottom magnet is N pole showing that emerged magnetic field for N pole go straight to S Pole.

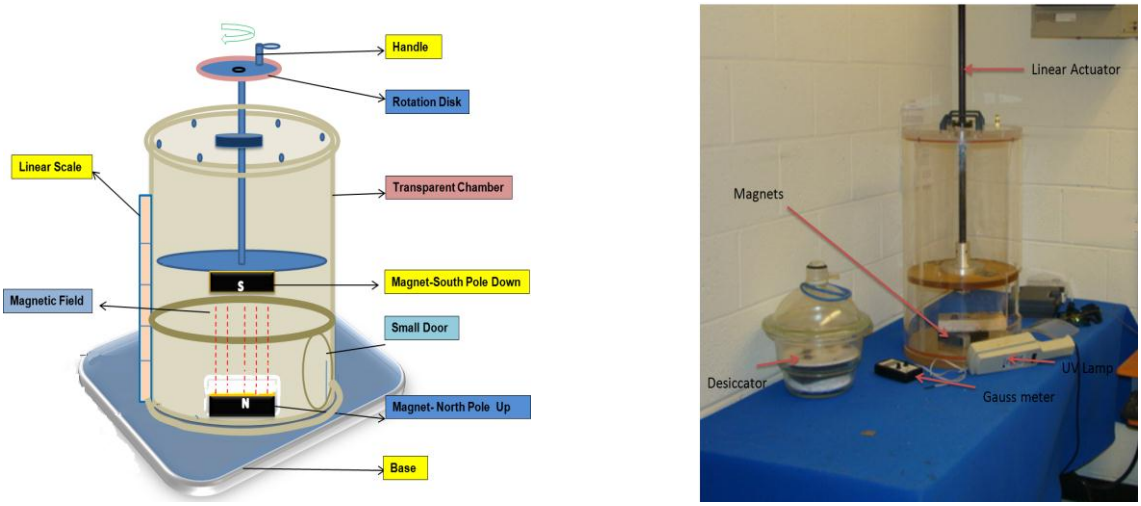

Figure 3.2 Chamber for magnetic exposure (a) schematic diagram (b) actual setup.

3.5 Composite Preparation

After the sample was cured it was then mounted on the stainless steel (Type: 430) cantilever beam 25.4 millimeters wide, 152.4 millimeters long and 0.30 millimeters thick. Three locations were chosen to mount the nanocoated PZT as shown in the Figure 3.3 (b). The other

composite structure as shown in Figure 3.3 (a) has a magnetic strip [Master Magnetics #07019 25.4 mm x 254 mm Flex Magnet Tape] attached over the cantilever beam to provide the magnetic field effect on the nanocoated PZT composite.

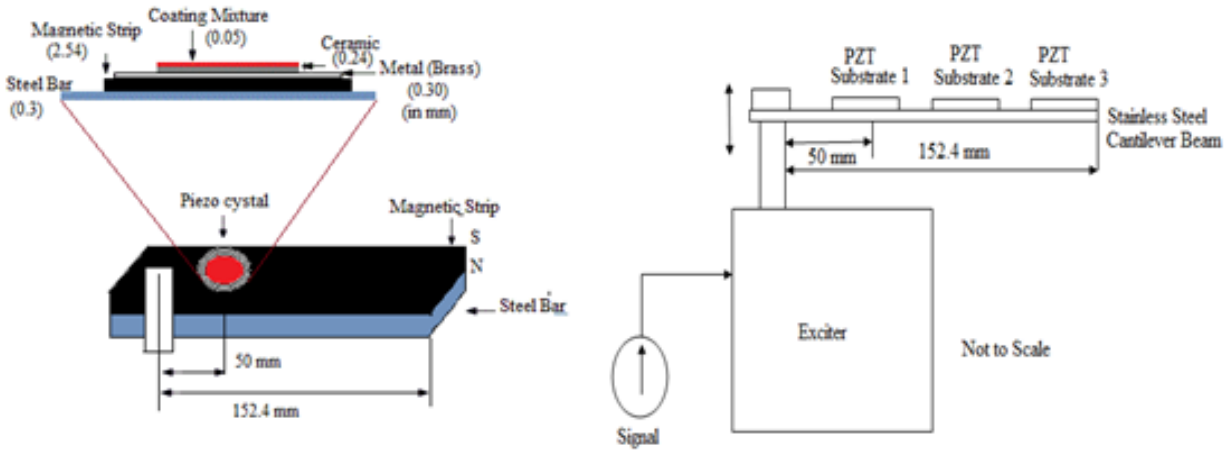

Figure 3.3 (a) Composite structure with magnetic strip and 1 nanocoated PZT (b) composite structure with 3 nanocoated PZT's.

3.6 Experimental Details for Energy Harvesting Using PZT

This composite structure (Figure 3.3) was vibrated using a vibration exciter (Bruel & Kjaer Model 4809) which is connected to the power amplifier (Stewart World 600) and the waves are generated by the function generator (Tektronic AFG-3021). The schematic diagram and actual experimental setup is shown in the Figure 3.4 (a) and (b) respectively. The signal input was a sine wave [Signal Details - Sine Curve, Phase - 0.00, Amplitude – 1.000 Vpp,]. The output voltage was measured using an oscilloscope (Tektronic TDS 3012). The current was measured using a multimeter (Fluke Process Calibrator Multimeter, NIST). The cantilever beam as shown in Figure 3.3 (a) and (b) were excited in a frequency range of 30 Hz to 1 kHz and the voltage and current outputs were measured for different composite structures respectively.

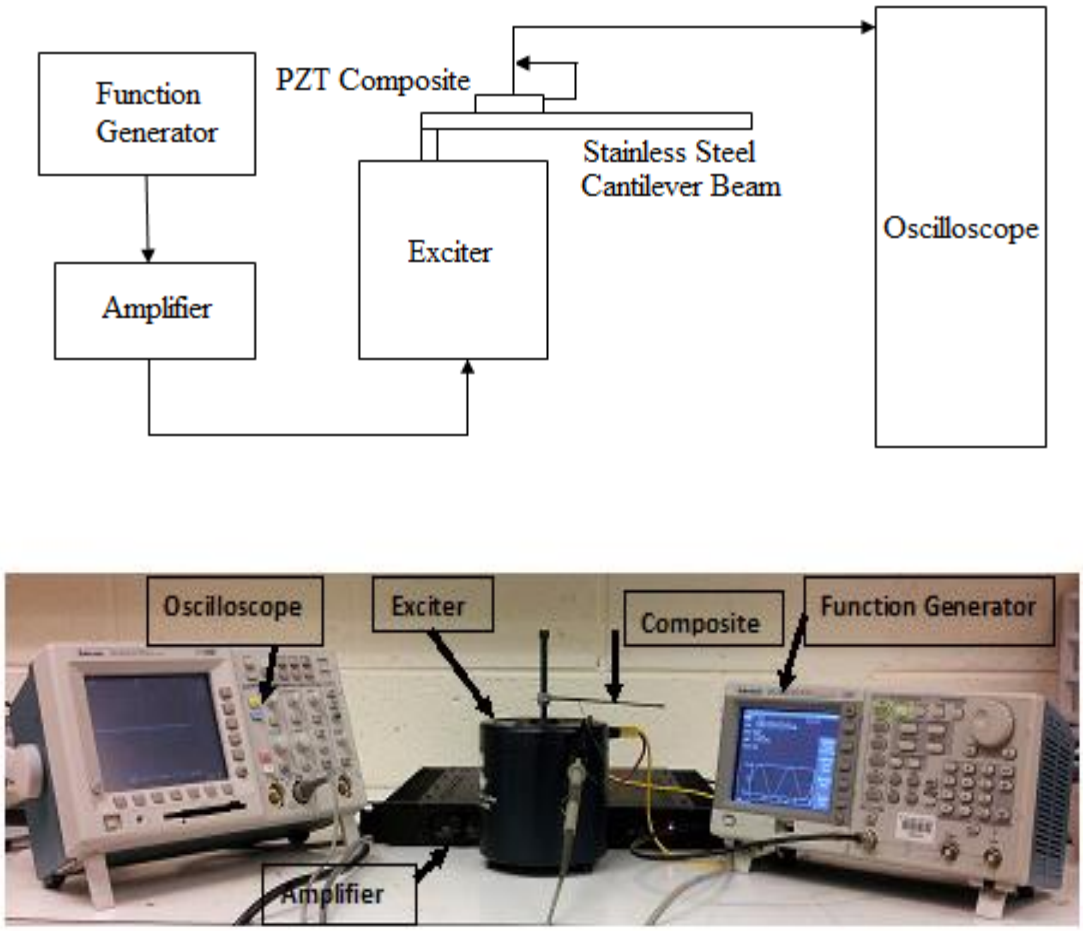

Figure 3.4 Experimental setup (a) schematic diagram (b) actual experimental setup.

The output was measured using the oscilloscope and the peak to peak voltage was determined. The peak to peak voltage was calculated directly from the output curve on the oscilloscope. The RMS voltage can be found by the measurement tool in the oscilloscope but because of the noise in the output signal the value is not very accurate. Thus, the RMS voltage was calculated from the peak to peak voltage using the relation $V_{pp} = 2\sqrt{2}V_{RMS}$. The current was measured using the fluke multimeter and the power was calculated by using the formula P = I x V where, P is the power in Watts, I is the current in Amperes, V is the RMS voltage in Volts. The results are shown in the subsequent chapters.

3.7 Gas Plasma Etching of Solar Cell

Gas plasma technology is used as surface treating tool in this experiment. Gas plasma etching is known to increase the surface energy of the substrate as well as can be used for cleaning surfaces of any residues or contamination, activation of various materials before adhering together and etching and partial removal of surfaces [47].

For this work Plasma Etch Model PE 100 from Plasma Tech was used to etch the solar wafer (MLS-156-MULTI, ML Solar). The plasma etching setup is composed of the etching gas (argon), compressed air, vacuum pump and the plasma etcher. Figure 3.5 (a) and (b) shows the schematic diagram and actual setup for gas plasma etching.

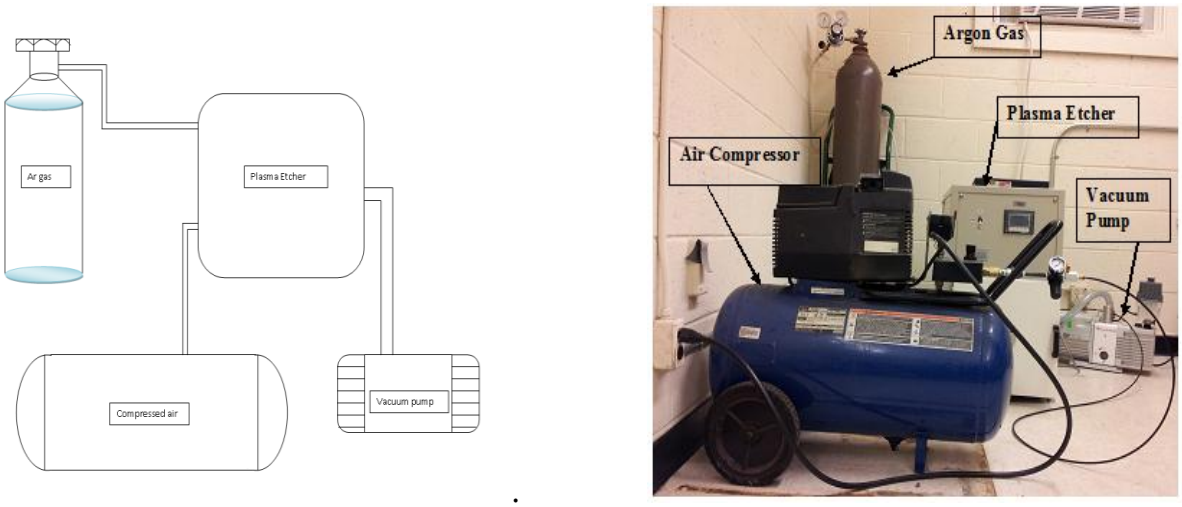

Figure 3.5 Setup for plasma etching (a) schematic diagram [48] (b) actual picture.

For the etching process Argon (Ar) was used. The air compressor pressure was set at 120 psi and the argon gas pressure was set at 25 psi. After the plasma system was started the crystalline solar cell was placed into the plasma etcher for the etching process. The etching time was set at 180 seconds. The vacuum created in the etcher for the cycle was 0.2 torrs.

After the solar cell was etched its output was measured under the sunlight. The output was measured using the fluke multimeter and the solar irradiance was measured using a solar power meter (General Tools DBTU1300). The output of the etched solar cell showed the effect of surface nanodents on its efficiency.

The second set of experiments was done by creating a magnetic field using a magnetic strip with 160 gauss magnetic field, as used in the cantilever beam structure in the previous section. Then the output was measured under the sunlight. The results showed the effect of plasma etching and magnetic field on solar cells.

CHAPTER 4

RESULTS

In the previous chapter, the experimental setups and procedures were outlined for coating process, plasma etching, and vibration testing. Using these setups, several experiments have been performed to study the effects of zinc oxide nanoparticles and magnetic field on the PZT composite and plasma etching and magnetic field on the solar cell. This chapter presents the results of these experiments.

4.1 Natural Frequency of the cantilever composite structure

Before discussing the results of the energy harvesting and solar cell efficiency it is important to mention the shape mode of a cantilever beam composite structure. This study was carried using the stainless steel beam structure in four different configurations.

1. Stainless steel beam
2. Stainless steel beam with one nanocoated PZT composite
3. Stainless steel beam with 3 nanocoated composites
4. Stainless steel beam with a mounted magnetic strip and one composite.

An accelerometer was attached on the end of the cantilever beam and five points were marked on the cantilever beam as shown in the Figure 4.1.

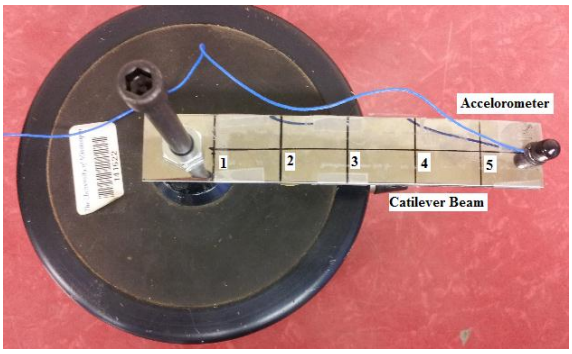

Figure 4.1 Cantilever beam marked at 5 points.

Impact force was applied on the five points and the frequency response functions were determined using the signal analyzer. Frequency response function (FRF) is the ratio of the output response (acceleration or force) of a structure to the applied force. The applied force and the response both are measured simultaneously. The measured time data is transformed from the time domain to the frequency domain using fast fourier transform (FFT) algorithm available in signal processing analyzer. This function contains complex numbers with real and imaginary components of magnitude and phase as shown in Figure 4.2.

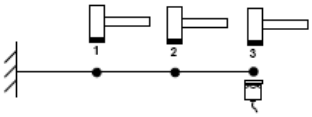

(a) Excitation at three points

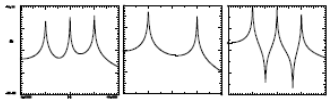

(b) Magnitude of FRF

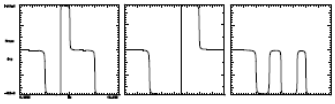

(c) Phase of FRF

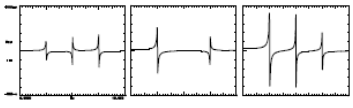

(d) Real component of FRF magnitude

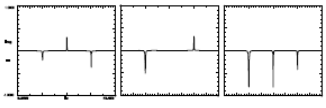

(e) Imaginary component of FRF magnitude

Figure 4.2 Frequency response function with different components.

Imaginary part of the frequency response function, Figure 4.2 (e) provides the required information to determine mode shape. The following are the results of the experiment conducted where the mass of accelerometer was also taken into account to calculate the theoretical value of the natural frequencies.

1. Natural Frequency for the Stainless Steel Beam

The first natural frequency of the cantilever beam is given as:

$$\omega_n = \sqrt{\frac{3EI}{l^3(m + 0.23m_b)}} \qquad (4.1)$$

where, m = mass of the accelerometer

m_b = mass of the cantilever beam

$$I = \frac{bh^3}{12} \qquad (4.2)$$

where, b = width of the beam

h = thickness of the beam

Cantilever beam (Stainless Steel Grade 430) has dimension 0.0254 m x 0.152 m x 0.0003 m i.e. width, length and thickness respectively.

As the metallic cantilever beam is set to vibration there is deformation in the piezocrystal mounted on the cantilever. The first mode shape is shown below for a cantilever beam.

l (length of the beam from fixed point) =0.133 m

$E = 200 \times 10^9 \text{ N/m}^2$

From equation 4.2, the area moment of inertia of the beam = $5.71 \times 10^{-14} \text{ m}^4$

$m = 1.5 \text{ grams} = 1.5 \times 10^{-3} \text{ kg}$

$m_b = 0.009071 \text{ kg} = 9.07 \times 10^{-3} \text{ kg}$

Theoretically the first natural frequency of the beam was calculated from equation 4.1; the value came out to be 10.14 Hz. The first natural frequency of the system from the experiment was 12 Hz which is very close to the theoretical frequency. The second, third and fourth natural frequencies from the experiment were found out to be at 76 Hz, 214 Hz and 414 Hz respectively for the cantilever beam.

These were obtained by collecting five recorded traces as shown in the Figure 4.3. These shows the mode shapes of the cantilever beam. Each figure has five pictures in it. To get the first mode shape, the first peak point of each picture is connected by a curve. Similarly, for the second mode shape, second peak point of each picture is connected by a curve and that's done for tracing the other natural frequencies as well. Each picture represents the imaginary mode shape vector output at the particular points selected on the cantilever beam as shown in the Figure 4.1.

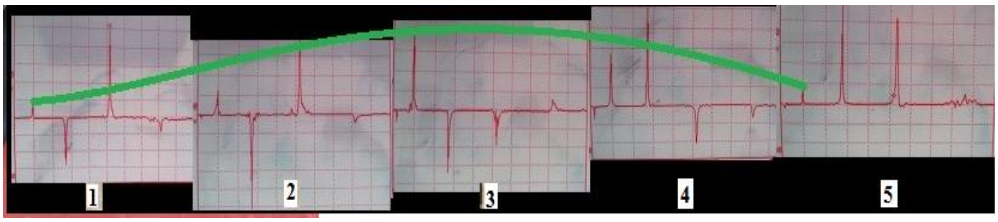

a) First mode shape of the cantilever beam.

b) Second mode shape of the cantilever beam.

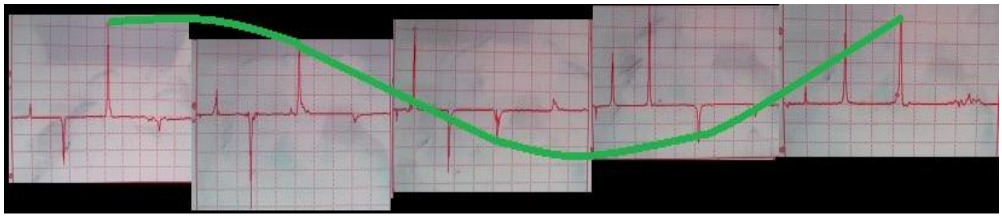

c) Third mode shape of the cantilever beam.

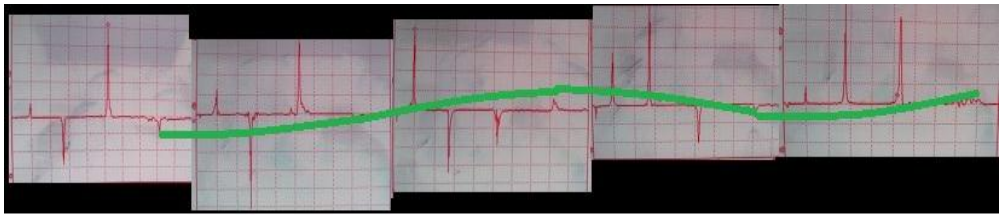

d) Fourth mode shape of the cantilever beam.

Figure 4.3 Mode shapes for cantilever beam.

2. Natural Frequency for the Stainless Steel Beam with one PZT Composite

m_b= 10.91 grams = 10.91 x 10^{-3} kgs

Using equation (4.1) and (4.2), theoretical first natural frequency = 9.59 Hz

First natural frequency of the system from the experiment was 12 Hz. The second, third and the fourth natural frequencies were 74 Hz, 202 Hz and 414 Hz respectively

3. Natural Frequency for the Stainless Steel Beam with three PZT Composites

m_b= 15.21 grams = 15.21 x 10^{-3} kgs

Using equation (4.1) and (4.1), theoretical first natural frequency = 8.59 Hz

First natural frequency of the system from the experiment was 10 Hz. The second, third and the fourth natural frequencies were 64 Hz, 192 Hz and 380 Hz respectively.

The first natural frequencies of the cantilever beam were in the range of 8 – 12 Hz, but due to experimental complications the frequency range chosen for this study was in the range of 30 – 1000 Hz.

4. Natural Frequency for the Stainless Steel Beam with magnetic strip and PZT Composite

m_b= 28.93 grams = 28.93 x 10^{-3} kgs

E_1 = Elastic modulus of stainless steel grade 430 = 200 x 10^9 N/m^2

E_2 = Elastic modulus of magnetic strip = 120 psi = 8.3 x 10^5 N/m^2

Dimension of stainless steel strip = 0.0254 m x 0.133 m x 0.0003 m

Dimension of magnetic strip = 0.0254 m x 0.133 m x 0.0025 m

Equivalent E of the composite is given by

$$E = E_1V_1+E_2V_2 \qquad (4.3)$$

where, $V_1 = A_1/A$, $V_2 = A_2/A$.

A = Total cross sectional area of the composite = 7.1 x 10^{-5} m^2

A_1 = Cross sectional area of stainless steel beam

A_2 = Cross sectional area of magnetic strip

V_1 = 0.107, V_2 = 0.894

Using equation (4.3), the equivalent modulus of elasticity of the composite = 2.1 x 10^{10} N/m^2

Using equation (4.2), the area moment of inertia = 4.65×10^{-11} m^4

Using equation (4.1), theoretical first natural frequency = 62.2 Hz

First natural frequency of the system from the experiment was 78 Hz. The second and third natural frequencies were 234 Hz and 380 Hz respectively.

4.2 Effect of PZT Composite Area Variation

This section includes the results of the experiments done with cantilever composites having different areas. The two composite beams that were tested for this study were:

a. Single area composite – One coated PZT composite mounted on the stainless steel cantilever beam as shown in Figure 4.4 (a). The area of the composite was 3.04×10^{-4} m^2. This composite structure has been identified as composite A.

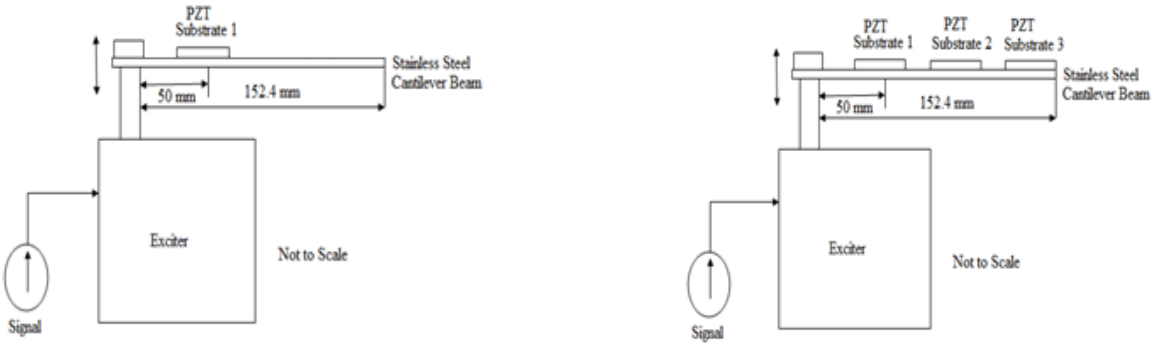

Figure 4.4 (a) Single PZT composite structure (b) Triple PZT composite structure.

b. Triple area composite – Three coated PZT composites mounted on the stainless steel cantilever beam as shown in the Figure 4.4 (b). The total area of the composite PZT's was 9.14×10^{-4} m^2. The coated PZT's were connected in series which increased the voltage output. This composite structure has been identified as composite B.

The coating type varies on the basis of the percentage of ZnO in PZT coatings. A total of 5 different percentage coatings 1, 10, 30 50 and 100 percent ZnO were used in this experiment. The power was calculated using the formula P = I x V, where P is the power, I is the current and V is the RMS voltage. The RMS voltage was calculated from peak to peak voltage which was determined experimentally. An average of 5 readings was taken for each frequency level. Tables 4.1 and 4.2 show the output for all the different coatings for composite A (single area composite) and composite B (triple area composite).

Table 4.1 Outputs of different coating types for composite A.

Freq (Hz)	Current (μA)					Voltage (mV)					Power (μW)				
	1%	10%	30%	50%	100%	1%	10%	30%	50%	100%	1%	10%	30%	50%	100%
30	2.4	1.9	1.9	3.3	2.9	0.3	0.2	0.2	0.6	0.6	0.8	0.4	0.4	2.1	1.8
45	3	2.5	2.2	3.6	3.4	0.5	0.4	0.3	0.7	0.8	1.4	0.9	0.7	2.6	2.7
60	4.3	2.9	2.9	5.4	4.7	0.7	0.5	0.5	1.2	1.2	3.2	1.4	1.5	6.6	5.7
75	8.9	6.8	6	11.3	9	1.8	1.4	1.3	2.9	2.6	16.2	9.4	7.8	32.3	23.7
90	9.4	5.8	5.5	13.1	10.8	1.9	1.2	1.2	3.4	3.2	18.2	6.7	6.5	44.3	34.8
120	2.4	1.7	1.7	2.7	2.4	0.3	0.2	0.2	0.5	0.5	0.8	0.3	0.3	1.3	1.2
150	1.7	1.6	1.7	1.7	1.5	0.2	0.2	0.2	0.2	0.2	0.3	0.2	0.3	0.3	0.3
180	2.4	1.9	2	2.6	2.3	0.3	0.2	0.3	0.5	0.4	0.8	0.4	0.5	1.2	1
220	6.8	5	4.8	6.3	5.4	1.3	1.0	1.0	1.5	1.4	9.1	4.8	4.8	9.4	7.8
250	7.2	4.6	3.9	10.9	7.7	1.4	0.9	0.7	2.8	2.2	10.4	4	2.9	30.2	16.9
300	2.6	2.2	2	3.1	2.5	0.4	0.3	0.3	0.6	0.5	1	0.6	0.5	1.8	1.3
400	1.6	1.6	1.5	1.6	1.7	0.2	0.1	0.1	0.2	0.2	0.2	0.2	0.2	0.3	0.4
500	3	1.8	1.7	3.2	2.7	0.5	0.2	0.2	0.6	0.6	1.4	0.3	0.3	2	1.5
750	2.2	2.1	1.7	1.8	1.8	0.3	0.2	0.2	0.2	0.3	0.6	0.5	0.3	0.4	0.5
1000	1.4	1.4	1.3	1.3	1.3	0.1	0.1	0.1	0.1	0.1	0.2	0.1	0.1	0.1	0.1

Table 4.2 Outputs of different coating types for composite B.

Freq (Hz)	Current (μA)					Voltage (mV)					Power (μW)				
	1%	10%	30%	50%	100%	1%	10%	30%	50%	100%	1%	10%	30%	50%	100%
30	2.1	2.1	1.6	2.4	2.4	1.0	1.0	0.6	1.9	1.8	2.1	2.1	1	4.5	4.4
45	2.5	2.4	1.9	2.7	2.8	1.4	1.3	0.9	2.2	2.4	3.5	3.2	1.8	5.9	6.7
60	3.4	3.4	2.5	3.8	3.8	2.2	2.3	1.6	3.7	3.7	7.6	7.7	3.9	13.9	13.9
75	6.9	6.2	4.2	7.5	7	5.5	4.9	3.3	8.6	7.9	37.8	30.6	13.8	64.3	55.2
90	7.3	6.4	5.7	8.7	8.3	5.8	5.2	4.8	10.1	9.7	42.4	33	27.6	88.2	80.3
120	1.9	2	1.6	2.1	2.1	0.8	0.9	0.6	1.4	1.4	1.6	1.9	0.9	2.9	3
150	1.5	1.5	1.5	1.5	1.4	0.6	0.5	0.6	0.6	0.6	0.8	0.8	0.8	0.9	0.8
180	2.1	2	1.9	2	2	1.0	1.0	0.9	1.4	1.3	2.1	2	1.7	2.7	2.6
220	5.3	5	4.3	4.4	4.2	4.0	3.8	3.4	4.5	4.3	21.2	19	14.7	19.8	18.2
250	5.7	4.7	4.2	7.1	6	4.3	3.5	3.4	8.0	6.6	24.7	16.5	14.2	56.8	39.5
300	2.2	2.4	2	2.3	2.2	1.1	1.3	1.0	1.8	1.6	2.5	3.1	2.1	4.1	3.5
400	1.5	1.6	1.5	1.4	1.5	0.5	0.6	0.5	0.5	0.7	0.7	0.9	0.7	0.7	1.1
500	2.4	2.2	1.9	2.4	2.3	1.4	1.2	1.0	1.9	1.7	3.3	2.6	1.9	4.5	3.9
750	1.9	1.8	1.6	1.5	1.6	0.9	0.7	0.6	0.7	0.8	1.6	1.3	0.9	1.1	1.3
1000	1.3	1.4	1.3	1.2	1.2	0.3	0.4	0.3	0.3	0.3	0.4	0.5	0.4	0.3	0.4

The voltage output for a PZT composite coating mixture having 50% ZnO in these two areas with the variation of frequency is shown in Figure 4.5.

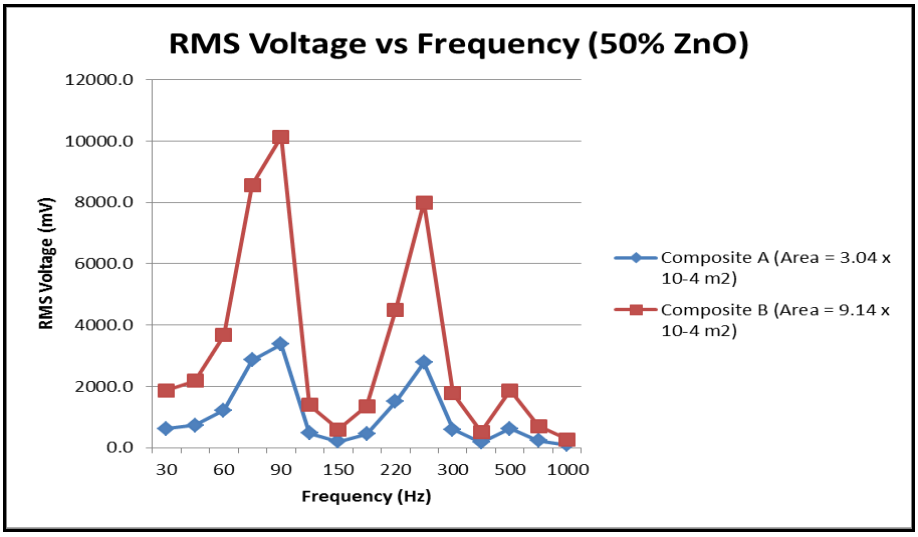

Figure 4.5 Voltage vs. frequency for different areas.

Table 4.3 shows the peak output values of the two composites A and B with different coating mixtures. The table clearly reflects the increase in the power output by increasing the area of the composite.

Table 4.3: Peak output values of composite A and composite B for different coatings.

Coating Type	**Peak Output Values Composite A**			**Peak Output Values Composite B**		
	Voltage (mV)	Current (µA)	Power (µW)	Voltage (mV)	Current (µA)	Power (µW)
1%	1937.5	9.4	18.21	5812.0	7.3	42.43
10%	1647.6	8	13.18	5154.0	6.4	32.99
30%	1308.1	6.1	7.98	4847.0	5.7	27.63
50%	3380.0	13.1	44.28	10139.0	8.7	88.21
100%	3224.4	10.8	34.82	9673.0	8.3	80.29

The following Figures 4.6, 4.7 and 4.8 show the peak current, peak voltage and peak power value comparison of these two composite structures respectively.

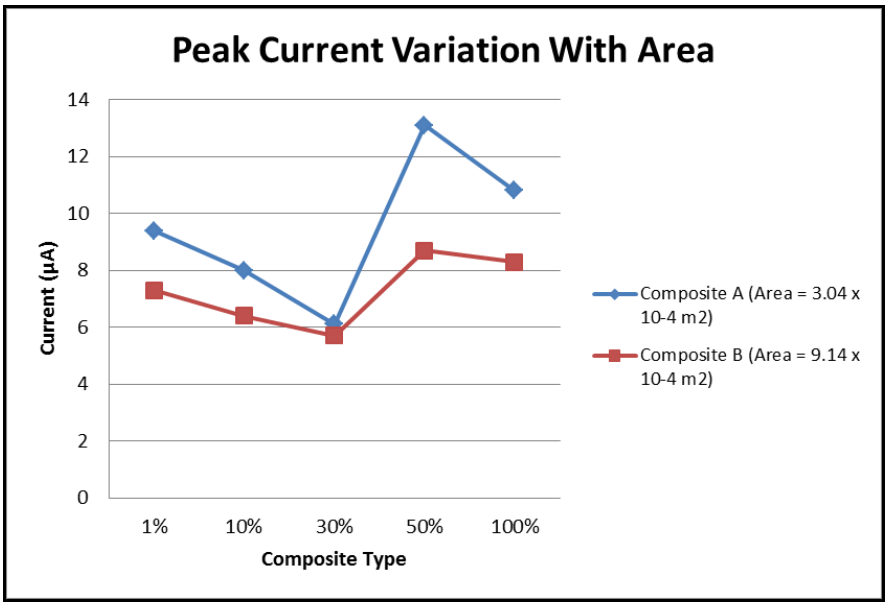

Figure 4.6 Variation of current with area.

Figure 4.6 shows the variation of peak current in micro amperes for different composites having different areas. Composite B has lower values of peak current as compared to composite A. This decrease in the value of output current is because of the losses in the connection and the increased resistance.

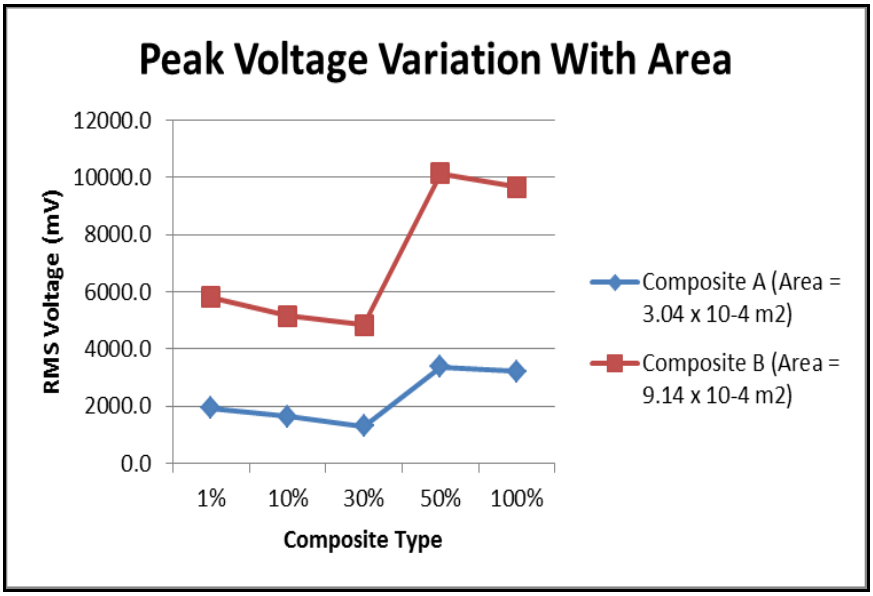

Figure 4.7 Variation of voltage with area.

Figure 4.7 shows the variation of peak voltage in millivolts for different composites having different areas. The peak voltage for composite A was 3380 mV as compared to 10,139 mV for the composite B.

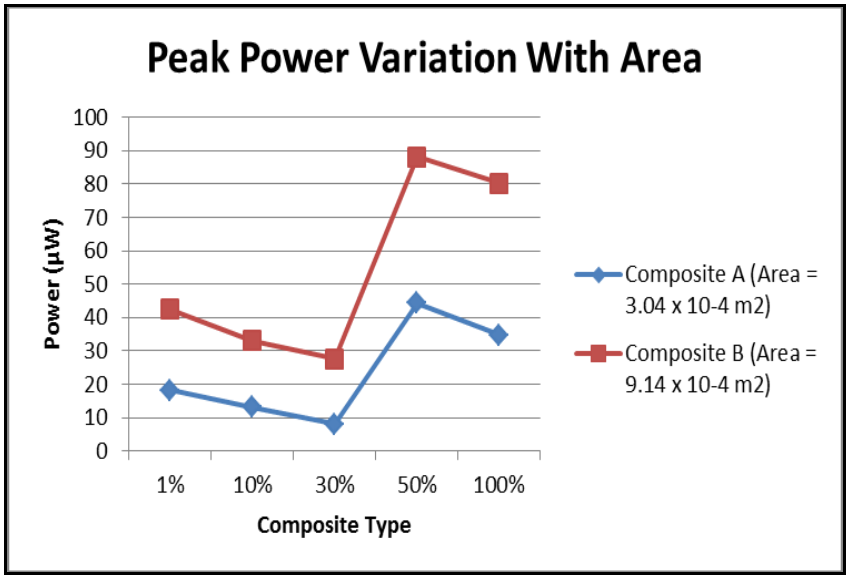

Figure 4.8 Variation of power with area.

Figure 4.8 shows the variation of peak power in microwatts for different composites having different areas. The peak power in case of composite A was 44.3 µW compared to 88.2 µW for composite B. The average increase in the power for composite B was 2.5 times as compared to composite A.

Discussion:

The four natural frequencies of the two composites were 12 Hz, 74 Hz, 202 Hz, 414 Hz and 10 Hz, 64 Hz, 192 Hz, 380 Hz respectively. The excitation frequency input range was from 30 – 1000 Hz and the peak values of voltage for both the composites A and B were at 90 Hz. In a cantilever beam the amplitude of vibration is highest at the resonant frequency. The voltage output of the composites increased from the 45 Hz to 90 Hz where it reaches its maximum value of 3380 mV and 10189 mV respectively. This increase is synonymous to the increase in

amplitude of vibration near the second natural frequency. After 90 Hz the voltage response drops to its lowest levels at 150 Hz. After that the output response increases again as the input vibrations approaches the third natural frequency of the composite and the resonant frequency as well.

The output response varies with the amplitude of vibration at a point on the beam. Therefore, the placement of PZT's on the cantilever beam should be on the points where the amplitude of vibration is the highest. The configuration made for this study had the first nanocoated PZT placed at the distance of 50 mm from the fixed end and the second 45 mm part from the first and the third was placed 45 mm apart from the second nanocoated PZT.

The area of the composite directly affects the power output of the system. The voltage output increases with a series connection and the current output increases with the parallel connection. Therefore, the kind of connection depends on its application. The area of composite can be increased by increasing the number of nanocoated PZT connected together.

For this study, the voltage and current outputs were calculated by taking an average of five readings. An average of 1 second is required to take one reading i.e. 5 seconds for 5 readings at a frequency level. Taking this into account the power output per sec can be calculated. In this study the output was not continuous as the process was stopped after each cycle to change the frequency, but when applied in the real world the input of vibration would be continuous, hence the power output would be continuous as well. Table 4.4 shows the output per second for the composites A and B.

Table 4.4 Power output in 5 seconds for the two composites.

Time (sec)	Power (µW) Composite A (Area = 3.04 x 10^{-4} m^2)	Power (µW) Composite B (Area = 9.14 x 10^{-4} m^2)
1	44.4	88.1
2	44.1	88.6
3	44.6	88.3
4	43.9	88.4
5	43.9	88.1

Figure 4.9 shows the different power readings of the two composites A and B having a 50% ZnO coating at 90 Hz frequency at which the system gives maximum output.

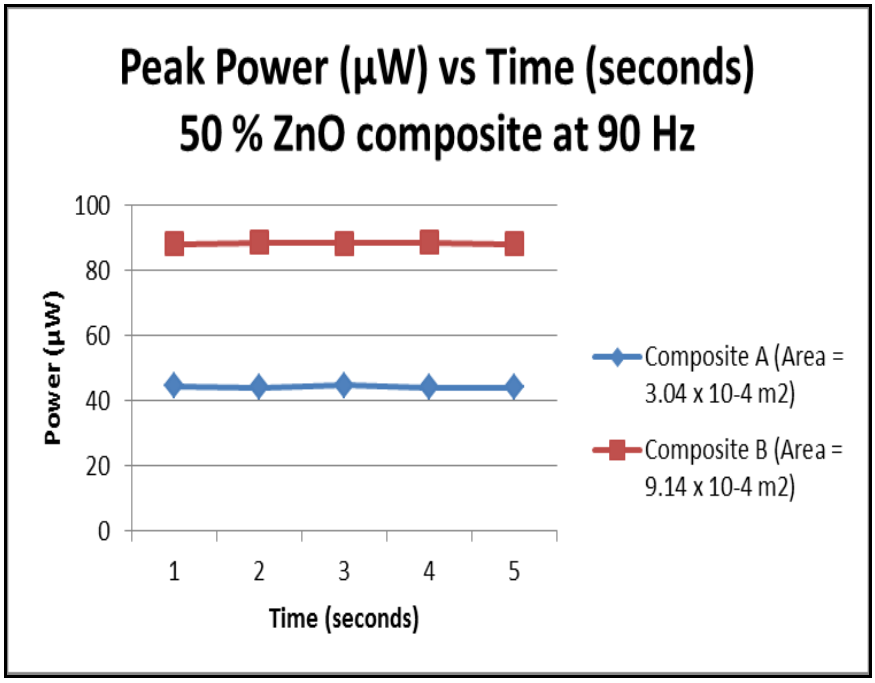

Figure 4.9 Peak power of 50% ZnO composites at 90 Hz vs time.

The total power generated by composite A during the 5 seconds was 220.9 µW as compared to 441.5 µW for composite B. Hence the average power generated per second for composite A and composite B is 44.18 µW/sec and 88.3 µW respectively.

4.3 Effect of the backup plates (Steel and Aluminum) on the Power Generation

The power output of the composite structure depends on the type of base plate used for the structure because of the various mechanical properties of the materials like the stiffness, modulus of elasticity etc. To find out the best material for the composite structure, two composite structures were compared, which were made of (a) aluminum and (b) stainless steel respectively. This section shows the variation of peak voltage, current and power outputs for these materials. Table 4.5 shows the tabulated output value comparison of the aluminum and stainless steel backup plates.

Table 4.5 Output of composites with aluminum and stainless steel backup plate.

S.No	Frequency (Hz)	Aluminum			Stainless Steel		
		Voltage (mV)	Current (μA)	Power (μW)	Voltage (mV)	Current (μA)	Power (μW)
1	30	360.62	1.6	0.58	332.3	2.4	0.80
2	45	420.73	2.8	1.18	466.7	3	1.40
3	60	565.69	3.4	1.92	749.5	4.25	3.19
4	75	760.14	4.3	3.27	1824.3	8.9	16.24
5	90	1272.79	6.5	8.27	1937.5	9.4	18.21
6	120	1647.56	7.2	11.86	325.3	2.4	0.78
7	150	1605.13	6.9	11.08	183.8	1.7	0.31
8	180	502.05	2.1	1.05	339.4	2.4	0.81
9	220	342.95	2.4	0.82	1336.4	6.8	9.09
10	250	381.84	2.7	1.03	1442.5	7.2	10.39
11	300	491.44	3.2	1.57	381.8	2.6	0.99
12	400	1187.94	6.1	7.25	155.6	1.6	0.25
13	500	332.34	2.4	0.80	473.8	3	1.42
14	750	219.20	1.9	0.42	289.9	2.2	0.64
15	1000	159.10	1.6	0.25	113.1	1.4	0.16

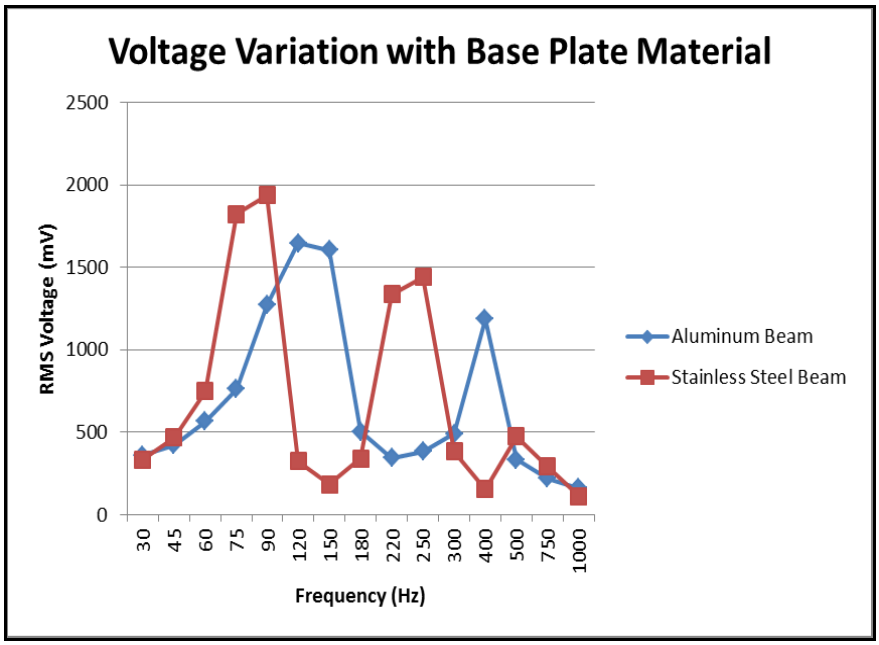

Figure 4.10 Voltage variation with base plate materials.

Figure 4.10 shows the difference in output voltage for the two different base plates. The coated PZT composite had a coating of 1% ZnO. The peak voltage for the aluminum base plate is 1647.6 mV at 120 Hz whereas for stainless steel base plate it was 1937.5 mV at 90 Hz.

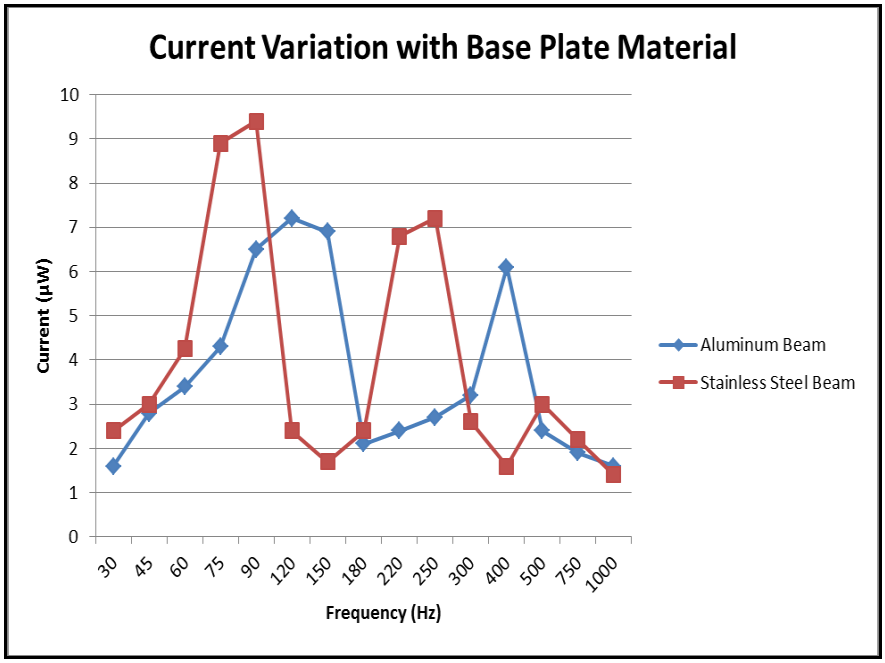

Figure 4.11 Current variation with base plate materials.

Figure 4.11 shows the current variation for the different base plates. The peak current for the aluminum base plate was 7.2 µA at 120 Hz vs 9.4 µA at 90 Hz for stainless steel base plate.

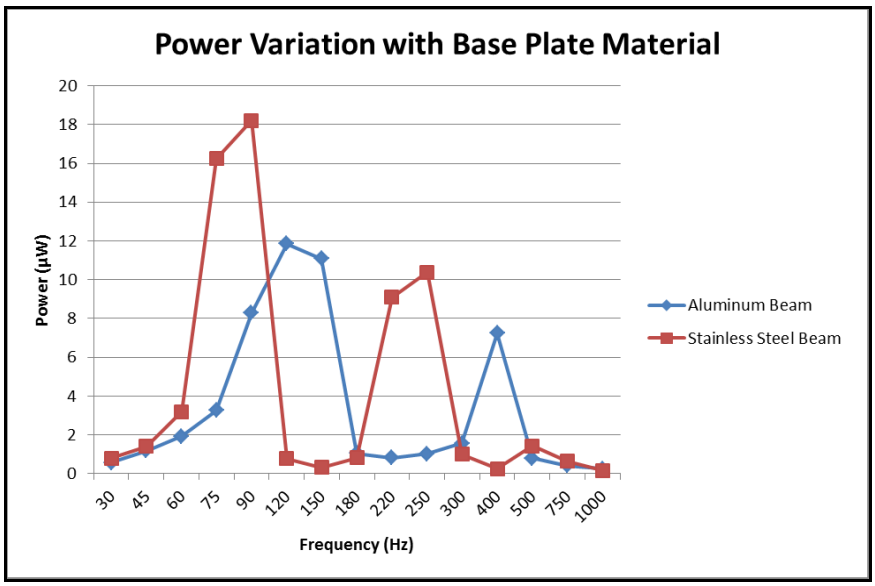

Figure 4.12 Power variation with base plate materials.

Figure 4.12 shows the power variation for these two base plates. The power was calculated using P= I x V. The peak values of power for aluminum and stainless steel plates were 11.8 µW at 120Hz and 18.2 µW at 90 Hz respectively. The above data clearly shows that the output is higher for the stainless steel beam and that is why it was decided to contibue the further experiments with stainless steel as the base for the composite structure.

Discussions:

The modulus of elasticity of Aluminum is 69 x 10^9 N/m^2 as compared to 200 x 10^9 N/m^2 for stainless steel. The stiffness (k) of the body is defined as

$k = \frac{AE}{L}$, where A - cross-sectional area, E – modulus of elasticity and L - length.

If the area and length for the beams remain constant the stiffness is direclty proportional to the moulus of elasticity i.e the material with higher elactic modulus would be having higher stifness or lower flexibility.

When a cantilever beam is vibrated the more stiffer material will have higher vibration levels as compared to lesser stiffer material as it has a tendency to flex. The levels of vibrations in a beam directly affects the strain generated in the nanocoated PZT. Figure 4.12 shows that the power output of stainless steel cantilever beam is more than the aluminum beam which is the direct consequence of the stiffness of the beams.

Also, the peak power outputs for the stainless steel and aluminum beam is coming at 90 Hz and 120 Hz respectively. This difference in the frequencies is also depenendent on the natural frequecies of the cantilever beams which is dependent on the dimensions, mass and mechanical properties of the material.

4.4 Effect of Zinc Oxide

To understand the effect of ZnO, different coating mixtures were made and the composite were tested to find out the peak values of current, voltage and power. In this segment the composites tested had no magnetic exposure.

Case 1: The sample tested in this case has the coating composition of 99.9% FNO + 0% ZnO + 0.1% Epoxy. Also there was no magnetic field exposure on this sample. The voltage and current output was measured for the frequency range 30 – 1000 Hz. Table 4.6 contains the respective voltage, current and power for coating mixture 1.

Table 4.6 Output values for coating mixture 1.

S.No	Frequency	Voltage (mV)	Current (μA)	Power (μW)
1	30	233.3	2	0.47
2	45	311.1	2.3	0.72
3	60	480.8	3.1	1.49
4	75	1923.3	9.4	18.08
5	90	1301.1	6.7	8.72
6	120	190.9	1.8	0.34
7	150	155.6	1.6	0.25
8	180	254.6	2.1	0.53
9	220	1329.4	6.8	9.04
10	250	841.5	4.6	3.87
11	300	297.0	2.3	0.68
12	400	169.7	1.7	0.29
13	500	304.1	2.3	0.70
14	750	254.6	2.1	0.53
15	1000	113.1	1.4	0.16

Figure 4.13 shows the variation of voltage with frequency. The peak voltage output comes at 75 Hz and the second peak comes at 220 Hz which is near the second and third natural frequencies of 74 Hz and 202 Hz of the cantilever beam with one PZT composite as shown in the section 4.1. The maximum RMS voltage for the nanocoated PZT composite with 0 % ZnO was 1923.3 mV.

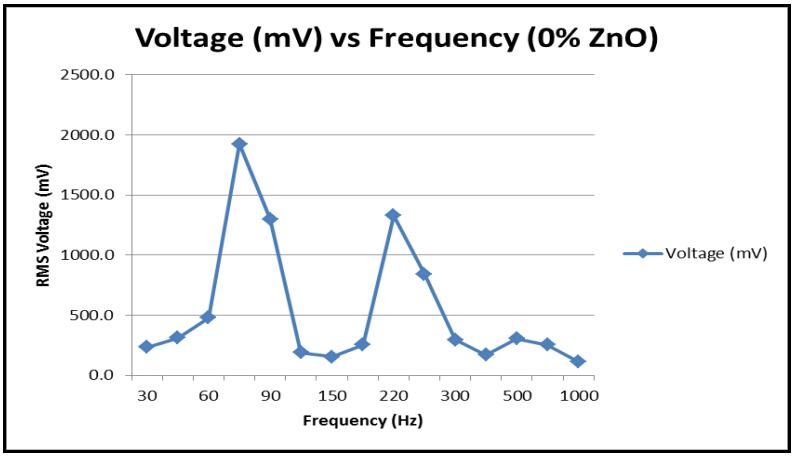

Figure 4.13 Variation of voltage with respect to frequency for composite without ZnO.

Figure 4.14 shows the current output for the composite. The maximum value of current is 9.4 µA at 75 Hz and the second highest is 6.8 µA at 220 Hz.

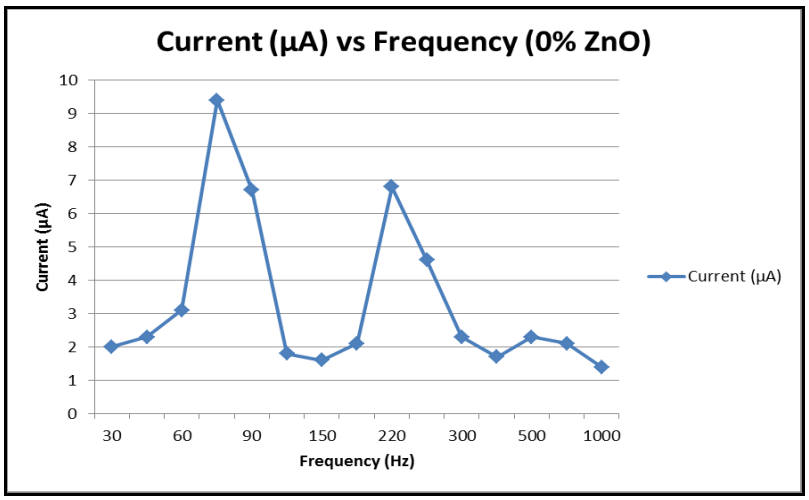

Figure 4.14 Variation of current with respect to frequency for composite without ZnO.

The power was calculated using P = I x V. As seen in Figure 4.15 the peak value of power is 18.1 µW at 75 Hz. The power output at lower frequencies is low and it increases from 30 Hz to 75Hz where it reaches it maximum output. There is a drop in output power from 75 Hz to 150 Hz where the minimum output is at 0.24 µW. The output increases again to 9.1 µW at 220 Hz and then drops again till 300 Hz after which the output stabilizes.

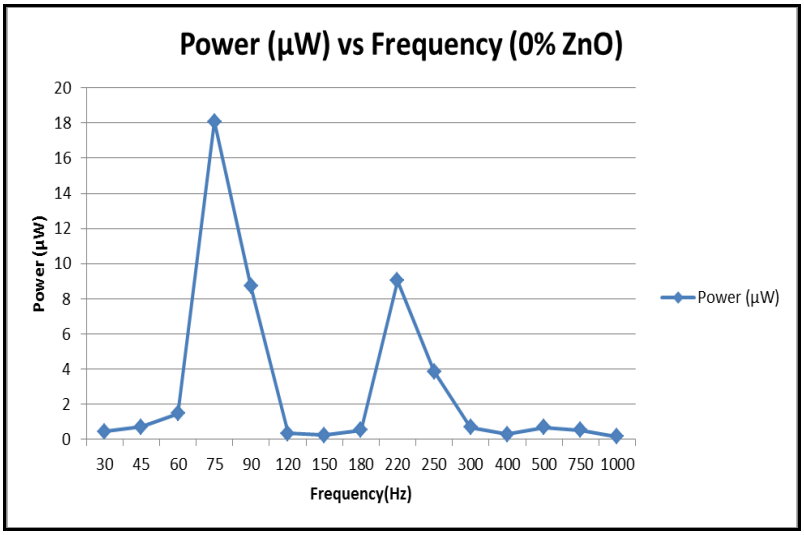

Figure 4.15 Variation of power with respect to frequency for composite without ZnO.

In the following cases only the power output is shown but they are calculated from RMS voltage and current like case 1.

Case 2: The sample tested in this case has the coating composition of 98.9% FNO + 1% ZnO + 0.1% Epoxy. Table 4.7 contains the respective voltage, current and power for coating mixture 2.

Table 4.7 Output values for coating mixture 2.

S.No	Frequency	Voltage (mV)	Current (μA)	Power (μW)
1	30	332.3	2.4	0.80
2	45	466.7	3	1.40
3	60	749.5	4.25	3.19
4	75	1824.3	8.9	16.24
5	90	1937.5	9.4	18.21
6	120	325.3	2.4	0.78
7	150	183.8	1.7	0.31
8	180	339.4	2.4	0.81
9	220	1336.4	6.8	9.09
10	250	1442.5	7.2	10.39
11	300	381.8	2.6	0.99
12	400	155.6	1.6	0.25
13	500	473.8	3	1.42
14	750	289.9	2.2	0.64
15	1000	113.1	1.4	0.16

As seen in Figure 4.16 the peak value of power is 18.2 μW at 90 Hz which is 0.1 μW more than the maximum output in case 1. The outputs at 75 Hz and 90 Hz are about the same and there is flatness in the curve at these points. Also, a similar flatness occurs at 220 Hz to 250 Hz which was not seen in the first case.

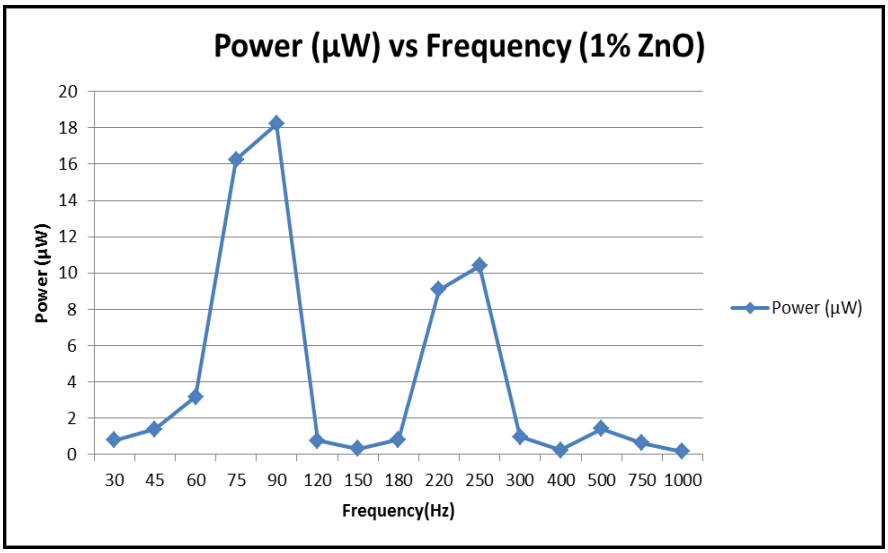

Figure 4.16 Variation of power with respect to frequency for composite with 1% ZnO.

Case 3: The composite mixture had the composition of 89.9% FNO + 10% ZnO +0.1% Epoxy. Table 4.8 contains the respective voltage, current and power for coating mixture 3.

Table 4.8 Output values for coating mixture 3.

S.No	Frequency	Voltage (mV)	Current (µA)	Power (µW)
1	30	339.4	2.4	0.81
2	45	445.5	2.8	1.25
3	60	763.7	4.2	3.21
4	75	1647.6	7.9	13.02
5	90	1647.6	8	13.18
6	120	346.5	2.5	0.87
7	150	169.7	1.7	0.29
8	180	332.3	2.4	0.80
9	220	1265.7	6.3	7.97
10	250	1166.7	5.9	6.88
11	300	431.3	2.8	1.21
12	400	190.9	1.8	0.34
13	500	388.9	2.6	1.01
14	750	240.4	2	0.48
15	1000	120.2	1.5	0.18

The maximum power output is 13.2 µW at 90 Hz and similar to case 2 which had flat curve at 75 Hz – 90 Hz and 220 Hz-250 Hz. There is a decrease in the maximum power from 18.2 µW to 13.2 µW.

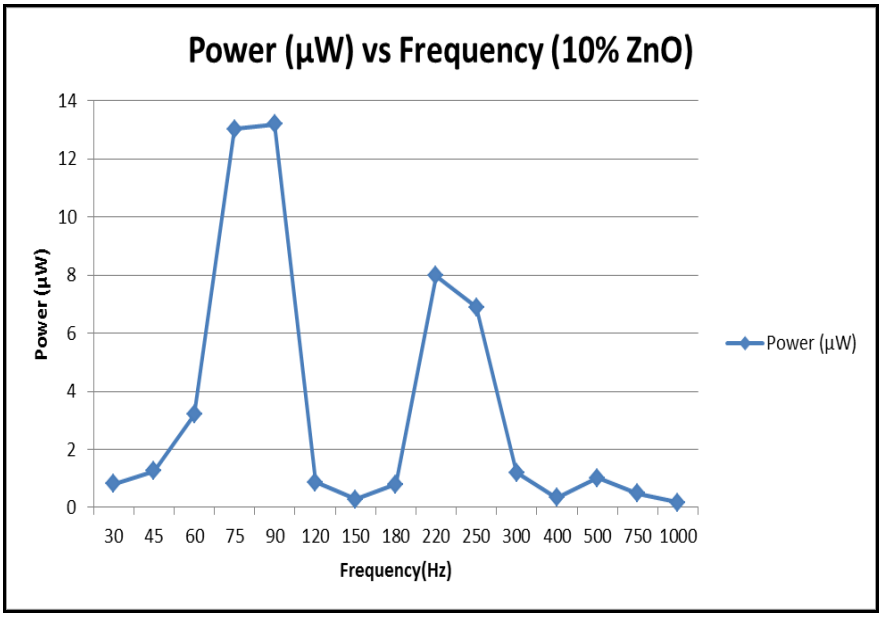

Figure 4.17 Variation of power with respect to frequency for composite with 10% ZnO.

Case 4: The composite had 79.9 % FNO + 20% ZnO + 0.1% Epoxy coating compostion. Table 4.9 contains the respective voltage, current and power for coating mixture 4.

Table 4.9 Output values for coating mixture 4.

S.No	Frequency	Voltage (mV)	Current (µA)	Power (µW)
1	30	438.4	2.8	1.23
2	45	544.5	3.2	1.74
3	60	830.9	3.4	2.82
4	75	2036.5	9.2	18.74
5	90	2149.6	9.6	20.64
6	120	297.0	2.2	0.65
7	150	190.9	1.8	0.34
8	180	346.5	2.4	0.83
9	220	1421.3	6.7	9.52
10	250	1520.3	7.1	10.79
11	300	410.1	2.6	1.07
12	400	162.6	1.6	0.26
13	500	381.8	2.5	0.95
14	750	240.4	1.9	0.46
15	1000	106.1	1.4	0.15

The maximum output increased from 13.2 µW to 20.6 µW at 90 Hz which is an increase of 57% for an increase of 10% ZnO. Also the outputs at 250 Hz increased from 7.9 µW in case 3 to 10.8 µW which translate in an increase in output by 36.7%.

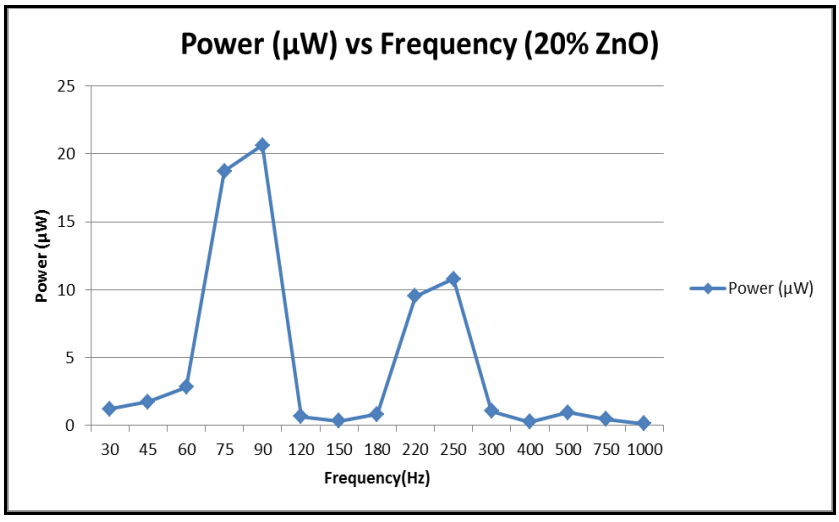

Figure 4.18 Variation of power with respect to frequency for composite with 20% ZnO.

Case 5: The composite had 69.9 % FNO + 30 % ZnO + 0.1% Epoxy coating compostion. The maximum output decreased from 20.6 µW to 8 µW at 90 Hz. The flow of the curve remained the same with the peak output coming at 90 Hz. Table 4.10 contains the respective voltage, current and power for coating mixture 5.

Table 4.10 Output values for coating mixture 5.

S.No	Frequency	Voltage (mV)	Current (µA)	Power (µW)
1	30	215.7	1.8	0.39
2	45	307.6	2.2	0.68
3	60	519.7	3	1.56
4	75	1308.1	6	7.85
5	90	1308.1	6.1	7.98
6	120	198.0	1.7	0.34
7	150	183.8	1.7	0.31
8	180	297.0	2.2	0.65
9	220	1138.4	5.4	6.15
10	250	1124.3	5.3	5.96
11	300	346.5	2.3	0.80
12	400	162.6	1.6	0.26
13	500	332.3	2.2	0.73
14	750	198.0	1.7	0.34
15	1000	99.0	1.3	0.13

Figure 4.19 shows the variation of power output with frequency.

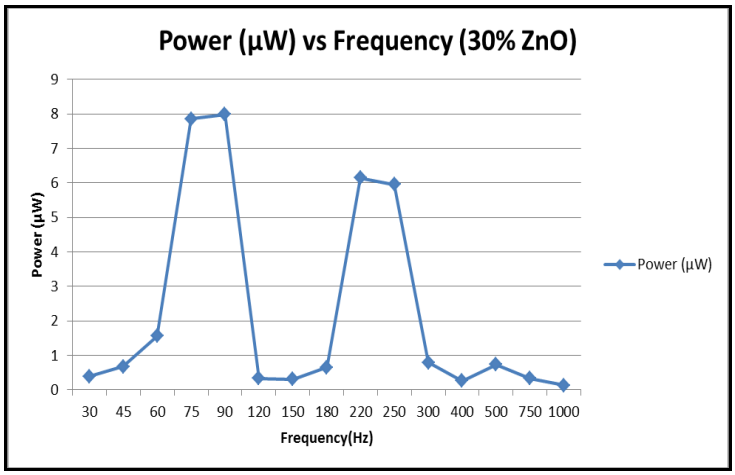

Figure 4.19 Variation of power with respect to frequency for composite with 30% ZnO.

Case 6: The composite had 59.9% FNO + 40% ZnO + 0.1% Epoxy coating compostion. Table 4.11 contains the respective voltage, current and power for coating mixture 6.

Table 4.11 Output values for coating mixture 6.

S.No	Frequency	Voltage (mV)	Current (µA)	Power (µW)
1	30	579.8	3.2	1.86
2	45	735.4	3.7	2.72
3	60	1159.7	5.3	6.15
4	75	2701.1	11.1	29.98
5	90	3323.4	13.4	44.53
6	120	424.3	2.5	1.06
7	150	198.0	1.7	0.34
8	180	480.8	2.8	1.35
9	220	1583.9	6.9	10.93
10	250	2573.9	10.6	27.28
11	300	537.4	3	1.61
12	400	162.6	1.6	0.26
13	500	834.4	4.1	3.42
14	750	254.6	1.9	0.48
15	1000	127.3	1.5	0.19

The maximum output incresed from 8 µW to 44.5 µW at 90 Hz which is an increase of more than 450%. This is the best coating composition for the composite as the power output is the maximum for this case as seen from Figure 4.25. Considering the volume of the composite is 0.062 cm^3 the maximum power will be 0.717 mW/cm^3.

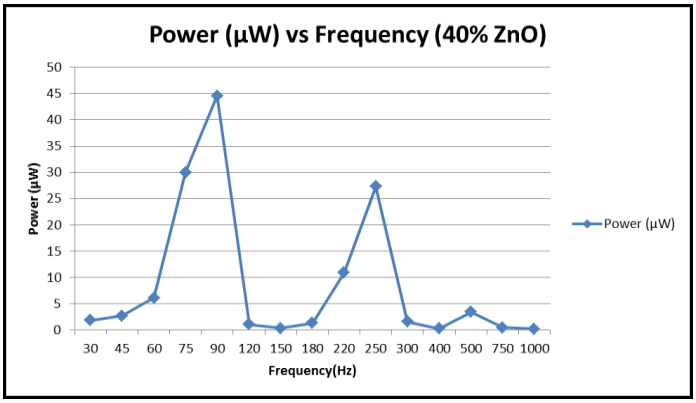

Figure 4.20 Variation of power with respect to frequency for composite with 40% ZnO.

Case 7: The composite had 49.9%FNO + 50% ZnO + 0.1% Epoxy coating compostion. Table 4.12 contains the respective voltage, current and power for coating mixture 7.

Table 4.12 Output values for coating mixture 7.

S.No	Frequency	Voltage (mV)	Current (µA)	Power (µW)
1	30	622.3	3.3	2.05
2	45	728.3	3.6	2.62
3	60	1223.3	5.4	6.61
4	75	2856.7	11.3	32.28
5	90	3380.0	13.1	44.28
6	120	466.7	2.7	1.26
7	150	198.0	1.7	0.34
8	180	452.5	2.6	1.18
9	220	1499.1	6.3	9.44
10	250	2771.9	10.9	30.21
11	300	594.0	3.1	1.84
12	400	169.7	1.6	0.27
13	500	622.3	3.2	1.99
14	750	233.3	1.8	0.42
15	1000	91.9	1.3	0.12

The maximum output dropped from 44.5 µW to 44.2 µW at 90 Hz. This is the best second coating composition for the composite as seen from Figure 4.25.

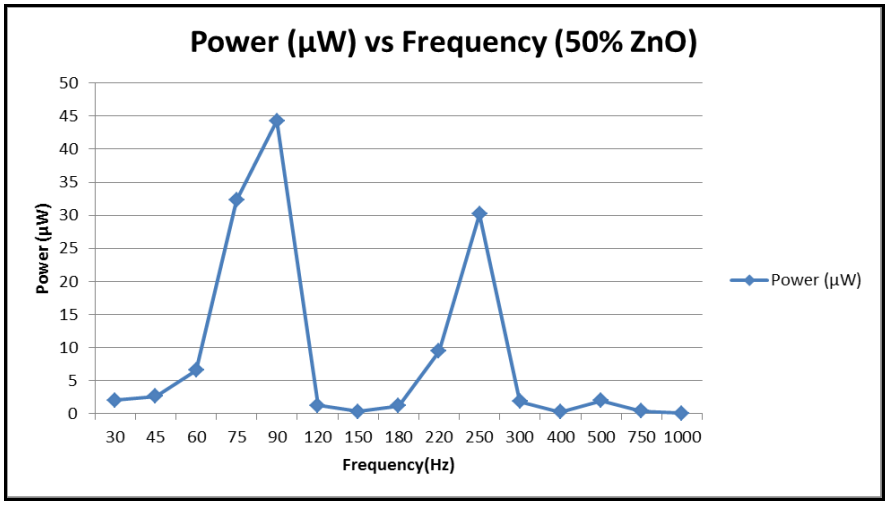

Figure 4.21: Variation of power with respect to frequency for composite with 50% ZnO

Case 8: The composite had 39.9% FNO + 60% ZnO + 0.1% Epoxy coating compostion. Table 4.13 contains the respective voltage, current and power for coating mixture 8.

Table 4.13: Output values for coating mixture 8.

S.No	Frequency	Voltage (mV)	Current (µA)	Power (µW)
1	30	625.8	3.2	2.00
2	45	749.5	3.6	2.70
3	60	1223.3	5.2	6.36
4	75	2778.9	10.6	29.46
5	90	3326.9	12.6	41.92
6	120	470.2	1.7	0.80
7	150	194.5	1.6	0.31
8	180	449.0	2.6	1.17
9	220	1481.4	6.4	9.48
10	250	2580.9	9.9	25.55
11	300	565.7	2.9	1.64
12	400	194.5	1.7	0.33
13	500	608.1	3.1	1.89
14	750	244.0	1.8	0.44
15	1000	91.9	1.3	0.12

The maximum output 41.9 µW at 90 Hz as shown in the Figure 4.22

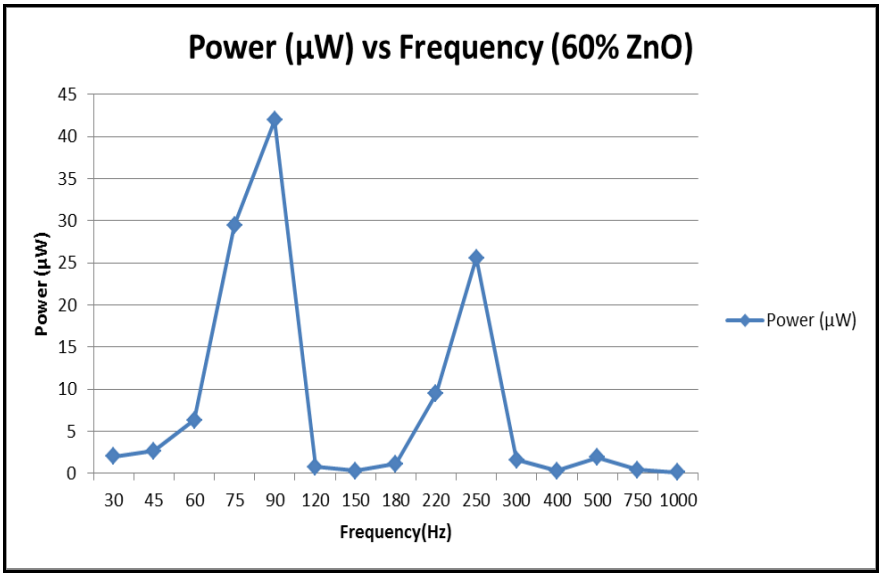

Figure 4.22 Variation of power with respect to frequency for composite with 60% ZnO.

Case 9: The composite had 19.9% FNO + 80% ZnO + 0.1% Epoxy coating compostion. Table 4.14 contains the respective voltage, current and power for coating mixture 9.

Table 4.14: Output values for coating mixture 9.

S.No	Frequency	Voltage (mV)	Current (µA)	Power (µW)
1	30	612.4	2.9	1.78
2	45	722.7	3.3	2.38
3	60	1190.8	4.8	5.72
4	75	2763.4	9.9	27.36
5	90	3255.5	11.6	37.76
6	120	458.2	2.5	1.15
7	150	189.5	1.6	0.30
8	180	441.2	2.4	1.06
9	220	1475.0	5.8	8.56
10	250	2597.9	9.4	24.42
11	300	567.1	2.8	1.59
12	400	168.3	1.5	0.25
13	500	601.0	2.9	1.74
14	750	229.1	1.7	0.39
15	1000	91.9	1.3	0.12

The maximum output 37.7 µW at 90 Hz as shown in the Figure 4.23

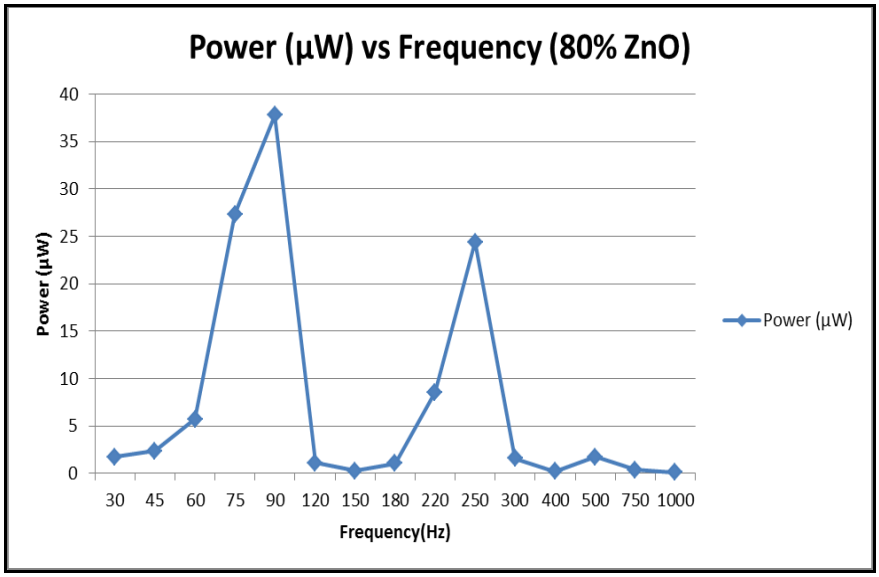

Figure 4.23 Variation of power with respect to frequency for composite with 80% ZnO.

Case 10: The composite had 0%FNO + 99.9% ZnO + 0.1% Epoxy coating compostion. Table 4.15 contains the respective voltage, current and power for coating mixture 10.

Table 4.15 Output values for coating mixture 10.

S.No	Frequency	Voltage (mV)	Current (µA)	Power (µW)
1	30	636.4	2.9	1.85
2	45	792.0	3.4	2.69
3	60	1223.3	4.7	5.75
4	75	2630.4	9	23.67
5	90	3224.4	10.8	34.82
6	120	480.8	2.4	1.15
7	150	183.8	1.5	0.28
8	180	438.4	2.3	1.01
9	220	1442.5	5.4	7.79
10	250	2192.0	7.7	16.88
11	300	523.3	2.5	1.31
12	400	240.4	1.7	0.41
13	500	565.7	2.7	1.53
14	750	268.7	1.8	0.48
15	1000	99.0	1.3	0.13

The maximum output 34.8 µW at 90 Hz as shown in the Figure 4.24

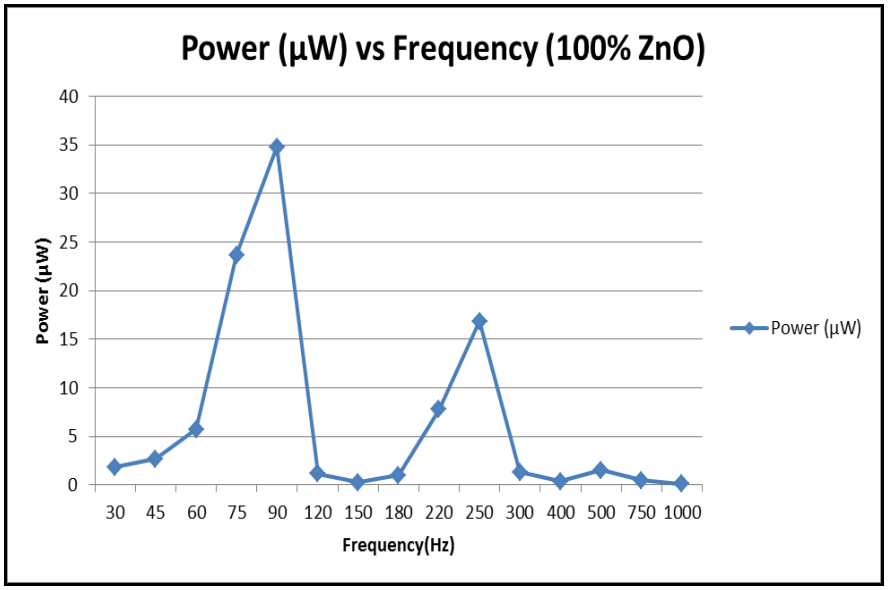

Figure 4.24 Variation of power with respect to frequency for composite with 100% ZnO.

Table 4.16 shows the peak power output of the all the coating mixtures.

Table 4.16 Peak power output for different coatings.

Coating Type	Peak Power (µW)
0%	18.08
1%	18.21
10%	13.18
20%	20.64
30%	7.98
40%	44.53
50%	44.28
60%	41.92
80%	37.76
100%	34.82

Figure 4.25 shows the maximum output of power for different composites. The power output varied with the percentage of ZnO nanoparticles in the coating mixture. The power increased first with the percentage of ZnO and then decreased. The maximum output was for a coating having 40% ZnO. It was observed that the output maxed out at 40% and then stabilized and didn't increase as the percentage of ZnO was increased. This shows that the saturation point of improvement in output occurs at 40%.

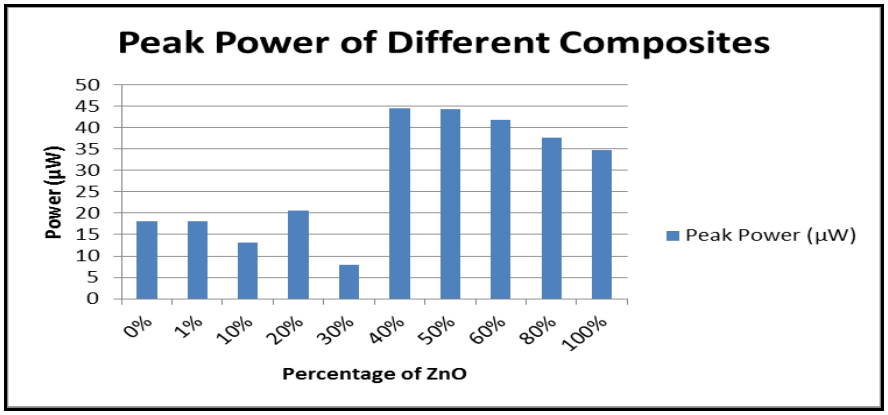

Figure 4.25 Peak power comparison of different composite.

Table 4.17 shows the peak power density in tabular form and Figure 4.26 shows the peak power density for different composites in graphical form and as seen in the previous results the max power density is for 40% ZnO at 0.72 mW/cm^3

Table 4.17 Peak power density for different coatings.

Coating Type	Peak Power Density (mW/cm^3)
0%	0.29
1%	0.29
10%	0.21
20%	0.33
30%	0.13
40%	0.72
50%	0.71
60%	0.68
80%	0.61
100%	0.56

It reaches the maximum limit for 40% and then it stabilizes as the ZnO percentage is increased. The sudden increase in the output is similar to the Zener Effect seen in semiconductors.

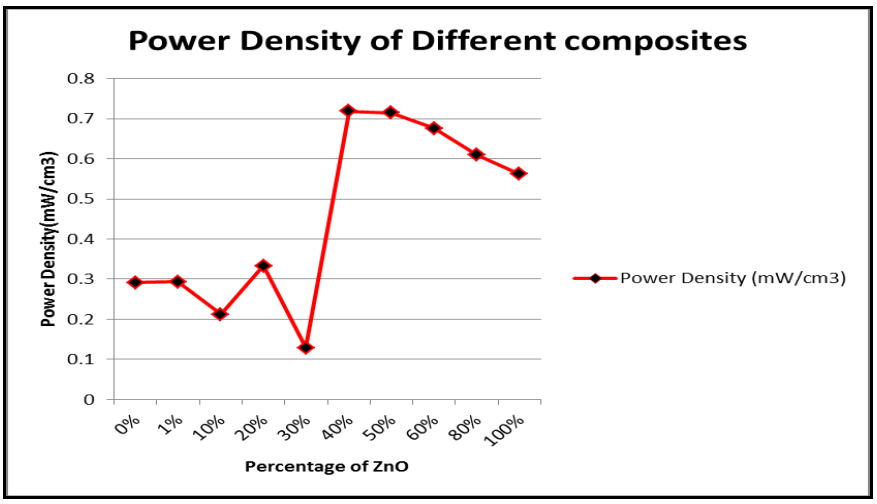

Figure 4.26 Peak power density comparison of different composite.

Discussions:

The power output for the different nanocoatings varied on the basis of the percentage of ZnO in them. Also capacitance of the semiconductor is effectively increased by the nanocoating.

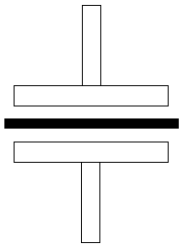

Figure 4.27 Dielectric material between parallel plates

The capacitance between plates for Figure 4.27 is defined as

$$C = \frac{\varepsilon_r \varepsilon_0 A}{d}$$

where, C = Capacitance in Farad

ε_r = dielectric constant of the insulating medium (for air, $\varepsilon_r = 1$)

ε_o = permittivity of air or free space (in vacuum); known as 8.885×10^{-12} F/m

A = overlapping area in plates, m^2

d = distance between electrodes or plates, m

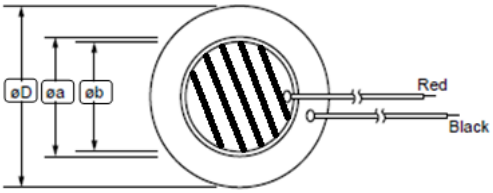

Figure 4.28 Nanocoated PZT.

The nanocoated PZT substrate has an uneven surface with defects like cones, cracks and difference in thickness which changed the surface area and consequently affected both the capacitance of the coated substrate and the dielectric constant as shown in Figure 4.29. Also,

presence of air entrapped pores is not ruled apart from filling of some pores on silver and piezo substrate. All these combination will change and increases the capacitance of the system as per variation shown in the above equation. .

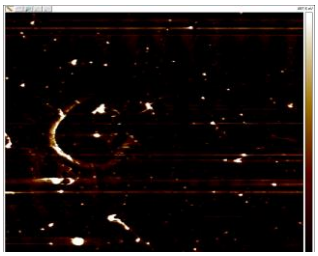

Figure 4.29 Atomic force microscope diagraph of nanocoated PZT.

The presence of ZnO nanoparticles increases the output of the composite as shown in the Figure 4.25 which compares the peak values of different coating mixtures. The output of the PZT remains fairly unchanged until the ZnO percentage reaches a critical point at 40 % level where the rise of the output is sudden and very high. The variation of the output of the composites from 0% ZnO coating to 100% ZnO coating can be attributed to the magnetization of ZnO. This variation can be possibly explained by the magnetic orientation of the ZnO nanoparticles. All the composites when made were exposed to magnetic field of 500 gauss and the lower output till 30% ZnO mixture maybe because the nanoparticles might not be getting magnetized or else if they are getting magnetized then the interaction between the particles is low. For the coating mixtures having more than 30% ZnO the magnetization would be resulting in inter particle interaction resulting in better output of the composite.

4.5 Effect of Magnetic Field

The effect of ZnO was analyzed the second composite was made with the magnetic strip which was then tested to find the effect of magnetic field on the performance of the composite. As seen from the previous works done in the field of PZT energy harvesting, the magnetic field has a major impact on the performance of the PZT. Some of the composites have shown power

output improvements in the range of 400-500 %. This experiment showed that the ME effect improves the output by a factor of 1.3-1.5. All the composites tested have coating compositions as shown in Table 3.1. The magnetic field at which the experiments were conducted was 160 gauss. All the other operating conditions remained the same as pervious experiment.

Case 1: The sample tested in this case has the coating composition of 99.9% FNO + 0% ZnO + 0.1% Epoxy. Also there was magnetic field exposure of 160 gauss on this sample. Table 4.18 contains the respective voltage, current and power for coating mixture 1.

Table 4.18 Output values for coating mixture 1 with magnetic field of 160 gauss.

S.No	Frequency	Voltage (mV)	Current (μA)	Power (μW)
1	30	265.2	2.2	0.58
2	45	353.6	2.6	0.92
3	60	601.0	3.7	2.22
4	75	2121.3	10.3	21.85
5	90	1387.7	7.1	9.85
6	120	221.0	2	0.44
7	150	176.8	1.8	0.32
8	180	327.0	2.4	0.78
9	220	1661.7	8.3	13.79
10	250	963.4	5.2	5.01
11	300	282.8	2.2	0.62
12	400	167.9	1.7	0.29
13	500	344.7	2.5	0.86
14	750	221.0	1.9	0.42
15	1000	141.4	1.6	0.23

As seen in Figure 4.30 the peak value of power is 21.9 μW at 75 Hz. This means the increase in output due to the magnetic field is around 20% when compared to the structure without the magnetic strip. Similar to the cases above the power output at lower frequencies is low and it increases from 30 Hz to 75 Hz where it reaches it maximum output. There is a drop in

output power from 75 Hz to 150 Hz where the minimum output is at 0.32 µW which is also higher by 0.4 µW compared to the composite without the magnetic field.

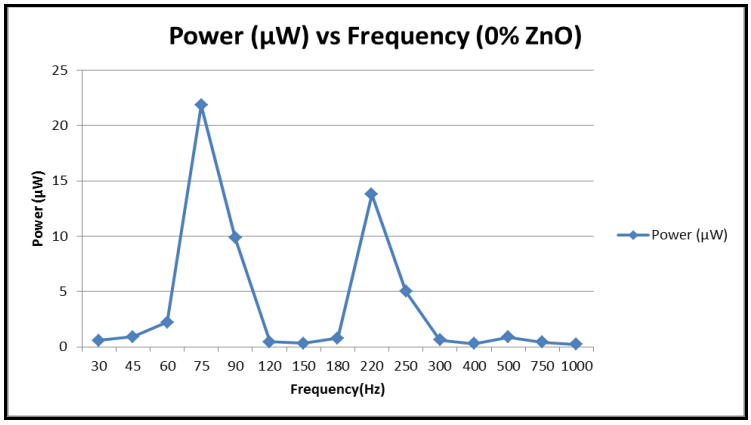

Figure 4.30 Variation of power with respect to frequency at 160 gauss for 0%ZnO.

Case 2: The sample tested in this case has the coating composition of 98.9% FNO + 1% ZnO + 0.1% Epoxy. Table 4.19 contains the respective voltage, current and power for coating mixture 2.

Table 4.19 Output values for coating mixture 2 with magnetic field of 160 gauss.

S.No	Frequency	Voltage (mV)	Current (µA)	Power (µW)
1	30	415.4	2.8	1.16
2	45	583.4	3.5	2.04
3	60	936.9	5.1	4.78
4	75	2280.4	11	25.08
5	90	2421.8	11.6	28.09
6	120	406.6	2.8	1.14
7	150	229.8	2	0.46
8	180	424.3	2.8	1.19
9	220	1670.5	8.3	13.87
10	250	1803.1	8.9	16.05
11	300	477.3	3.1	1.48
12	400	194.5	1.9	0.37
13	500	592.2	3.6	2.13
14	750	362.4	2.6	0.94
15	1000	141.4	1.6	0.23

As seen in Figure 4.31 the peak value of power is 28.1 μW at 90 Hz which is 50 % higher compared to 18.2 μW output for the same coating mixture composite without the magnetic field.

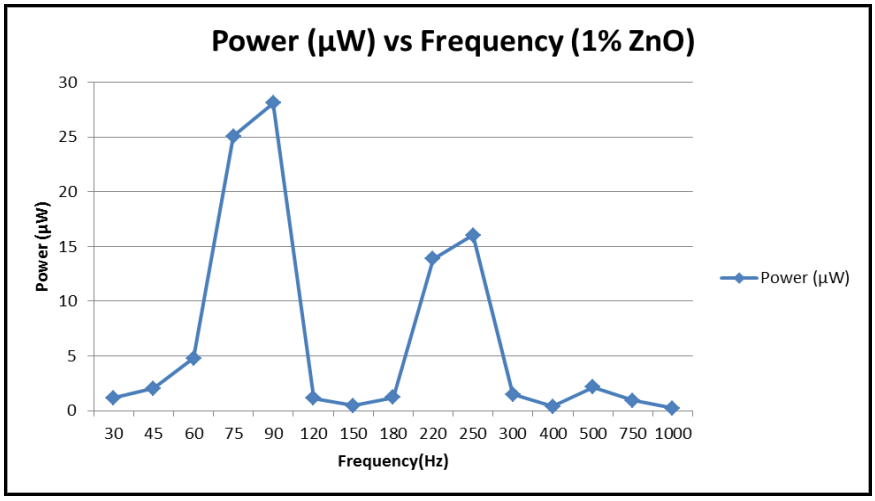

Figure 4.31 Variation of power with respect to frequency at 160 gauss for 1%ZnO .

Case 3: The composite mixture had the composition of 89.9% FNO + 10% ZnO +0.1% Epoxy. Table 4.20 contains the respective voltage, current and power for coating mixture 3.

Table 4.20 Output values for coating mixture 3 with magnetic field of 160 gauss.

S.No	Frequency	Voltage (mV)	Current (μA)	Power (μW)
1	30	424.3	2.50	1.06
2	45	556.8	3.00	1.67
3	60	954.6	4.50	4.30
4	75	2059.4	8.50	17.51
5	90	2059.4	8.60	17.71
6	120	433.1	2.50	1.08
7	150	212.1	1.80	0.38
8	180	415.4	2.50	1.04
9	220	1582.2	6.80	10.76
10	250	1458.4	6.40	9.33
11	300	539.2	2.00	1.08
12	400	238.6	1.90	0.45
13	500	486.1	2.80	1.36
14	750	300.5	2.10	0.63
15	1000	150.3	1.60	0.24

The maximum power output is 17.7 μW at 90 Hz which is 4.5 μW higher than the composite without magnetic field. The curve is similar to the above case it had flat curve at 75 Hz – 90 Hz and 220 Hz-250 Hz..

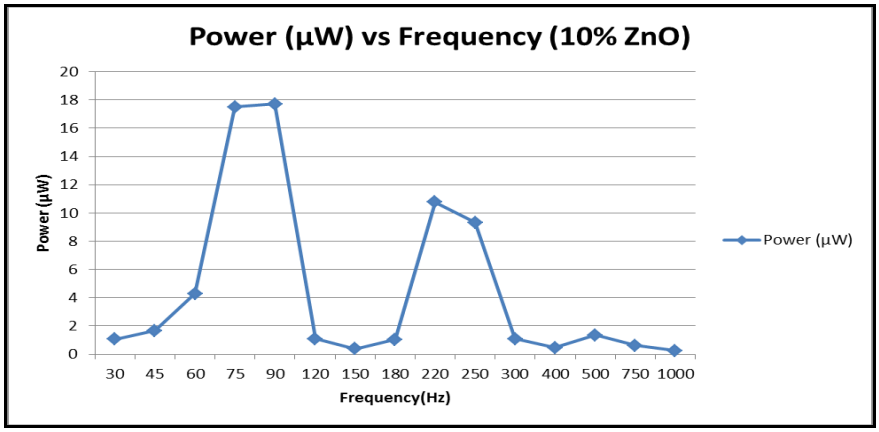

Figure 4.32 Variation of power with respect to frequency at 160 gauss for 10%ZnO.

Case 4: The composite had 79.9% FNO + 20% ZnO + 0.1% Epoxy coating compostion. Table 4.21 contains the respective voltage, current and power for coating mixture 4.

Table 4.21 Output values for coating mixture 4 with magnetic field of 160 gauss.

S.No	Frequency	Voltage (mV)	Current (μA)	Power (μW)
1	30	548.0	3.2	1.75
2	45	680.6	3.7	2.52
3	60	1038.6	5.2	5.40
4	75	2545.6	11.3	28.77
5	90	2687.0	11.8	31.71
6	120	371.2	2.5	0.93
7	150	238.6	1.9	0.45
8	180	433.1	2.7	1.17
9	220	1776.6	8.2	14.57
10	250	1900.3	8.7	16.53
11	300	512.7	3.1	1.59
12	400	203.3	1.8	0.37
13	500	477.3	2.9	1.38
14	750	300.5	2.2	0.66
15	1000	132.6	1.5	0.20

The maximum output was 31.7 μW at 90 Hz which is an increase of 54% as compared to the non-magnetic composite as shown in Figure 4.33.

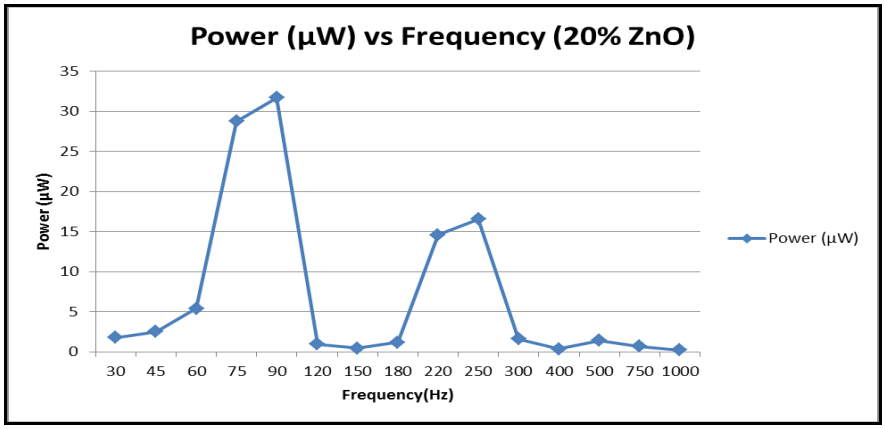

Figure 4.33 Variation of power with respect to frequency at 160 gauss for 20%ZnO.

Case 5: The composite had 69.9% FNO + 30% ZnO + 0.1% Epoxy coating compostion. Table 4.20 contains the matrix containing the respective voltage, current and power for coating mixture 5

Table 4.22 Output values for coating mixture 5 with magnetic field of 160 gauss.

S.No	Frequency	Voltage (mV)	Current (μA)	Power (μW)
1	30	269.6	2	0.54
2	45	384.5	2.5	0.96
3	60	649.7	3.5	2.27
4	75	1635.2	7.3	11.94
5	90	1635.2	7.5	12.26
6	120	247.5	1.9	0.47
7	150	229.8	1.8	0.41
8	180	371.2	2.4	0.89
9	220	1423.1	5.5	7.83
10	250	1405.4	5.4	7.59
11	300	433.1	2.7	1.17
12	400	203.3	1.8	0.37
13	500	415.4	2.6	1.08
14	750	247.5	1.9	0.47
15	1000	123.7	1.5	0.19

The maximum is 12.3 µW 90 Hz. The flow of the curve remained the same with the peak output coming at 90 Hz. Figure 4.34 shows the variation of power output with frequency.

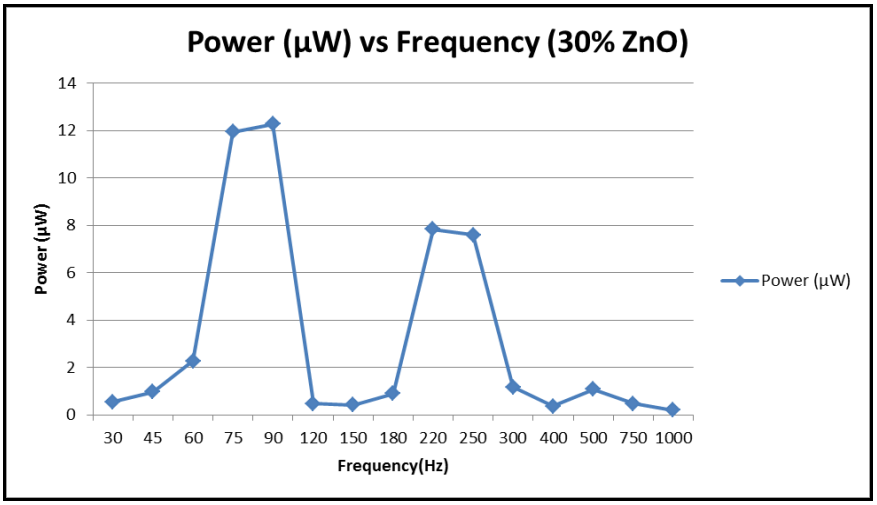

Figure 4.34 Variation of power with respect to frequency at 160 gauss for 30%ZnO.

Case 6: The composite had 59.9% FNO + 40% ZnO + 0.1% Epoxy coating compostion. Table 4.23 contains the respective voltage, current and power for coating mixture 6.

Table 4.23 Output values for coating mixture 6 with magnetic field of 160 gauss.

S.No	Frequency	Voltage (mV)	Current (µA)	Power (µW)
1	30	724.8	3.8	2.75
2	45	919.2	4.4	4.04
3	60	1449.6	6.4	9.28
4	75	3376.4	13.6	45.92
5	90	4154.3	16.5	68.55
6	120	530.3	2.9	1.54
7	150	247.5	2	0.49
8	180	601.0	3.2	1.92
9	220	1979.9	8.4	16.63
10	250	3217.3	12	38.61
11	300	671.8	3.5	2.35
12	400	203.3	1.8	0.37
13	500	1043.0	4.9	5.11
14	750	318.2	2.2	0.70
15	1000	159.1	1.6	0.25

The maximum output incresed to 68.5 μW from 44.5 μW at 90 Hz which is an increase 54% for the magnetic composite. As seen in the above experiment this remained the best coating composition for the composite as the power output is the maximum for this case as seen from Figure 4.35. Also, the maximum power density increased from 0.717 mW/cm^3 to 1.11 mW/cm^3.

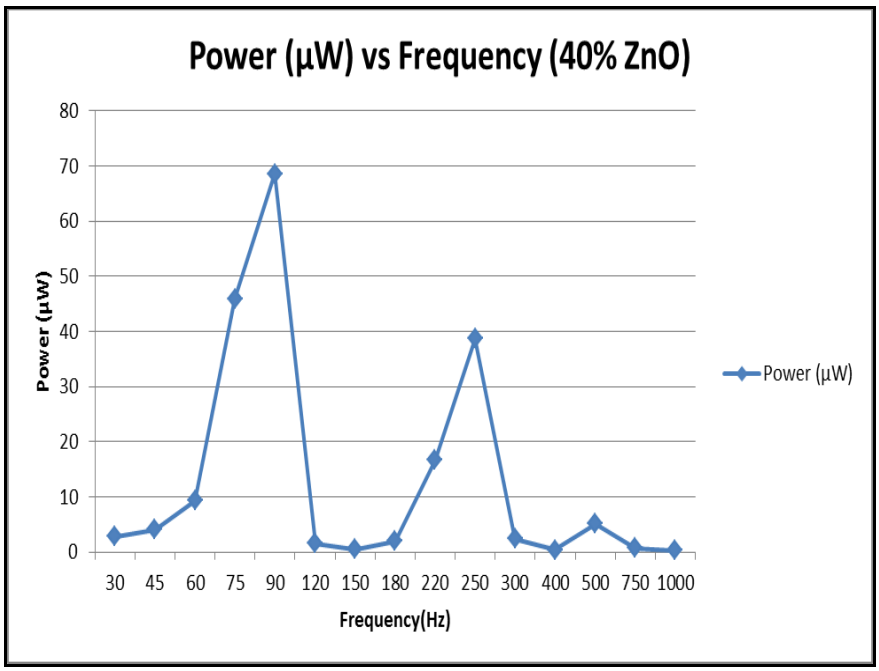

Figure 4.35 Variation of power with respect to frequency at 160 gauss for 40%ZnO.

Case 7: The composite had 49.9% FNO + 50% ZnO + 0.1% Epoxy coating compostion. Table 4.24 contains the respective voltage, current and power for coating mixture 7.

Table 4.24 Output values for coating mixture 7 with magnetic field of 160 gauss.

S.No	Frequency	Voltage (mV)	Current (µA)	Power (µW)
1	30	777.8	3.8	2.96
2	45	910.4	4.3	3.91
3	60	1529.1	6.5	9.94
4	75	3570.9	13.9	49.64
5	90	4225.0	16.2	68.44
6	120	583.4	3.1	1.81
7	150	247.5	1.9	0.47
8	180	565.7	3	1.70
9	220	1873.8	7.7	14.43
10	250	3464.8	13.6	47.12
11	300	742.5	3.6	2.67
12	400	212.1	1.7	0.36
13	500	777.8	3.8	2.96
14	750	291.7	2	0.58
15	1000	114.9	1.4	0.16

The maximum output is 68.4 µW at 90 Hz as shown in Figure 4.36.

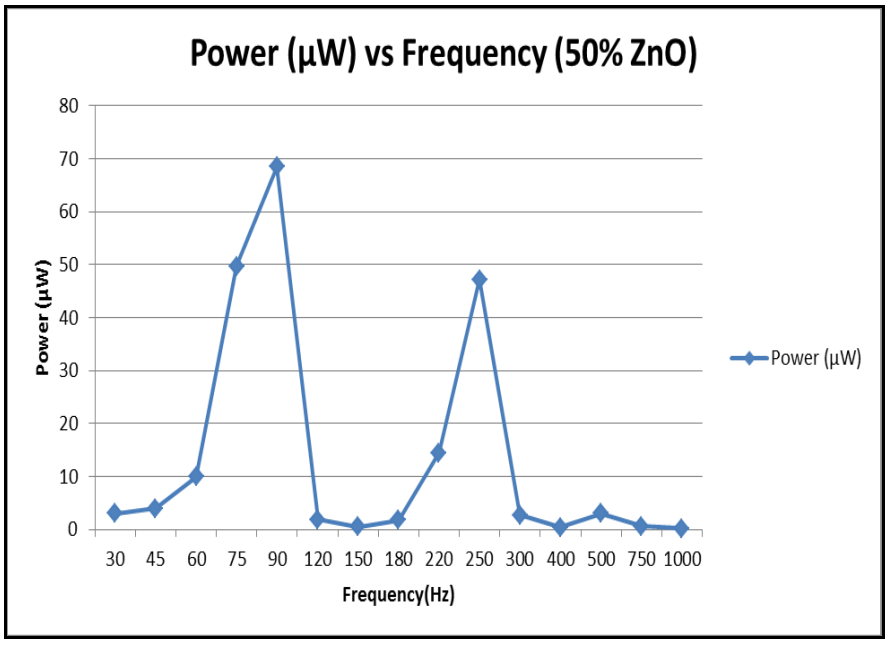

Figure 4.36 Variation of power with respect to frequency at 160 gauss for 50%ZnO .

Case 8: The composite had 39.9% FNO + 60% ZnO + 0.1% Epoxy coating compostion. Table 4.25 contains the respective voltage, current and power for coating mixture 8.

Table 4.25 Output values for coating mixture 8 with magnetic field of 160 gauss.

S.No	Frequency	Voltage (mV)	Current (µA)	Power (µW)
1	30	782.2	3.7	2.89
2	45	936.9	4.3	4.03
3	60	1529.1	6.3	9.63
4	75	3473.7	13.1	45.50
5	90	4158.7	15.4	64.04
6	120	587.8	3	1.76
7	150	243.1	1.8	0.44
8	180	561.3	2.9	1.63
9	220	1851.7	7.4	13.70
10	250	3226.2	12	38.71
11	300	707.1	3.4	2.40
12	400	243.1	1.8	0.44
13	500	760.1	3.6	2.74
14	750	304.9	2.1	0.64
15	1000	114.9	1.4	0.16

The maximum output 64 µW at 90 Hz as shown in the Figure 4.37.

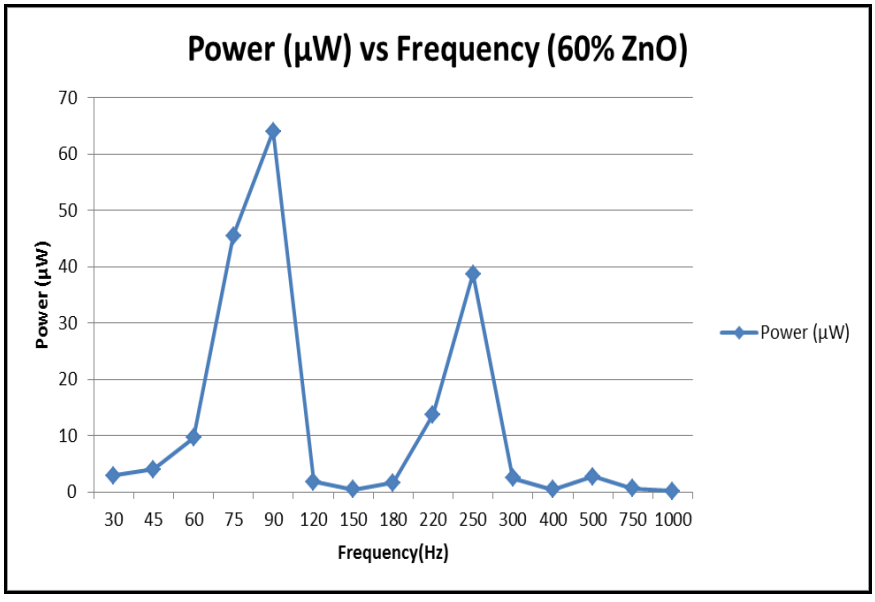

Figure 4.37 Variation of power with respect to frequency at 160 gauss for 60% ZnO.

Case 9: The composite had 19.9% FNO + 80% ZnO + 0.1% Epoxy coating compostion. Table 4.26 contains the respective voltage, current and power for coating mixture 9.

Table 4.26 Output values for coating mixture 9 with magnetic field of 160 gauss.

S.No	Frequency	Voltage (mV)	Current (µA)	Power (µW)
1	30	765.4	3.5	2.68
2	45	903.3	3.9	3.52
3	60	1488.5	5.8	8.63
4	75	3454.2	12.2	42.14
5	90	4069.4	14.1	57.38
6	120	572.8	2.8	1.60
7	150	236.9	1.8	0.43
8	180	551.5	2.8	1.54
9	220	1843.8	6.9	12.72
10	250	3247.4	11.5	37.34
11	300	708.9	3.3	2.34
12	400	210.4	1.7	0.36
13	500	751.3	2.4	1.80
14	750	286.4	1.9	0.54
15	1000	114.9	1.4	0.16

The maximum output 57.3 µW at 90 Hz which is 19.6 µW higher as compared to non-magnetic composite as shown in Figure 4.38.

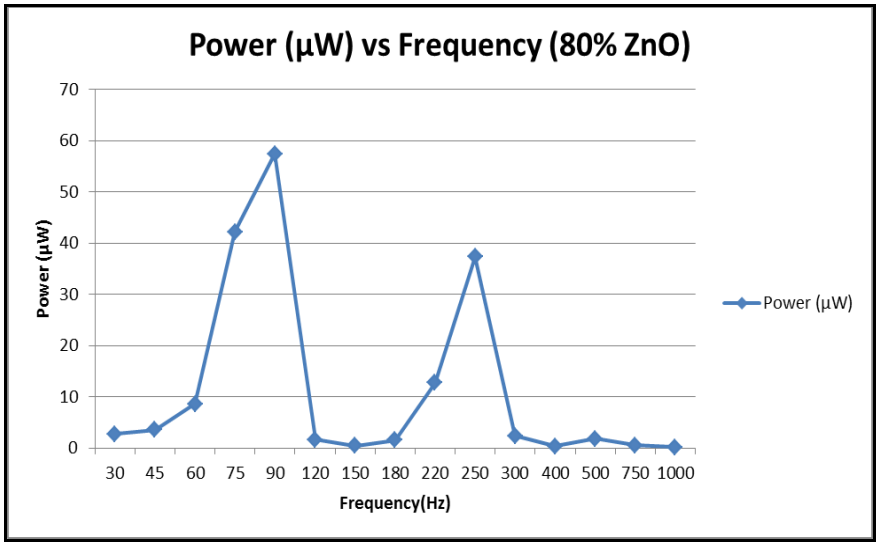

Figure 4.38 Variation of power with respect to frequency at 160 gauss for 80% ZnO.

Case 10: The composite had 0% FNO + 99.9% ZnO + 0.1% Epoxy coating compostion. Table 4.27 contains the respective voltage, current and power for coating mixture 10.

Table 4.27 Output values for coating mixture 10 with magnetic field of 160 gauss.

S.No	Frequency	Voltage (mV)	Current (µA)	Power (µW)
1	30	795.5	3.4	2.70
2	45	989.9	4	3.96
3	60	1529.1	5.7	8.72
4	75	3288.0	11	36.17
5	90	4030.5	13.1	52.80
6	120	601.0	2.8	1.68
7	150	229.8	1.7	0.39
8	180	548.0	2.6	1.42
9	220	1803.1	6.4	11.54
10	250	2740.0	9.3	25.48
11	300	654.1	2.9	1.90
12	400	300.5	1.9	0.57
13	500	707.1	3.1	2.19
14	750	335.9	2	0.67
15	1000	123.7	1.3	0.16

The maximum output is 52.8 µW at 90 Hz as shown in the Figure 4.39 which is 1.5 times that of the non-magnetic composite as shown in Figure 4.24.

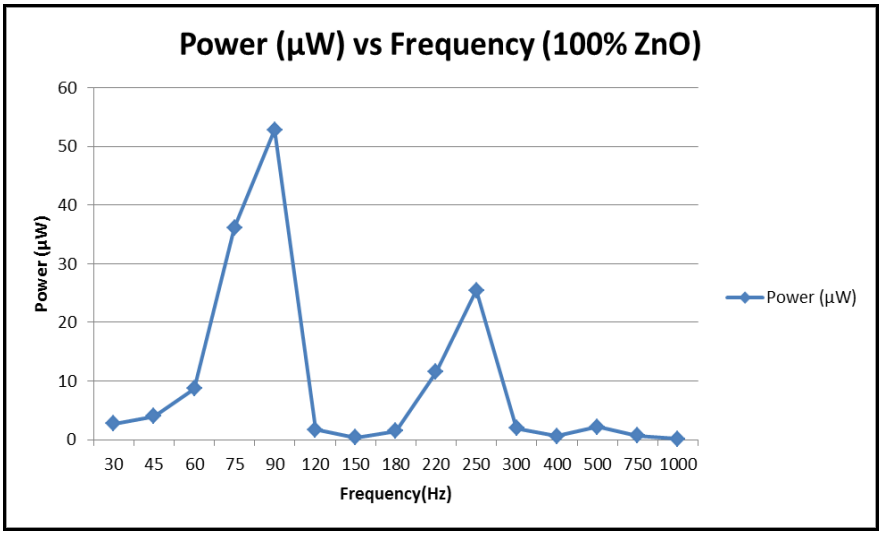

Figure 4.39 Variation of power with respect to frequency at 160 gauss for 100% ZnO.

Table 4.28 shows the maximum output of power for different composites. The power output varied with the percentage of zinc oxide nanoparticles in the coating mixture and it increased due to the effect of magnetic field. As in case of the non-magnetic composite the maximum output was for a coating having 40% ZnO. Similarly, it was observed that the output maxed out at 40% and then stabilized.

Table 4.28 Peak power output for different coatings with magnetic field of 160 gauss.

Coating Type	Peak Power (µW)
0%	21.85
1%	28.09
10%	17.71
20%	31.71
30%	12.26
40%	68.55
50%	68.44
60%	64.04
80%	57.38
100%	52.80

Figure 4.40 shows the comparison of the peak power output of the different composites having different coating mixtures.

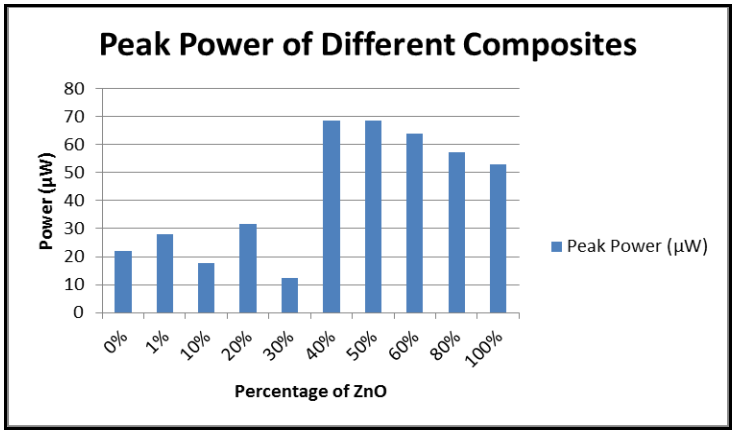

Figure 4.40 Peak power comparison of different composite at 160 gauss.

Table 4.29 shows the peak power outputs of the different coating composites with and without the magnetic field. The magnetic field strength as shown above is 160 gauss. The maximum power increased by a factor of 1.2 to 1.55 for different composites thereby proving the theory that PZT output increases when it is subjected to magnetic field.

Table 4.29 Peak power output for different coatings with and without magnetic field.

Coating Type	Peak Power (µW)	Peak Power with 160 Gauss field (µW)
0%	18.08	21.85
1%	18.21	28.09
10%	13.18	17.71
20%	20.64	31.71
30%	7.98	12.26
40%	44.53	68.55
50%	44.28	68.44
60%	41.92	64.04
80%	37.76	57.38
100%	34.82	52.80

Figure 4.41 compares the peak power outputs for the magnetic and non-magnetic composites.

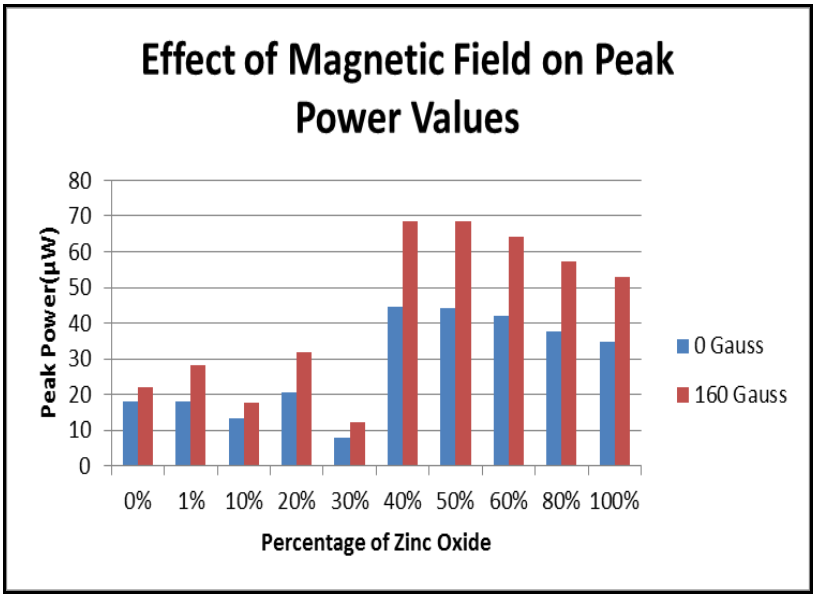

Figure 4.41 Peak power comparison with and without magnetic field

Table 4.30 shows the peak power density of the composites with and without the magnetic field. As shown in the previous section of this chapter the power density was calculated by dividing the power with the volume of the nanocoated PZT.

Table 4.30 Peak power density for different coatings with and without magnetic field.

Coating Type	Peak Power Density (mW/cm^3)	Peak Power Density with 160 Gauss field (mW/cm^3)
0%	0.29	0.35
1%	0.29	0.45
10%	0.21	0.29
20%	0.33	0.51
30%	0.13	0.20
40%	0.72	1.11
50%	0.71	1.10
60%	0.68	1.03
80%	0.61	0.93
100%	0.56	0.85

Figure 4.42 compares the peak power density outputs for the magnetic and non-magnetic composites. The maximum power density increased from 0.72 mW/cm^3 to 1.11 mW/cm^3 which shows an improvement of 54%.

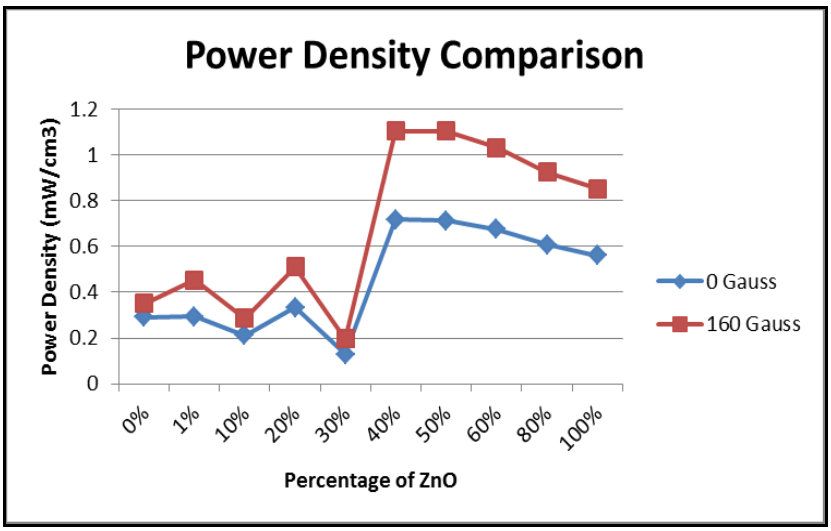

Figure 4.42 Peak power density comparison with and without magnetic field.

Discussion:

The optical, magnetic and semiconducting properties of ZnO combined with the magnetic properties of ferrofluid lead in improvement in the power output of the PZT composite. The increase in output is caused by the strain produced in the coating due to the magnetostrictive effect which the nanocoating exhibits under the influence of magnetic field. The improved output of the nanocoated composite under the influence of magnetic field is a magneto-electric effect is the product property of the composite.

When the magnetic field is applied to the PZT composite strain is induced in the PZT and also the magnetostrictive coating restricts the magnetic field which increases the strain in the PZT, subsequently leading to improved performance of the composite as shown in Figure 4.43.

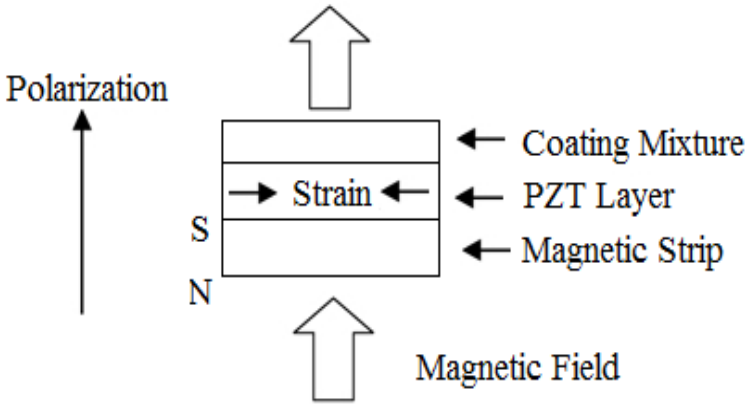

Figure 4.43 Nanocoated PZT under magnetic field.

Also, coating mixture may flow in the cracks on the surface of PZT and when the magnetic field is applied and coating is cured by UV on the PZT different level of strains will be produced in between the PZT surface and on the surface thereby causing more strain in the system and hence better output.

4.6. Power Output from Solar Cell

In this section, the voltage and current output of the Ar- gas plasma etched solar cell was compared with that of plane solar cell and that of etched solar cell under magnetic field.

Effect of Etching and Magnetic Field

Recent developments in the field of photovoltaics have shown that the efficiency of solar cell increases with the exposure to magnetic field [49]. Also, etching the solar cell wafer increases the surface energy of the surface and also enhances the internal reflection capacity of the solar cells. The main purpose of this study is to improve the efficiency of solar cells by these techniques. The following Steps were taken to study the effect of etching and magnetic field on the solar cell output.

1. Firstly, output of normal solar cell was taken without subjecting it to any improvement processes.

2. Then the normal solar cell was the subjected to magnetic field of 160 gauss to study the effect of magnetic field.

3. After the above two experiments were done, then the solar cell was etched using the Ar-gas plasma etch machine for 3 minutes. After the etching that cell's output was taken to understand the effect of plasma etching on the solar cell.

4. The solar cell which was etched was then subjected to magnetic field of 160 gauss and then its output was taken, this data helped in understanding the cumulative effect of etching and magnetic field. Figure 4.44, 4.45 and 4.46 show the Current, Voltage and Power outputs respectively.

Table 4.31 shows the output of the solar cell after each process like etching and under the magnetic field. The values are the average of 5 readings.

Table 4.31: Solar cell outputs under different conditions.

	Plain Solar Wafer	With Magnet	Etched Solar Wafer	Etched with Magnet
Voltage(Volts)	0.49	0.51	0.52	0.53
Current(Amps)	7.25	7.58	7.65	7.79
Power	3.55	3.87	3.96	4.16

Current Variation: Figure 4.44 shows the average current outputs for solar cell after each process was done. The current for plain solar cell was 7.24 amps which increased to 7.6 amps when exposed to magnetic field. After that the solar cell was itched using the plasma etch machine for 180 secs or 3 mins the current increased to 7.6 amps and along with the magnetic exposure this solar cell gave a current output of 7.8 amps which is an increase of 7.5%.

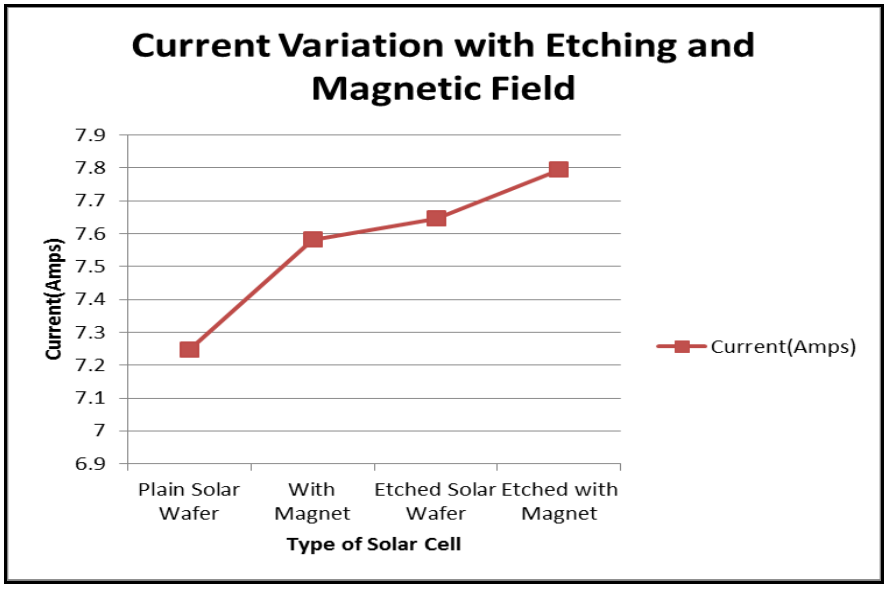

Figure 4.44 Current variation for different solar cells.

Voltage Variation: Figure 4.45 shows the average open circuit voltage outputs for solar cell after each process was done. Similar to the outputs of current the voltage output also increased

with the etching process and magnetic field. Voltage and current outputs were taken simultaneously. The voltage output improved from 0.49 V for plain solar cell to 0.51 V when exposed to magnetic field. After that the solar cell was itched using the plasma etcher for 180 secs or 3 mins the voltage further increased to 0.52 V and along with the magnetic exposure this solar cell gave a voltage output of 0.53 V which is an increase of 9 % over the plain solar cell.

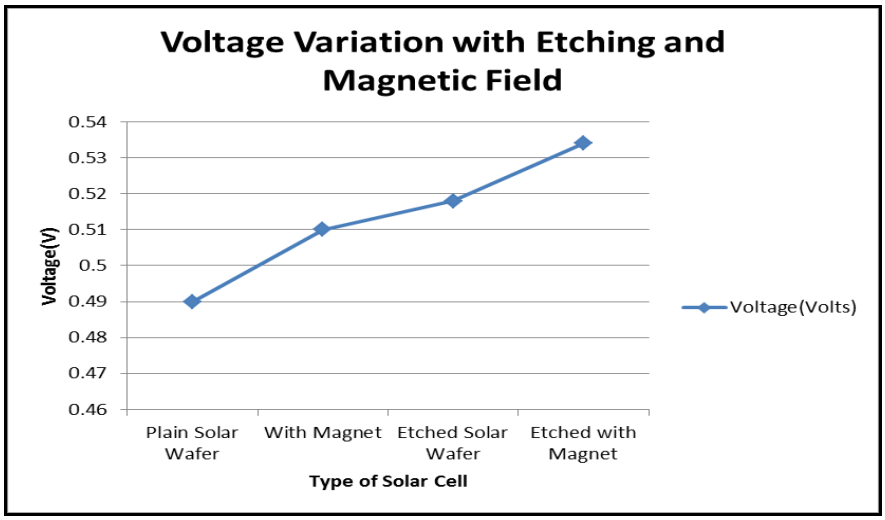

Figure 4.45 Voltage variation for different solar cell.

Power Variation: Figure 4.46 shows the average power outputs for solar cell after each process was done. This was calculated using the relation P = I x V, similar to the outputs of current and voltage the power also increased with the etching process and magnetic field. For plain solar cell the power was 3.5 W and it increased to 3.89 W with magnetic field. The power output after etching was 3.96 W which increased to 4.16 W for the etched solar cell exposed to magnetic field. The percentage increase was 17%.

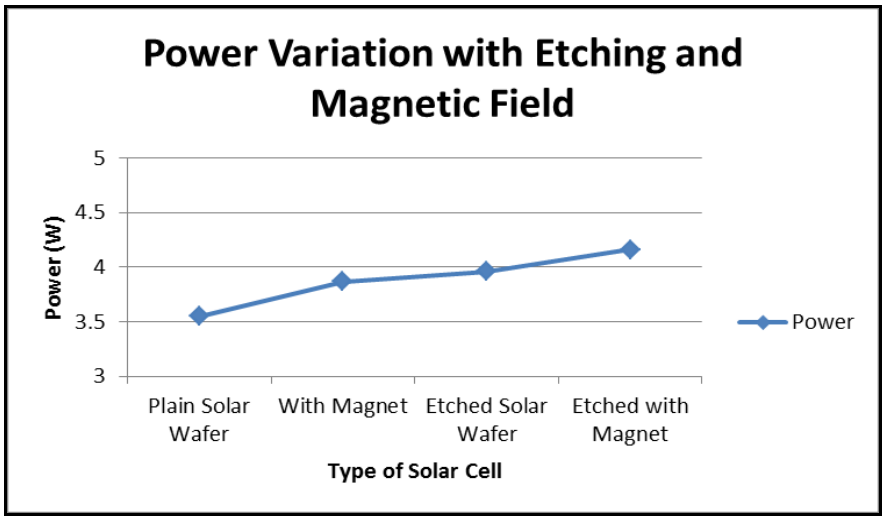

Figure 4.46: Power variation for different solar cells.

Efficiency Variation: Table 4.32 shows the efficiencies of solar cells subjected to various efficiency improvement methods.

Table 4.32 Solar cell efficiency under different conditions.

Processing Type	Efficiency (%)
Plain Solar Wafer	14.59
With Magnet	15.89
Etched Solar Wafer	16.27
Etched with Magnet	17.10

The efficiency of the solar cell was calculated using equation 9 from chapter 2. Area of the Solar Cell was 0.023 m^2 and the irradiance was 1000 W/m^2. Maximum power is found using the values of current and voltage.

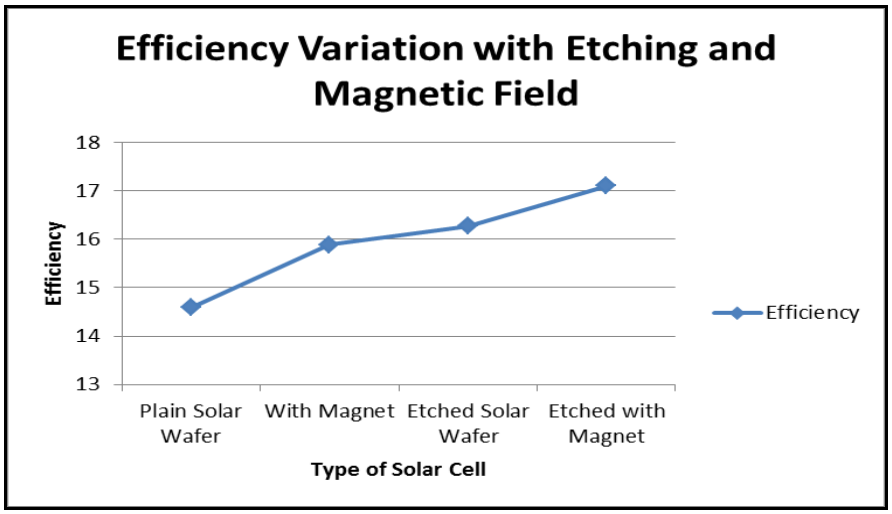

Figure 4.47 Efficiency variation for different solar cells.

Figure 4.47 and 4.48 shows the variation of efficiency for the solar cell after each procedure. The efficiency improved from 14.5% to 17.1% which is an improvement of 2.6%.

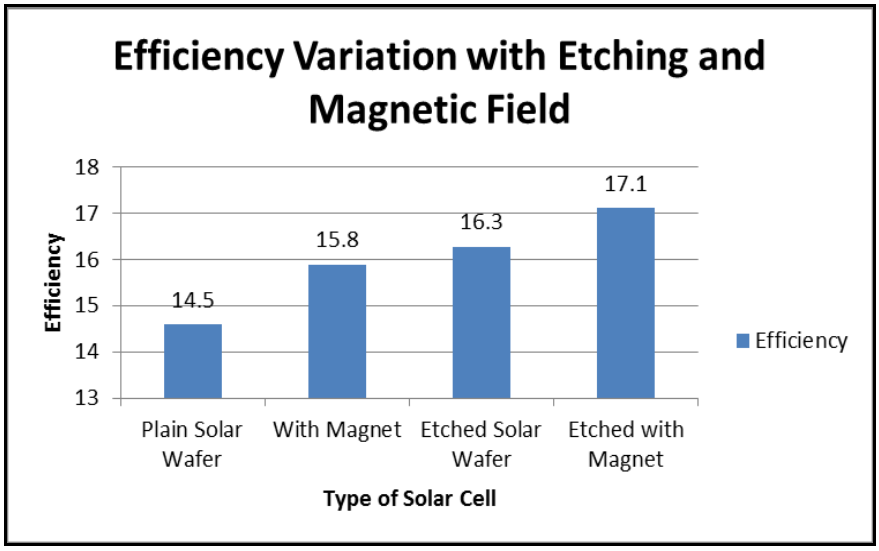

Figure 4.48 Efficiency variation histogram.

Discussion:

Gas plasma etching with argon gas causes nanodents in the structure of the solar cell as seen in Figure 4.49. Argon is an inert gas and doesnot react with the surface. Thus the etching only increases the surface energy of the solar cell by knocking the loosely bounded electrons

from the solar cell. If the gas was reactive then the surface material's electron would react with the electrons from the gas and the efficiency would not increase.

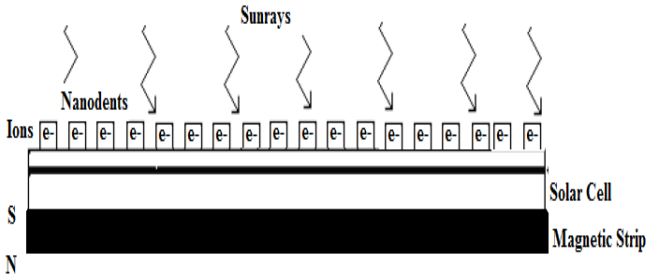

Figure 4.49 Etched solar cell with nanodents under magnetic field.

The nanodents cause the light rays to be diffracted and also cause the internal reflection of the rays reducing the reflectance of the solar cell and improving the efficiency of the solar cell. Also the increase in the surface energy and loosening of electrons on the surface of solar cell would increase the output of the solar cell.

The improvement in the performance of solar cell under the magnetic field can be attributed to the increase in the spectrum of light which hits the solar cell due to the magnetic field's attraction. Thus, the combination of gas plasma etching and the magnetic field has an immense scope in the improvement in the performance of the solar cell.

CHAPTER 5

CONCLUSION

In this chapter the results are discussed and conclusions are drawn from the results. The chapter is divided into three segments; the first contains the review of the effect of PZT composite area variation, effects of backup plate on power generation, etc., the second segment contains the hypothesis and the third segment contains the summarized conclusions of this study.

Effect of PZT composite area variation: The output increases with the area of the PZT. The area of the PZT can be increased by attaching multiple PZT together in series or parallel connections. Also, the area of the power generating surface can be increased by the nanocoatings. The nanocaotings as shown in the Figure 5.1 shows the patterned coating which increases the output of the composite by increasing the effective area for electron generation.

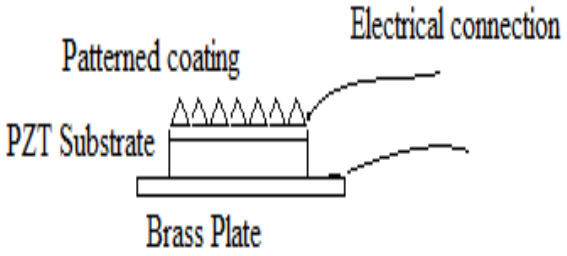

Figure 5.1 Nanocoated PZT substrate.

The capacitance between plates is given by $C = \frac{\varepsilon_r \varepsilon_0 A}{d}$

The effective area of the composite increases due to the coating but the distance between the electrodes remains the same, and thus the capacitance increases.

Effect of backup plate on power generation: The properties of the backup plate of the composite are very critical to determine the power generated by the energy harvester. The natural frequency of the cantilever beam is $\omega_n = \frac{1}{2\pi}\sqrt{\frac{k}{m}}$

Where, k = stiffness of the beam

m = mass of the beam

The stiffer the beam, the more is the power generated by it because the stress waves travel faster in a stiffer beam as well as the vibrations do not dampen out quickly in a stiff beam. $k_{aluminum} < k_{stainless\ steel}$, therefore the power generated would be more in stainless steel as compared to aluminum for a beam having same dimensions as shown in the previous section. Moreover the variation in the natural frequency determines the frequency at which the peak outputs will be obtained. The mode shapes would determine the points where the PZT substrate should be attached to get maximum output. The mode shapes and the points of highest amplitude of vibration also vary with the material of backup plate. Also, the amplitude of vibration defined in terms of 'g' – acceleration values is higher for stainless steel as compared to aluminum.

The other important factor that governs the output of the composite is the joint between the PZT and the backup plate. When the joint is not strong or if there is a gap between the PZT substrate and the backup plate then the level of stain transferred from plate to the PZT would be low and thus the output would be low.

Effect of ZnO: The output of the composite varies with the percentage of ZnO and the optimum percentage of ZnO leads to very high increase. The other effect of ZnO which is seen for the coatings having 0% to 30 % ZnO is the flattening of the output curves with respect to frequency

at 75 Hz – 90 Hz level. This phenomenon of the flattening of the curve ends for the coatings having more than 40% ZnO in them.

The flattening of the curve at the frequencies means that the output of the composite at these frequencies is about the same. This effect can lead to further exploration for finding more compositions of the coatings for a consistent output from the PZT composite.

Effect of magnetic field: The magnetic field improves the performance of the nanocoated PZT composite, which is due to magnetostrictive properties of the nanocoating as well ME effect of the PZT. This is a product property, which means that either the coating's or PZT's alone do not exhibit such behavior. To further enhance the output of the PZT composite, variation of its performance with the different levels magnetic field can be researched.

Effect of etching and magnetic field on solar cell efficiency: The improvement in the solar cell efficiency is due to gas plasma etching which produced an energized surface with extra loose ions to generate power as well created nanodents which lowered the reflectance of the solar cell by improving the internal reflection and refraction of the sunrays.

The magnetic field helped in increasing the spectrum of light which is striking the solar cell and causing more ions to be displaced in the semiconductor causing higher output. The wider spectrum means more photons and phonons are hitting the surface of the solar cell and due to the nanodents are entrapped for a longer time and the energy is getting transferred more effectively.

Hypothesis: Nanoparticle coating on the PZT under the influence of magnetic field improves the energy generating capabilities of the system. The effect may be similar to the law of Fleming's Left Hand Rule as shown in Figure 5.2 [50] below.

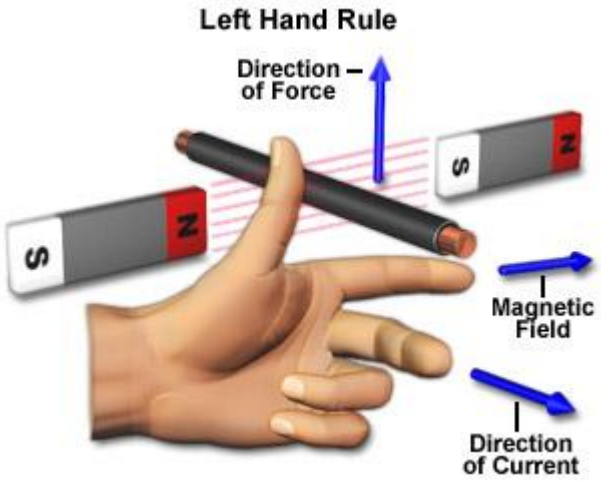

Figure 5.2 Fleming's Left hand rule [50].

The hypothesis recommended in this work suggests that the energy generated increases because of the combination of the piezoelectric effect of the PZT, Magneto Electric Effect and the charged particles in the coating mixture working under the left hand rule. The charged nanoparticles present in the coating mixture flow into the cracks of the PZT surface as well causing an additional strain in conjunction with the strain induced due to the vibrations. When all the factors are taken into account the sudden increase in the output of the composite formed can be explained.

Furthermore, according to the work previously done, the effect of increase in the surface area of the coating could possibly increase the output of the composite structure exponentially. To increase the surface area of the composite a layer of nanocones can be formed on the surface using the effects of magnetic field on ferrofluid. The surface having cones is shown in Figure 5.3.The advantage of the surface having cones would be as follows:

1) Increase in the surface area.
2) Orientation of the charged nanoparticles

3) Additional induced strain in the Zinc nanoparticles in the cones which will improve the piezoelectric effect of Zinc nanoparticles.

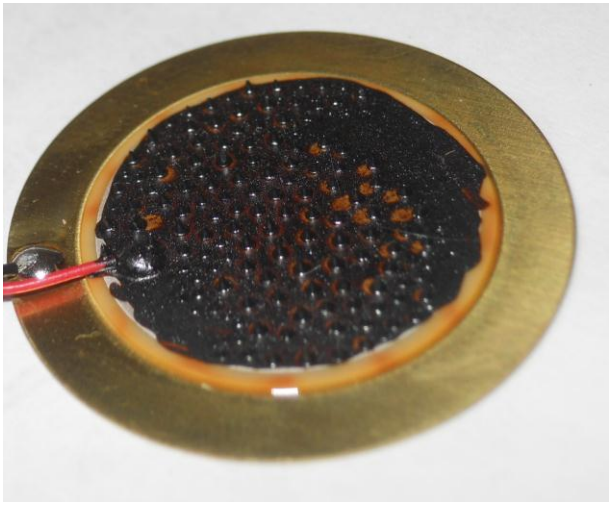

Figure 5.3 Structure nanocones on the PZT substrate.

Hence, looking at the posible applications and scope of further improvement in this field of energy harvesting, the work needs to be further explored and imporved upon.

Conclusions:

In this work, PZT substrate was coated with nano-mixture of ferrofluid and zinc oxide nanoparticle and a composite was made to analyze its energy harvesting capability. Also, the effect was magnetic field was studied for PZT energy harvesting. Solar cell's efficiency was also studied under magnetic field and the effect of etching the solar cell was analyzed.

The study included determining the natural frequency of the cantilever beam, effect of area variation of the PZT on the power generation, comparison of the backup plate material for power generation, effect of ZnO on the power generation capability of the nanocoating, best coating mixture composition, effect of magnetic field on the composite and the effects of surface

texturing and magnetic field on the performance of silicon solar cell. The conclusions of these experiments are summarized below.

1. Natural frequency of cantilever stainless steel beam used in this study was 12 Hz and the theoretical natural frequency derived for the same beam came out to be 10.14 Hz which are very similar and hence proved that the experimental setup was working well.

2. The second, third and fourth natural frequencies for the stainless steel cantilever beam were 76 Hz, 214 Hz and 414 Hz.

3. The natural frequencies for the cantilever beam with one nanocoated PZT mounted on it were 12 Hz, 74 Hz, 202 Hz and 414 Hz

4. The natural frequencies for the cantilever beam with three nanocoated PZT mounted on it were 10 Hz, 64 Hz, 192 Hz and 380 Hz

5. The natural frequencies for the cantilever beam with magnetic strip and a nanocoated PZT mounted on it were 78 Hz, 234 Hz and 380 Hz

6. The peak current output for the composite having area 9.14×10^{-4} m^2 was 8.7 μA as compared to 13.1μA for the composite having area 3.04×10^{-4} m^2

7. The peak voltage output for the composite having area 9.14×10^{-4} m^2 was 10,139 mV as compared to 3380 mV for the composite having area 3.04×10^{-4} m^2

8. The effect of composites area on the output was also studied and the composite structure having 9.14×10^{-4} m^2 area of PZT performed 2.5 times better by generating 88.2 μW compared to 44.3 μW than the composite having area 3.04×10^{-4} m^2 .

9. The nanocoatings were also subjected to different magnetic fields to find the optimum level of magnetic exposure for highest power outputs and upon comparison between composites exposed to different levels of magnetic field it was found that composite exposed to 500 gauss performed the best. So, all the other composites were then exposed to the same magnetic field.

10. The optimum percentage of ZnO nanoparticles for the best output was at 40% at 90 Hz frequency, where the power output was 48.5μW. Experiments in this study showed the best composition for highest power generation to be 59.9% ferrofluid, 40% ZnO nanoparticles and 0.1% binder.

11. The performance of the composite for energy harvesting can further be improved by application of magnetic field. It was shown that the power output could be improved from 48.5 μW to 68.5 μW by applying a magnetic field of 160 gauss.

12. The current for plain solar cell was 7.24 amps which increased to 7.6 amps when exposed to magnetic field.

13. In the solar cell itched using the gas plasma etch machine for 180 secs or 3 mins, the current increased to 7.6 amps from 7.24 amps of normal solar cell. Comparing the performance of plasma etched solar cell with one which is not etched, it was found that the plasma etched one is found to be 10% better in terms of power output.

14. The voltage output improved from 0.49 V for plain solar cell to 0.51 V when exposed to magnetic field.

15. Solar cell etched for 180 secs or 3 mins the produced a voltage output of 0.52 V as compared to 0.49 V of non-etched solar cell.

16. Along with the magnetic exposure this solar cell gave a voltage output of 0.53 V which is an increase of 9 % over the plain solar cell.

17. When the effect of etching and magnetic field is combined and that solar cell is compared to the non-etched one, it was found to be 17% better in terms of power output. The combination of the use of magnetic field and plasma etching using argon gas improved the performance of the solar cell. The efficiency of the Solar cell improved from 14.6% to 17.1%, a 2.5% improvement by the processes done on the solar cell.

In conclusion, the research performed in this study has shown that the nano-coated composite developed based on the concepts presented works reasonably well. The trends in this study indicate that there is a great potential that further research can lead to this composite being able to harness the ambient energy at low vibration levels. Also, the efficiency of the solar cells can also be improved further by subjecting them to the magnetic field and texturing.

LIST OF REFERENCES

LIST OF REFERENCES

[1] Mittal, S., "Tapping the Untapped: Renewing the Nation." Centre for International Trade, Economics and Environment, 2010.

[2] Green, A. M., Emery, K., Hishikawa, Y., and Warta, W. "Solar cell efficiency Tables (version 37)" Progress in Photovoltaics: Research and Applications , Vol. 19, Issue 1, p. 84–92, 2011.

[3] Tsuo, Y.S., Wang, T.H., and T.F. Ciszek "Crystalline-Silicon Solar Cells for the 21st Century" NREL/CP-590-26513, 1999.

[4] Grogg K. "Harvesting the Wind: The Physics of Wind Turbines", 2005.

[5] Sodano, H. A., and Inman, D. J., "Comparison of Piezoelectric Energy Harvesting Devices for Recharging Batteries", Journal of Intelligent Material Systems and Structures, 2005.

[6] V. Kulkarni, D.Waechter, R.Ben Mrad, T. El-Diraby, N. Somayajula, S. Nemana and E. Prasad, "Development of energy harvesting modules based on piezoceramics ," International Workshop, Smart Materials and Structures, 2009.

[7] Shearwood, C. and Yates, R. B., "Development of an electromagnetic microgenerator," Electronics Letters, vol. 33, p. 1883-1884, 1997.

[8] Amirtharajah, R, Chandrakasan, A., "Self-powered signal processing using vibration-based power generation," IEEE Journal of Solid-State Circuits, vol. 33, p. 687-695, 1998.

[9] Amirtharajah, R, Meninger S., Mur-Miranda, J. O., Chandrakasan, A., and Lang, J., "A micropower programmable DSP powered using a MEMS-based vibration-toelectric energy converter", 2000.

[10] Li, W. J., Chan, G. M. H. , Ching, N. N. H. , Leong, P. H. W. and Wong H. Y., "Dynamical modeling and simulation of a laser-micromachined vibration-based micro power generator," Int. J. Nonlinear Sci. Simulation, vol. 1, p. 345-353, 2000.

[11] Meninger, S., Mur-Miranda, J. O., Amirtharajah, R, Chandrakasan, A., and Lang, J., "Vibration-to-electric energy conversion," IEEE Transactions on Very Large Scale Integration (VLSI) Systems, vol. 9, p. 64-76, 2001.

[12] El-hami, M., Glynne-Jones, P., White, N. M., Hill, M., Beeby, S., James, E., Brown, A.D., and Ross, J.N., "Design and fabrication of a new vibration-based electromechanical power generator," Sensors and Actuators, A: Physical, vol. 92, p. 335-342, 2001.

[13] Ching, N. N. H. , Li, W. J., Leong, P. H. W. and Wong H. Y., "A laser micro-machined multi-modal resonating power transducer for wireless sensing systems", 2002.

[14] Roundy, S. and Wright, P. K. “A piezoelectric vibration based generator for wireless electronics”, Smart Materials and Structures, vol. 13, no. 5, p. 1131-1142, 2004.

[15] Chao, L., Chi-Ying T., and Wing-Hung K., "Vibration Energy Scavenging and Management for Ultra Low Power Applications", 2007.

[16] Dongna, S. “Piezoelectric energy harvesting devices for low frequency vibration applications” Thesis, 2011.

[17] Angel, J. “Wind Roses and Wind Frequency Tables for Illinois” 2000.

[18] Wang, Z. L., and Song, J., “Piezoelectric Nanogenerators Based on Zinc Oxide Nanowire Arrays” Science, Vol. 312, p. 242-246, 2006.

[19] Lukas, S.M., and MacManus-Driscoll, J.L., "ZnO – nanostructures, defects, and devices." Material Today. vol.10, issue 5, p. 40-48, 2007.

[20] Veeregowda, D.H., "Tribo acoustics tool for stick slip friction and energy harvesting using nanoparticles" Thesis, 2007.

[21] Bhagmar, S. "Patterned NANO coated energy harvester composites from vibration" Thesis, 2009.

[22] Jing, M., Jiamian, H., Zheng, L., and Ce-Wen, N., "Recent Progress in Multiferroic Magnetoelectric Composites: from Bulk to Thin Films" Advanced Materials, vol. 23, pp 1062-1087, 2011.

[23] Shenqiang, R., and Manfred, W., "Magnetoelectric nano Fe3O4/CoFe2O4// PbZr0.53Ti0.47O3 Composite", 2008.

[24] Jungho, R., Shashank, P., Kenji, U., and Hyoun-Ee, K., "Magnetoelectric Effect in Composites of Magnetostrictive and Piezoelectric Materials", 2002.

[25] Pan, D.A., Bai, Y., Volinsky, A.A., Chu, W.Y., and Qiao, L.J., "Giant magnetoelectric effect in Ni-Lead zirconium titanate cylindrical structure," Applied Physics Letters, vol. 92, 2008.

[26] Sodano, H.A., Magliula, E. A., Park, G. and Inman D. J., "Electric power generation using piezoelectric materials", Proceedings of the Thirteenth International Conference on Adaptive Structures and Technologies, p. 153-161, 2002.

[27] Zheng, Q. and Xu, Y., "Asymmetric air-spaced cantilevers for vibration energy harvesting", Smart Materials and Structures, vol. 17, no. 5, 2008.

[28] Glynne-Jones, P., Beeby, S. P. and White, N. M., "Towards a piezoelectric vibration powered microgenerator", IEEE Science Measurement and Technology, vol. 148, no. 2, p. 68-72, 2001.

[29] Marinkovic, B. and Koser, H., "Smart sand: a wide bandwidth vibration energy harvesting platform", Applied Physics Letters, vol. 94, no. 10, p. 103-105, 2009.

[30] Renaud, M., Sterken, T., Fiorini, P., Puers, R., Baert, K and van Hoof, C., "Scavenging energy from human body: design of a piezoelectric transducer", The Thirteenth International Conference on Solid-State Sensors and Actuators Transducers, p. 784–787, 2005.

[31] "Piezoelectric Ceramics: Principles and Applications", APC International Ltd, Chapter 2, 2002.

[32] DoITPoMS, Shaw, R., and Mathur, N., "Functional Behaviour of Materials: Piezoelectric Materials", Core-Materials, 2010.

[33] Wolf, H., Sauer, H.M. and Birringer, R. "Magnetic Field Induced Spontaneous Pattern Formation in Aerosol Particle Deposits", Europhysics Letters, 60(4), p. 573-579, 2002.

[34] Sai Sunder, Development of Nanoparticle Treated Sensors and Bearing Diagnostics using Fluctuation based processing. Thesis, 2004.

[35] Zheng, H., Wang, J., "Multiferroic BaTiO3-CoFe2O4 Nanostructures", Science, 2004.

[36] Fisher, W. M., Rand, S. C., "Optically-induced charge separation and terahertz emission in unbiased dielectrics" Journal of Applied Physics, 109(6), 2011.

[37] Sargent, T., Nortel Networks–Canada Research Chair in Emerging Technologies http://www.news.utoronto.ca/bin6/050110-832.asp.

[38] Wang, Z. L. and Song, J. “Piezoelectric Nanogenerators using Zinc Oxide Nanowires”, Science 312(5771),p. 242-246, 2006.

[39] Wang, Z. L. ,“Zinc oxide nanostructures: growth, properties and applications”, J. Physics : Condensed Matter 16, p. 829-858, 2004.

[40] Albrecht, C., Bührer "First observation of ferromagnetism and ferromagnetic domains in a liquid metal (abstract)". Applied Physics a Materials Science & Processing, 1997.

[41] Butter, K., “Iron (oxide) ferrofluids: synthesis, structure and catalysis”, Thesis, 1975.

[42] Meirovitch, L., Analytical Methods in Vibrations. 1st Edn., Macmillan Publishing Co. Inc., NY, USA., ISBN: 0023801409, p: 135-154. 1967.

[43] Knier, G. “How do Photovoltaics work”, NASA, 2002.

[44] National Renewable Energy Laboratory (NREl), Golden, CO, USA, 2010.

[45] Ryu, S., Yang, C., Yoo, W.J, “ Effects of Nanostructures formed by plasma etching on the reflectance of solar cells”, Journal of Korean Physical Society, Vol. 54, No. 3, p. 1016~1020, 2009.

[46] Murata USA - http://www.murata.com/products/catalog/pdf/p37e.pdf.

[47] Ion- and electron-assisted gas-surface chemistry—An important effect in plasma etching Coburn, J. W.; Winters, Harold F.; Journal of Applied Physics, 2009.

[48] Yebo, D. “Improving Sample Collection of Trace Particles of Mock Explosive on Nano Coated Sensor”, Thesis, 2011.

[49] Shakya, P., Desai, P., Kreouzis, T. Gillin, W. P, Tuladhar, S. M., Ballantyne, A. M,, and Nelson J. “The effect of applied magnetic field on photocurrent generation in poly-3-hexylthiophene:[6,6]-phenyl C61-butyric acid methyl ester photovoltaic devices”, 2008.

[50] http://www.magnet.fsu.edu/education/tutorials/java/handrules/index.html.
Accessed on 02/15/2012.

APPENDIX

APPENDIX

Definitions

I. Piezo related definitions

Piezoelectricity - Piezoelectricity is the charge which accumulates in certain solid materials in response to applied mechanical stress. The word piezoelectricity means electricity resulting from pressure.

Piezoelectric Effect- The piezoelectric effect is a reversible process in that materials exhibiting the direct piezoelectric effect (the internal generation of electrical charge resulting from an applied mechanical force) also exhibit the reverse piezoelectric effect (the internal generation of a mechanical strain resulting from an applied electrical field).

Dielectric constant (k) - Dielectric Constant is a number relating the ability of a material to carry alternating current to the ability of vacuum to carry alternating current.

Electromechanical Coupling - It represents the piezoelectric efficiency of a piezoelectric ceramic. Electromechanical coupling constant (K) for a piezoelectric material is defined as the root mean square of the energy accumulated within the crystal in a mechanical form. This accumulated energy reflects the electrical output.

Piezoelectric dielectric constant- Dielectric constant is an electrical displacement when a unity electric field is applied under no stress.

Piezoelectric Distortion Constant (d) - Piezoelectric Distortion Constant is the distortion of the piezoelectric material under the applied electric field of uniform strength with no stress.

Piezoelectric voltage output coefficient (g) - Piezoelectric voltage output coefficient is the piezoelectric voltage output under uniform external stress applied and no electrical displacement.

Curie temperature - Curie temperature refers to the temperature at which the piezoelectric materials loose there polarization capability and hence, the piezoelectric property. Curie temperature for the PZT film is 2800C (553K).

Coercive Field - Piezoelectricity is a property of ferroelectric materials. During poling, the domain structures are aligned along the direction of the applied electric field. When the applied electric field is removed, polarization produces the hysteresis loop. The reverse electric field required to cancel the remnant polarization is called as coercive field.

II. Magnetism related definitions

Magnetic flux (Φ) **-** It is a measure of quantity of magnetism, taking into accounts the strength and the extent of a magnetic field. The SI unit of magnetic flux is the weber.

Orientation of dipole - It actually means alignment of dipoles under influence of any magnetic or electric field.

Flux density – It is the amount of magnetic flux per unit area of a section, perpendicular to the direction of flux.

Magnetic field strength - strength is a measure of the intensity of a magnetic field, given in teslas (T), the SI unit.

Ferromagnetic - Materials that can be magnetized by an external magnetic field and remain magnetized after the external field is removed.

Diamagnetic – Diamagnetic materials are repelled by magnetic fields.

Paramagnetic - Paramagnetic material is only attracted when in the presence of an externally applied magnetic field and the material does not retain the magnetic properties when the external field is removed.

Permeability - It is the degree of magnetization that a material obtains in response to an applied magnetic field.

Magnetic Reluctivity: The reciprocal of magnetic permeability is magnetic reluctivity.

Magnetic Susceptibility (χm) - In electromagnetism, the magnetic susceptibility (χm) is a dimensionless proportionality constant that indicates the degree of magnetization of a material in response to an applied magnetic field.

MagnetoElectric (ME) Effect - ME effect can be defined as coupling of magnetic, mechanical and dielectric behaviors. Composite magnetoelectrics are combinations of magnetostrictive and electrostrictive materials, such as ferromagnetic and piezoelectric materials.

Multiferroic materials - Multiferroics have been formally defined as materials that exhibit more than one primary ferroic order parameter simultaneously. The basic primary ferroic order parameters are ferromagnetism.

Magnetostriction - It is a property of ferromagnetic materials that causes them to change their shape or dimensions during the process of magnetization. Magnetostrictive materials can convert magnetic energy into kinetic energy, or the reverse.

III. Coating definitions

Ferrofluid - Ferrofluids are colloidal liquids made of nanoscale ferromagnetic, or ferrimagnetic, particles (20-50nm) suspended in a carrier fluid (usually an organic solvent or water). Each tiny particle is thoroughly coated with a surfactant to inhibit clumping. It becomes strongly magnetized in the presence of a magnetic field.

Nanoparticles –Nanoparticles are particles sized between 100 and 1 nanometers.

IV. Material related definitions:

Young's modulus (E) - Young's modulus is a measure of the stiffness of an elastic material and is a quantity used to characterize materials. It is defined as the ratio of the uniaxial stress over the uniaxial strain in the range of stress in which Hooke's Law holds.

Stiffness (k) – It is the resistance of an elastic body to deformation by an applied force.

Poisson's ratio (ν) – When a material is compressed in one direction, it usually tends to expand in the other two directions perpendicular to the direction of compression. This phenomenon is called the Poisson effect. Poisson's ratio ν (nu) is a measure of the Poisson effect. The Poisson ratio is the ratio of the fraction (or percent) of expansion divided by the fraction (or percent) of compression, for small values of these changes.

V. Photovoltaics related definitions:

Photovoltaic effect – The photovoltaic effect is the creation of voltage or electric current in a material upon exposure to light.

Solar Cell - A solar cell (also called photovoltaic cell or photoelectric cell) is a solid state electrical device that converts the energy of light directly into electricity by the photovoltaic effect.

Semiconductors - A semiconductor is a material with electrical conductivity due to electron flow (as opposed to ionic conductivity) intermediate in magnitude between that of a conductor and an insulator.

Band Gap - The term "band gap" refers to the energy difference between the top of the valence band and the bottom of the conduction band measured in eV.

Photon - Photons exhibit wave–particle duality i.e. exhibiting properties of both waves and particles.

Phonons - A phonon is a quantum mechanical description of a special type of vibrational motion, in which a lattice uniformly oscillates at the same frequency.

Electron mobility (μ) - In solid-state physics, the electron mobility characterizes how quickly an electron can move through a metal or semiconductor, when pulled by an electric field.

Monocrystalline -Monocrystalline silicon or single-crystal Si, or mono-Si consists of silicon in which the crystal lattice of the entire solid is continuous, unbroken (with no grain boundaries) to its edges.

Multicrystalline or Polycrystalline silicon -Polycrystalline are composed of a number of smaller crystals or crystallites. Polycrystalline silicon is a material consisting of multiple small silicon crystals. Polycrystalline cells can be recognized by a visible grain, a “metal flake effect”.

Amorphous Silicon - (a-Si) is the non-crystalline allotropic form of silicon.

Reactive ion etching (RIE) - Texturization of silicon in chlorine plasma is a dry isotropic etching process that creates a surface with a high density of steep etching pits, with typical dimensions below 1 μm.

VITA

Sudhanshu Sharma, son of Mrs. Shakuntala Sharma and Mr. Shri Ram Sharma, was born in Indore, India. He received his Bachelor of Engineering (B.E) degree in Industrial & Production Engineering, from Shri G S Institute of Technology and Science, Indore, India, in May 2007. Before he enrolled at the University of Mississippi in August 2009, he had been working as a Deputy Manager in Indore, India. He attended graduate school, and obtained his Master of Science in Engineering Science from the Department of Mechanical Engineering at the University of Mississippi in May 2012.